To

my

Mother Prabhavati,

and

Father Pundalik.

I hereby declare that the matter embodied in the thesis entitled " **ELECTROCATALYTIC REDUCTION OF OXYGEN ON COBALT OXIDE SPINEL IN ALKALINE FUEL CELL** ", is based on the results of the investigation carried out by me in the Department of Chemistry in the Goa University, under the supervision of Dr. Jayant Budkuley.

In keeping with general practice of reporting scientific observation, due acknowledgements have been made wherever the work described is based on the finding of other investigators.

6/8/2002

Miss Harsha Pundalik Uskaikar

9/1/2003.
Guiding Teacher.

Jan. 9, 2003
External Examiner.

Certified that the work

" ELECTROCATALYTIC REDUCTION OF OXYGEN

ON

COBALT OXIDE SPINEL IN ALKALINE FUEL CELL ",

presented in this thesis has been carried out by Miss Harsha Pundalik Uskaikar under my supervision and the same has not been submitted for a degree of other universities.

6.8.2001

Dr. Jayant Budkuley

PROFESSOR & HEAD
DEPARTMENT OF CHEMISTRY
GOA UNIVERSITY

CONTENTS

CHAPTER I

LITERATURE SURVEY

LIST OF TABLES

CHAPTER I

CHAPTER III

CHAPTER IV

LIST OF FIGURES

CHAPTER I

CHAPTER II

CHAPTER III

CHAPTER I

CHAPTER ONE

LITERATURE SURVEY

INTRODUCTION

Any country's economy reflects the amount of energy consumed by that country or we can say that the standard of living of a given country is directly related to per capita income energy consumption. Man has needed and used energy at an increasing rate for his sustenance and well being ever since he came to earth a few million years ago [1].

Today man draws its energy needs from a variety of sources, which can broadly be categorized as renewable and non-renewable sources. In the non - renewable sources we have wood, Coal, fossil fuels, hydroelectric power and nuclear power. While the renewable sources include fuel cells, solar energy, tidal energy, sea, wind energy, geothermal energy, biomass etc. Wood was main source of energy in the pre-industrialization era. Once oil was introduced the coal and coke were replaced by it as a major source of energy. Nuclear energy looks to be attractive but there are some limitations in the use of nuclear energy such as difficulties associated with disposal of radioactive waste. Renewable sources such as wind energy can be utilized where the high wind velocity is available. Geothermal energy can be derived from the heat in the center of the earth. Biomass, which is in the form of wood, agricultural residues may prove as an important fuel source for rural areas [2].

Solar energy which has the greatest potential of all the sources of renewable energy if used in proper way can find number of applications, where sunlight is available in abundance [3].

In the past few years it has become obvious that the fossil resources are fast depleting and the fossil fuel era is gradually coming to an end. Even though the large scale use of commercial energy has led to better quality of life, it has created many problems.

The most serious of these is harmful effect on the environment. The combustion of the fossil fuel has caused several problems in many areas because of the localized release of large amounts of the waste heat from a power plant that has caused thermal pollution in lakes and rivers leading to the destruction of many forms of plants and animal life. It will be conflict between energy and environment to supply more energy to a burgeoning industrialized world. Without increasing the adverse environment effects of energy production. The global economy will be affected by the production and distribution of energy in all sectors. More and more industrialization of world requires sustainable and highly efficient energy production. One such energy source which can satisfy all these needs and also provide high thermodynamic efficiency, very low emission noise levels, excellent part load characteristics, rapid response times low pollution emission behavior, simplicity of mechanical engineering, good power/weight ratio, modularity of construction, is the **FUEL CELL** which can be an ideally flexible power provision. The application of fuel cell technology may be the most important technological advancement of the next decade [4].

1.1 HISTORY OF FUEL CELL

The fuel cell, invented in 1839 by Sir William Grove [5], had hydrogen and oxygen as reactant gases with sulfuric acid as an electrolyte. This device was not a proper fuel cell but a prototype of a chemical power source with gaseous electrodes. The research on Grove's fuel cell (Fig. 1.1) got the further boost after W. Oswald [6] published a paper on this.

In 1889, Ludwig Mond and Charles Langer repeated the earlier work of Grove and tried to make the fuel cell more practical by using air instead of oxygen and impure industrial gas, obtained from coal, instead of pure hydrogen. The first fuel cell development project, that led to a successful device, was started in 1932 by Francis T. Bacon [7]. He realized that expensive platinum catalyst must be replaced by a cheaper catalyst in the acid cell to make the fuel cell commercially viable. He switched from acid to less corrosive alkaline electrolyte and was able to use porous nickel metal as the electrode material. He also realized that it is necessary to use porous gas diffusion electrodes in order to get sufficiently large active electrode surface areas with three-phase contact. In 1959, after more than a quarter of a century of research, Bacon was able to announce that he and his co-workers had developed, built and demonstrated a 5KW fuel cell unit. Later it was used in NASA space program, as one of the important units which enabled man to fly to the moon in 1968.

In 1955, K. Kordesch developed prototype of low temperature O_2-H_2 fuel cell with carbon electrodes containing small amounts of oxides and platinum catalyst [8]. E. Justi and his coworkers [9] developed non - platinum catalysts namely raney nickel and

silver, for H_2 and O_2 fuel cell. This was a further step in the development of fuel cell electrodes.

It was soon discovered that the fuel cell was suitable as an electrical power source on the aerospace flights. A fuel cell with solid polymer electrolyte was used on the Gemini space flights. Later, this was changed to alkaline electrolyte, such as potassium hydroxide, in Apollo space flights, since solid polymer electrolyte had some limitations. One important or major advantage of fuel cell for the generation of electrical power on space flights is that the reaction product in this cell, water, could be used by the crew for drinking purpose [10,11].

Mid 1970's showed an interesting change in the direction of fuel cell technology. An alkaline fuel cell that had gained importance in space program was replaced in worldwide research by Phosphoric Acid Fuel Cell (PAFC). Which was better suited for the power plants [12].

During 1980's, the thrust in the research was on the Molten Carbonate Fuel Cell (MCFC), since it has the advantage of better overall efficiency together with the heat from a high temperature. Similarly, during 1990's the research and development in Solid Oxide Fuel Cell (SOFC) got the prime place and the membrane fuel system was found to be interesting and as such focus was on its development work [13]. Inspite of all research and development in membrane fuel cell for so many years, its drawbacks such as the high cost of membrane, and the expensive auxiliary system for heat and water still remains.

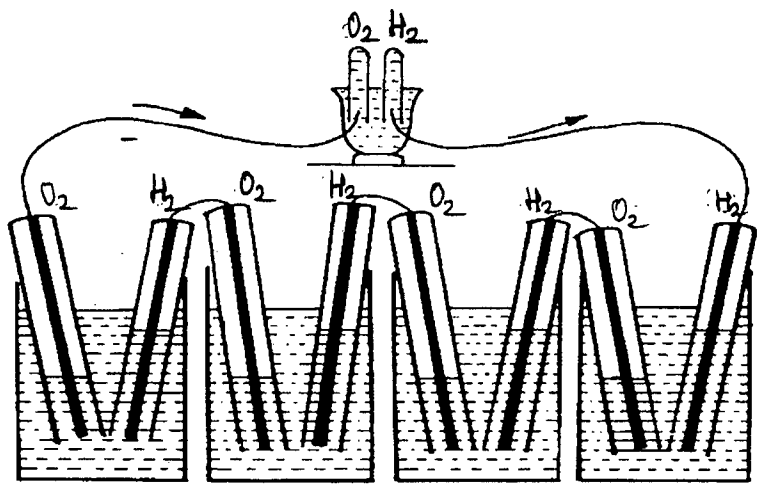

Fig. 1.1 The Grove's fuel cell.

1.1.1 OPERATING PRINCIPLE OF FUEL CELL

A fuel cell is an electrochemical cell, which can continuously convert the chemical energy of a fuel and an oxidant to electrical energy by using an electrode – electrolyte system [14]. The oxidant is fed to the cathode and the fuel to anode and the two electrodes are separated by the electrolyte. The simplest type of fuel cell, typical one for example, an alkaline $H_2 - O_2$ fuel cell is shown schematically in Fig. 1.2. It is possible to drive a fuel cell based on any chemical reaction that has negative free energy. The maximum voltage obtained from such a cell is given by the equation (1.1)

$$E = -\Delta G/nF, \qquad 1.1$$

Where 'n' is the number of electrons involved in each half-cell reaction, and F = 96500 C mol^{-1} is the faraday. Fig 1.2 shows the mode of operation of an alkaline fuel cell [15]. The electrolyte used is potassium hydroxide. The cell consists of two electrodes, the cathode and the anode. Hydrogen is oxidized to water at the anode by the reaction,

$$H_2\,(g) + 2OH^- \longrightarrow 2H_2O + 2e^- \qquad 1.2$$

And oxygen (or air) is reduced to hydroxide ions at the cathode, thus

$$^1/_2O_2(g) + H_2O + 2e^- \longrightarrow 2OH^- \qquad 1.3$$

The net chemical reaction, the sum of the cathode and the anode reactions, is given by

$$H_2 + {}^1/_2O_2 \longrightarrow H_2O \qquad 1.4$$

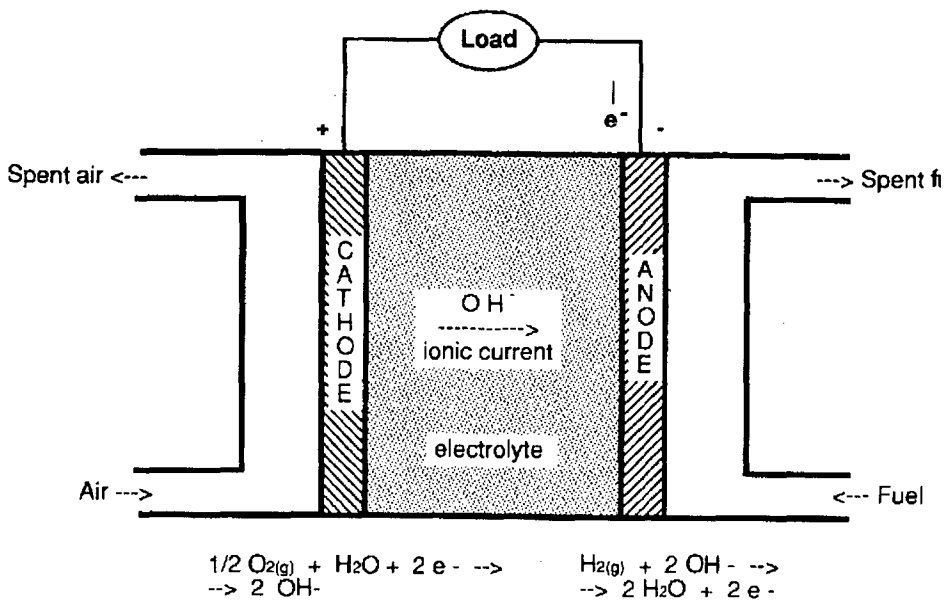

Fig 1.2 operating principle for an alkaline fuel cell.

1.1.2 CURRENT VOLTAGE CHARACTERISTIC OF FUEL CELL

The characteristic of the current voltage of a fuel cell during its operation can be shown by a typical current-voltage curve as shown in Fig 1.3 which shows the variation of cell potential with current density and also conversion efficiency of fuel to electrical power.

Depending on the type of the fuel cell, the electrode processes that occur, the temperature at which the cell operates and the thermodynamic reversible cell potential (E) is found to be in the range of 1-1.5V and determines the intrinsic maximum efficiency, which is usually equal to 80% [16].

As is seen from the Fig 1.3, the cell potential V decreases as the current drawn from the cell increases and deviates from the ideal cell potential - current relationship and maximum efficiency.

The region, where the cell potential decreases with increase in current density, the decrease is due to activation overpotential. The region where the cell potential is almost linear to the current density is attributed to the ohmic losses.

The region, where there is rapid decrease in cell potential at high current density represents the mass transport of fuel, oxygen and the reactant product in the cell [17].

Presence of an electrocatalyst in the electrode material plays a significant role in determining current-voltage relationship, especially in the initial stages of the cell voltage curve where voltage loss due to activation overpotential results in a dominating impact of cell performance.

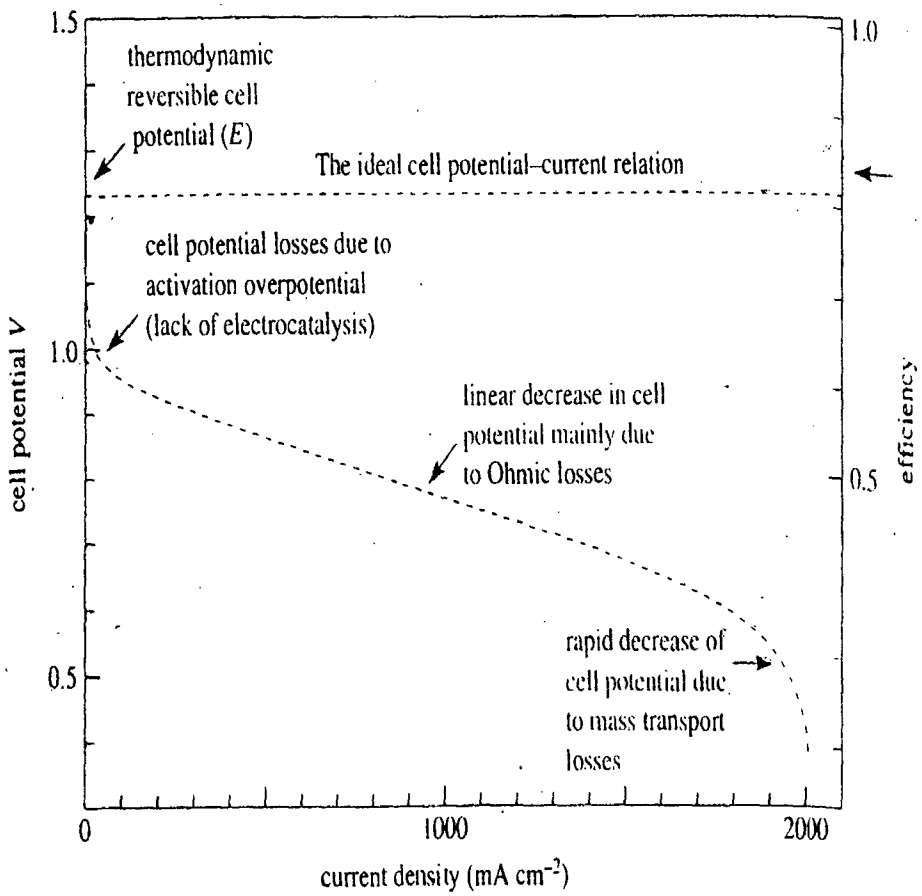

Fig. 1.3 The current voltage characteristics of a fuel cell

1.1.3 CHARACTERISTICS OF FUEL CELL SYSTEMS

One of the important characteristics of fuel cell is the direct conversion of chemical energy to electrical energy intrinsically, which makes its efficiency free from Carnot's theorem. Other advantages shown by fuel cell are efficiency, reliability, economy, cleanliness, unique operating channel, planning flexibility and future development potential [18].

** High efficiency and reliability: Ideal fuel cell is capable of converting 90% of the energy present in the fuel into usable electric power and heat. Phosphoric acid fuel cell gives 42% electrical conversion efficiency. Fuel cell efficiency is independent of its size and can operate at half of its rated capacity and still maintain high fuel use efficiency.

** The cost of the transmission lines can be reduced for the fuel cells, which can be located near the loads. Hence saving transmission losses [19].

** Another important characteristic of the fuel cell is its ability to co-generate, i.e. it can simultaneously produce hot water and low temperature steam with generation of electricity. Its ratio of electric to thermal output is approximately 1.0, while for the gas turbine the ratio is 0.5.

** Fuel cell power plants emissions are 10 times lesser than specified by most stringent environment regulations.

** Since water is one of the by products of the electrochemical reaction of fuel cell, very less water is required for plant usage. The low water usages of fuel cell have advantage over conventional power plants, which require large quantity of water for cooling.

** The other advantages of fuel cells are simple, clean, and quiet operation; site adaptability, due to their modular nature; can operate over any desired temperature range; and multi fuel capability: fuel cells can run on almost any fuel like naptha, methanol, natural gas, or any hydrogen rich fuel.

** Fuel cells produce D. C. electricity and hence find applications in chlor alkali and aluminium industry.

** Fuel cells have excellent part load heat rate and can immediately react to transient loads [20].

** Since the fuel cell power plant can be built within two years and since it is independent of plant size, utility system capacity can be increased slowly step-by-step with respect to customers satisfaction.

1.2 DIFFERENT TYPES OF FUEL CELLS

Fuel cells are classified into direct, indirect and regenerative fuel cell. Reformer and the biochemical cells are classified under indirect fuel cells. The direct types have been further classified according to the working temperature: high, medium and low (ambient) temperature systems, or referring to the pressure of operation: high, medium and low (atmospheric) pressure systems. They can be further classified on the basis of fuels intake and / the oxidants they use [21,22].

(1) Gaseous reactants (such as hydrogen, ammonia, air and oxygen).

(2) Liquid fuels (alcohols, hydrazine, hydrocarbons)

(3) Solid fuels (e.g. coal, hydrides).

Fuel cells are also classified based on the types of electrolyte used. The electrolytes used may be acid (phosphoric acid), alkali (potassium hydroxide), molten carbonates (Li^+, K^+, Na^+, CO_3^{-2}), solid oxides Y_2O_3 /ZrO_2 YSZ (Yttria stabilized zirconia), solid polymers (RSO_3H).

1.2.1 PHOSPHORIC ACID FUEL CELL (PAFC)

In acidic fuel cells, hydrogen ion conducts through the electrolyte. Platinum or platinum alloys are employed as electrocatalysts with carbon or (graphite) based electrodes [23]. Phosphoric acid at room temperature is slightly dissociated showing very low conductivity in concentrated solution. These cells find wide application in large power units (10KW). The working temperature is found to be between 463-473K.

Reactions involved in the PAFC are as follows.

At cathode. $^1/_2O_2 + 2H^+ + 2e^- \longrightarrow H_2O$ 1.5

At anode. $H_2 \longrightarrow 2H^+ + 2e^-$ 1.6

The important factor, which limits the performance of fuel cell for oxygen reduction reaction, is the slow kinetics of this reaction [24]. Workability at high temperatures and tolerance to carbon dioxide are some of the advantages offered by PAFC. Air can also be used as an oxidant and the other hydrocarbon products can be used as fuel [25]. The support that is commonly used in phosphoric acid fuel cell is Cabot Corporation's Vulcan XC-72R. This material is a conductive furnace black, and has very high conductivity and high specific surface area 250 $m^{-2}g$.

1.2.2 SOLID OXIDE FUEL CELL (SOFC)

The electrolyte used in the Solid Oxide Fuel Cell or SOFC is the ceramic material based on zirconium dioxide with the composition $ZrO_{2\cdot 0.17}$ or $ZrO_2.0.11Y_2O_3$. The conductivity of the first electrolyte is 0.02 ohm^{-1} cm^{-1}. And that of the second is about 0.12 ohm^{-1} cm^{-1} at 1273K. If the temperature is decreased, the conductivity decreases very sharply. The current carriers in the oxide electrolyte are oxygen ions (O_2^-). Anodes can be made from platinum as well as from the iron group metals. Nb-Zr-Y-O has been synthesized [26] from metals and some oxide compositions with semiconductor properties and used as anode material. Cathodes are made of platinum, silver or semi conducting oxides (based on oxides of zinc and zirconium). SOFC have many advantages over aqueous fuel cells, as this does not employ any liquid and hence the problems associated with flooding of porous electrodes and maintenance of three phase interface do not arise. The composition of the fuel and oxidant is the only factor to be taken into consideration. Also since the cell operates at high temperature, losses due to activation overpotential are lessened and hence the use of noble metal catalysts is avoided. The disadvantages are associated with high temperature of operation and several material problems imposed at these temperatures [27].

Reactions involved in SOFC are

At cathode, $^1/_2O_2 + e^- \longrightarrow {}^1/_2O_2^-$ 1.7

At Anode $H_2 + {}^1/_2O_2^- \longrightarrow H_2O + e^-$ 1.8

1.2.3 MOLTEN CARBONATE FUEL CELL (MCFC)

Extensive research has been carried out in Molten Carbonate Fuel Cell (MCFC) for the last decade as a second-generation fuel cell system. Still substantial development work is required to be carried out for the commercialization of the cell. It operates between 873- 923K. In MCFC, with molten electrolyte, the anodic process consumes carbonate ions:

$$H_2 + CO_3^{2-} \longrightarrow H_2O + CO_2 + 2e^- \qquad 1.9$$

Whereas carbon dioxide from the exhaust gas added to the oxygen for cathodic reaction and carbonate ions are regenerated in the reaction. Thus, transfer of an additional CO_2 molecule for each two electrons accompany the current producing reaction. CO_2 is transferred through the electrolyte from the cathodic space to anodic space, which returns to the cathodic space via gaseous phase. The slower cathodic process and the formation of oxides is explained by, [28.29].

$$\tfrac{1}{2} O_2 + CO_2 + 2e^- \longrightarrow CO_3^{2-} \qquad 1.10$$

Silver, lithium containing (lithiated) nickel oxide and some other oxides constitute the oxygen electrode. The fuel electrode can be made from platinum, palladium, silver, nickel or palladium coated graphite. The main disadvantages observed in MCFC are the instability of electrolyte carriers, corrosion of the electrodes and structural materials and also sealing problems. Scientists have designed a cell which has oxygen electrode made from lithiated nickel oxide. The hydrogen electrode has been made from a nickel cobalt

alloy and the electrolyte has been prepared from electrolyte immobilized with lithium aluminates.

1.2.4 SOLID POLYMER FUEL CELLS (SPFC)

Grubbs was first to introduce the cation exchange membrane in fuel cell technology [30]. The electrolyte used is an ion exchange membrane is of the type RSO_3H. The cation exchange resins are used because they offer higher conductivity and stability as compared to anion exchange resins. Solid Polymer Fuel Cell (SPFC) found its first major application in Gemini space flights. The main advantages of SPFC in the space applications are (a)high power and energy densities with respect to weight and volume, (b)high efficiency, (c)few moving parts, (d)minimum noise and vibration and (e)reliability.

The general electric solid polymer electrolyte fuel cell system with power of 1KW, was used as an auxiliary power source in the space vehicles. The byproduct in this fuel cell reactions, namely, pure water, could be used for drinking purpose by the astronauts.

Eventhough the fuel cell performed well for space missions for 1-2 weeks, there were some problems associated with the cell such as the power densities attained were not high enough ($<50mW\ cm^{-2}$). In addition, the polystyrene sulfonate ion exchange membrane was not stable under the electrochemical environments in the SPFC and the platinum loading was quite high. It is for these reasons that the alkaline fuel cell was chosen for the later Apollo programs and the space shuttle flights.

The General Electric Company continued the development of solid polymer electrolyte fuel cell even after the problem faced by Gemini space flights. The major breakthrough came when they discovered perfluorinated sulfonic acid polymer, Nafion, produced by Dupont, as the electrolyte.

The cell reactions are.

At the cathode $^{1}/_{2}O_{2} + 2H^{+} + 2e^{-} \longrightarrow H_{2}O$ 1.11

At the anode $H_{2} \longrightarrow 2H^{+} + 2e^{-}$ 1.12

Even the Ballard power system pursued the research on SPEFC and they were successful in reducing the cost of the SPEFC, by lowering the platinum loading [31]. Also they were successful in discovering a new sulfonated fluorocarbon ion conducting polymer membrane [32].

SPEFC finds major application for traction due to its higher power density. Ballard have recently designed and constructed a bus that uses compressed hydrogen in cylinders as the fuel [33,35].

1.2.5 DIRECT METHANOL FUEL CELL (DMFC)

Hydrogen has been the common fuel used in all the above mentioned types of fuel cell. But for traction use, as is in the case of Ballard bus, it requires tanks for the transport of fuel, which increases the weight of the bus. Hence an alternative for hydrogen is considered in form of methanol. The fuel cell, that can oxidize methanol directly at the anode and also maintain high power/weight ratio, is preferred.

The reactions occurring in the DMFC are:

And at the cathode, $^3/_2O_2 + 6H^+ + 6e^- \longrightarrow 3H_2O$ 1.13

At the anode $CH_3OH + H_2O \longrightarrow CO_2 + 6H^+ + 6e^-$ 1.14

Different alloys, such as Pt/Sn [36], Pt/Pd [37], Pt/Ru [38,40] have been developed as electrode materials. The problem associated with this cell is, poor electrode kinetics observed at the anode. Inspite of these difficulties the DMFC-SPE can be looked upon as a promising fuel cell for transport applications as it is cheap and potentially very competitive with the internal combustion engine, and can give high efficiency at low load and the most important feature of this cell is that it is pollution free.

1.2.6 ALKALINE FUEL CELL (AFC)

The cell which was developed by T. Bacon and which was used in Apollo space shuttle was alkaline fuel cell. The electrolyte used in the alkaline fuel cell was potassium hydroxide, and the cell operated at 523K. Hydroxyl ion provides ion conduction in AFC. Usually the concentration of KOH used in this fuel cell is 35-45% [41,42].

The half-cell reactions occurring in the cell are:

At the cathode, $O_2 + 2H_2O + 4e^- \longrightarrow 4OH^-$ 1.15

At the anode $2H_2 + 4OH^- \longrightarrow 4H_2O + 4e^-$ 1.16

The net cell reaction is;

$O_2 + 2H_2 \longrightarrow 2H_2O$ (1.23V) 1.17

Among several advantages offered by the AFC's their ability to operate at room temperature, to yield the highest voltage (at comparable current densities) of all the fuel

cell systems. And AFC's can achieve a long operating life (i. e. 15000h), have been demonstrated [43].

For alkaline fuel cell, wide choices of electrocatalysts are available compared to acid fuel cell. It is not restricted only to platinum group metal and tungsten carbide. The important electrocatalysts used in AFC's are platinum, silver [44] nickel [45] and raney nickel alloy [46,47]. The platinum group metals as well as cheaper catalyst can be used in the alkaline electrolyte, both for the hydrogen electrode (raney nickel) and the oxygen electrode (activated carbon promoted with various additives). In the Bacon cell, the electrodes were manufactured from nickel powder. The material was subjected to a special oxidation treatment and lithium oxide was added to it. The electrodes of the low temperature cells contained platinum group metals, in which the attempts were made to decrease the amount of these metals to 0.1-1mg/cm^2. The level of 0.1mg/cm^2 corresponds to platinum consumption of about 1.5g per 1KW of the rated power, which is quite acceptable economically [48].

The rated working current density of the alkaline oxygen-hydrogen cells is 50-200mA/cm^2 for voltages of 0.8-0.9V. The electrodes with platinum catalyst make it possible for the cell to operate at higher current densities up to 0.4-0.8A/cm^2.

Oxygen reduction kinetics is more rapid in alkaline electrolytes than in acid electrolytes. The alkaline fuel cell is the simplest Grove's fuel cell and actually a low temperature fuel cell in concept and operation and is shown schematically in Fig. 1.1 and 1.2 two types of the construction have been developed and used for oxygen hydrogen cells with alkaline electrolyte, namely, one with free (circulating) electrolyte solution and

other with matrix electrolyte. In matrix electrolyte, the electrolyte is held in 0.2-0.6mm sheets of asbestos or synthetic fibers (of potassium titanate) [49,50].

When exposed to CO_2, the life of the alkaline fuel cell is reduced since alkali reacts with carbon dioxide to form carbonate which blocks electrolyte pathways:

$$CO_2 + 2OH^- \longrightarrow CO_3^{2-} + H_2O \qquad 1.18$$

This difficulty can be overcome if pure hydrogen is used as a fuel. And scrubbers are used for removing the CO_2.

1.2.6.1 COMMERCIALLY AVAILABLE ALKALINE FUEL CELLS

Various multinational companies have been marketing alkaline fuel cells [51,52].

(1) The unit commercialized by Union Carbide Batteries (USA) has catalytically active layers of the electrodes which consist of activated carbon with the addition of oxide catalyst (spinels) for the oxygen electrode and small amount of platinum (less than $1mg/cm^2$) for the hydrogen electrode. The current densities observed are 50 and $100mA/cm^2$ for operation with aerial oxygen and pure oxygen and voltage observed is 0.80-0.85V. At the beginning of the seventies, Union Carbide ceased research development work in the field of fuel cells.

(2) The Allis Chalmers Batteries (USA) unit has a single cell consisting asbestos matrix impregnated with 30% KOH solution on both sides, on which highly porous (85%) nickel plates coated with platinum-silver catalyst are pressed.

(3) Pratt and Whitney Battery (USA) acquired the patent rights to the medium temperature Bacon cell in 1959 and begun further development. In 1962, work was

started on the development of the power source for the Apollo spacecraft. The cells employed had two layer nickel electrodes with platinum catalysts. The electrolyte used was potassium hydroxide solution, which is solid crystal hydrate at room temperature and melts at 423K.

(4) VARTA (West Germany) developed fuel cell with bilaterally operating gas diffusion electrodes.

(5) The Elenco fuel cell system has a circulating 6.6 N aqueous KOH electrolyte, which is also used as a coolant. The anodes and cathodes are multilayer gas diffusion electrodes. They consist of a PTFE powder carbon catalyst mixture, which is rolled extensively to cross link the PTFE.

(6) India and Sweden were involved in joint development of bio-fuels power plant AFC generator.

(7) Bipolar AFC concept was developed by the Technical University of Graz in 1985, where low cost PTFE bonded carbon fuel cells were operated with air and hydrogen.

1.2.6.2 OXYGEN REDUCTION IN ALKALINE FUEL CELL

The commonly used oxidant in alkaline fuel cell is oxygen or air. Since oxygen is cheaper and easily available, it is preferred over other oxidants. If ambient air is used as an oxidant then the cost of the fuel cell is reduced. Moreover, eliminating the use of storage tanks, it reduces the weight and volume of the cell. In alkaline fuel cell the reduction reaction occurs at cathode in the presence of oxygen. Whether oxygen is reduced by two e^- process to peroxide or by four e^- process to water, the reduction

depends on the catalyst used and not on the electrode substrate. The substrate should be electronically conductive. With the help of simple methods, such as chemical or electrochemical methods [53], it is possible to pinpoint the peroxide formation in the intermediate.

Depending on the electrolyte used in fuel cell, the ORR occurring in the cell is represented as follows.

In acid, $O_2 + 4H^+ + 4e^- \longrightarrow 2H_2O$ $\Delta E^\circ = +1.229V$ 1.19

In base, $O_2 + 2H_2O + 4e^- \longrightarrow 4OH^-$ $\Delta E^\circ = +0.401V$ 1.20

Due to the complexities and difficulties associated in the formation and breaking of the O=O bond in oxygen, almost all catalysts show very poor electrocatalytic activity in oxygen reduction reaction.

1. In acid and alkali solutions most of the metals and alloys have instability problem in the region where reaction occurs.

2. Reaction rates are slow (i_o of the order of 10^{-10} mA/cm^{-2}) with respect to other electrode reactions.

3. The formation of the oxide on the electrode blocks the progress of the ORR.

4. Also, the formation of H_2O_2 as an intermediate slows down the reaction.

Oxygen reduction reaction has been assumed to proceed by the following pathways [54,55].

DIRECT 4-ELECTRON PATHWAY

(a) In alkaline solution,

$O_2 + 2H_2O + 4e^- \longrightarrow 4OH^-$ $E = 0.401V$ 1.21

(b) In acid solution,

$$O_2 + 4H^+ + 4e^- \longrightarrow 2H_2O \qquad E = 1.229V \qquad 1.22$$

PEROXIDE PATHWAY

(a) In alkaline solution,

$$O_2 + H_2O + 2e^- \longrightarrow HO_2^- + OH^- \qquad E = -0.065V \qquad 1.23$$

Further followed by either the reduction reaction,

$$HO_2^- + H_2O + 2e^- \longrightarrow 3OH^- \qquad E = +0.867V \qquad 1.24$$

Or the decomposition reaction

$$2HO_2^- \longrightarrow O_2 + 2OH^- \qquad 1.25$$

(b) In acid solutions

$$O_2 + 2H^+ + 2e^- \longrightarrow H_2O_2 \qquad E = 0.67V \qquad 1.26$$

Followed by, either

$$H_2O_2 + 2H^+ + 2e^- \longrightarrow 2H_2O \qquad E = 1.77V \qquad 1.28$$

Or,

$$2H_2O_2 \longrightarrow 2H_2O + O_2 \qquad 1.29$$

(The potentials correspond to the standard state values vs. the Normal Hydrogen Electrode (NHE) at 298K.)

All the electrocatalysts do not support the peroxide pathway. In fact, some of them facilitate the 4-electron pathway. Some electrode surfaces are capable of breaking the O=O bond in molecular dioxygen in reaction sequence by 4 electron pathway.

Platinum in the form of Pt/C electrodes, with platinum loading as low as few mg/cm^1, remains the most practicable electrocatalyst in alkaline fuel cell [56]. Lot of

work has been reported [57,67] in recent times for metal oxide catalysts and transition macrocycles (e.g. Fe or Co phthalocyanines and porphyrins [68,70].

The following parallel series represents the path for the electroreduction of molecular oxygen.

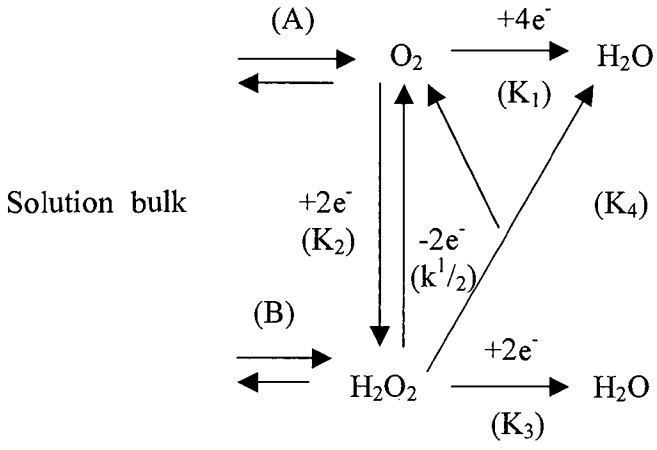

The scheme was proposed for metal electrodes [71], which can also be applied to metal oxide. According to this scheme, the electrochemical reaction, occurring either by H_2O_2 or 4 e^- pathway, depends on how the O=O bond is adsorbed, whether by splitting before adsorption or absorbed without splitting, in such case the electrochemical reduction of oxygen yield water directly (with a rate constant k_1) or hydrogen peroxide (with rate constant k_2). The hydrogen peroxide formed in the process will get reduced either to water (k_3), or may be oxidized ($k_{1/2}$), or may undergo catalytic decomposition on the surface (k_4) or may be released in the bulk of the solution.

There had been two viewpoints on the path of the electro-reduction of oxygen on oxide catalysts. According to some workers [72,73] it is said that the oxygen reduction occurs only via intermediate formation of H_2O_2, and further, the decomposition of the

H_2O_2 is accelerated. Another viewpoint is that the electroreduction may occur on metal oxide directly by 4-e pathway to water [74].

The ring electrode method has confirmed the formation of H_2O_2 as an intermediate on simple oxides for the electro-reduction of oxygen [75,76]. Whereas, on spinel type oxides, the electro-reduction of oxygen occurs either by the formation of H_2O_2 or a parallel reaction of direct reduction to water. The cobaltite spinels deposited on carbon black shows the presence of only one oxygen reduction current plateau corresponding to the addition of the four e^- as shown in Fig. 1.4.

For electro-reduction of molecular oxygen, the rate constants for different steps occurring in the proposed reaction scheme are shown in Table 1.1. Since the O-O bond breaks in both the cases, certain relationship is observed for the fractions of reaction of reduction to water and the rate constant of reduction of hydrogen peroxide to water. Similar results are observed for the spinel synthesized by thermal oxidation of cobalt or cobalt alloyed with nickel [77,79].

It is found that in the potential range 0.8-0.9 V, the H_2O_2 formed is 15% of the total process with Co_3O_4, and is found to be 10% with $NiCo_2O_4$ electrocatalyst. If the potential is shifted in negative direction than the H_2O_2 formation increases to 30-40% at E_r = 0.5V for Co_3O_4, and 50-60% at E_r = 0.3V for $NiCo_2O_4$.The electrochemical activity for different spinels studied under similar conditions have been in the following order

$$MnCo_2O_4 > MgCo_2O_4 > CdCo_2O_4 > CoCo_2O_4$$

This order differs for the activity of homomolecular oxygen exchange and is given in the following manner

$$CoCo_2O_4 > ZnCo_2O_4 > NiCo_2O_4 > MgCo_2O_4 > MnCo_2O_4$$

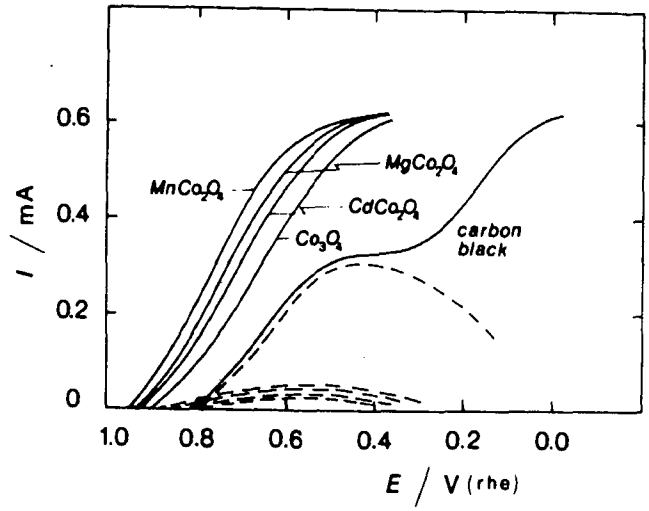

Fig. 1.4 Polarisation curves of oxygen reduction on carbon black promoted by various spinel oxide in 0.1 mol dm^{-3} KOH.

Table 1.1 Kinetic Parameters of Electroreduction of Oxygen on various Cobaltites

Spinel	k_1/k_2	$10^3 \times k_3$/cm s^{-1}
Co_3O_4	4.0	0.20
$CdCo_2O_4$	5.2	0.55
$Mg\ Co_2O_4$	5.9	0.75
$Mn\ Co_2O_4$	7.0	0.96
$Ni\ Co_2O_4$	10.0	----

The influence of the surface states of Co_3O_4 and $NiCo_2O_4$ on the cathodic reduction of oxygen has been studied. The electrodes in this were subjected to electrochemical oxidation at E_r = 1.2-1.6 V [77,78], or to reduction at 0.0V. It is reported that the electrochemical oxidation did not have any influence on the electrode reaction of spinels but the reduction at 0.0V changed the reaction route. Further, it resulted in a sharp reduction in fraction of direct reduction to water and in a concurrent increase in the rate of further conversion of H_2O_2. These changes are ascribed to the decomposition of spinel catalyst to simple oxides like NiO, CoO, Co_2O_3.

In order to explain the mechanism of oxygen reduction reaction, wherein the nature of adsorption is the criterion, the reaction mechanism depends on how reacting molecule is adsorbed i.e. whether in the end or in the side position, since oxygen is paramagnetic in nature, contains two unpaired electrons. If the O-O bond is broken then the two electrons will get adsorbed on two adsorption centers on the side position [79]. Some authors believe that the adsorption of molecules occur in the end position with the formation of sigma bond between the π^*-orbital of the metal and e_g orbital of oxygen.

Oxygen reduction reaction proceeds by peroxide pathway on most of the carbon substrate, and the resulting electrode potential to be equivalent to 2 e^-. Ring disk electrode (RRDE) studies on platinum and platinum alloys show that oxygen reduction of these materials precedes via 4 e^- and peroxide, with 4-electron being predominant. Oxygen reduction kinetics is higher in alkaline electrolyte than in acid medium. Different oxides with spinel, perovskite and pyrochlore structure show high catalytic activity for oxygen reduction [80]. Activated carbon itself is a good electrocatalyst for oxygen reduction reaction in alkaline media. Various kinds of carbon have been studied as

oxygen reducing electrode. Coconut shell carbon is found to reduce dioxygen to water without peroxide formation [81].

The electrochemical reduction of oxygen at thin platinum film prepared on titanium substrate has been studied in alkaline solution. The Tafel plots with two different slope region were observed for oxygen reduction in 0.1M KOH. At low current densities the slope is around –60mV/dec, whereas at higher current densities the slope was varying between –260 - 490mv/dec [82].

In alkaline solution, the gas activated carbon acts as a catalyst for oxygen reduction reaction and it is found that there is no formation of H_2O_2 as an intermediate [83].

Lanthanum manganates [84] were used to correlate the solid-state physicochemical character and the heterogeneous electrocatalytic activity for oxygen reduction reaction in alkaline fuel cell and both bulk and surface properties were evaluated.

The oxygen reduction reaction was studied for cobalt/iron tetraphenyl porphyrin or silver on carbon and the electrodes showed the potential of –186mV vs. Hg/HgO at $1Acm^{-2}$ at $40^{o}C$ for 5 M KOH [85].

The electrocatalytic activity of NiO doped with different % of lithium [86] has been studied. It is reported [87] that surface state of carbon plays an important role in determining the catalytic activity of oxygen reduction reaction.

Electrodes made from $LaNiO_3$ have been tried as an oxygen electrode [88] and it is found that these electrodes can withstand load current density of $30mAcm^{-2}$ with a

polarization of < 0.2V. MnO_2. Manganese oxyhydroxide has been synthesised [89] and for its electrocatalysis on ORR.

Some transition metal oxides such as $LaTiO_3$, $SrFeO_3$, $SrVO_3$, $SrRuO_2$, $V_{0.2}Ti_{1.8}O_3$, and $La_{1-x}Sr_xMO_3$ having metallic conductivity were investigated for their catalytic activities. The conclusion drawn from the study is it must have sigma σ band and band must contain electrons [90].

Several authors have reported methods of preparation of spinel (metal oxides) and electrodes. Lot of work has been reported for oxygen evolution reaction in alkaline solution for spinels like $NiCo_2O_4$ and Co_3O_4 [91]. But not much work has been reported for Co_3O_4 in oxygen reduction reaction in alkaline solution. It is reported that oxygen reduction with spinels and mixed metal oxides as electrocatalysts, decrease with time and this is proved for Co_3O_4 spinels in 1-1.2 M KOH [92]. And it is found that the decrease in catalytic activity is due to the changes in crystal structure of the surface layer of the electrodes. Inspite of several attempts to develop a suitable catalyst, platinum dispersed on carbon with platinum loading of $0.5mg/cm^2$ remains to be the most practical catalyst [93].

1.2.6.3 DIFFERENT COMPONENTS IN ALKALINE FUEL CELL

Electrodes, electrolyte, electrocatalyst are the important components in Alkaline Fuel Cell.

1.2.6.3.1 ELECTRODES IN AFCs

In fuel cells, electrodes are the active centers for the energy conversion reaction i.e. for fuel, the oxidation occurring at the anode and for oxygen reduction occurring at the cathode. The important criterion which should be satisfied by the electrodes is that it should be porous and should have higher surface area, since the reaction involves gases. The main function of the porous gas diffusion electrode is to give a large reaction zone area and provide very small amount of mass transport hindrance for the reactants and also for the removal of products. Increasing electrode area increases the electrode potential and the current density per unit area. Thus affecting the cell performance [94].

Adding fillers to the electrode can enhance the porosity of the electrodes. The surface of electrodes can be said to be hydrophobic or hydrophilic based on the basic structure and added binder [95]. Hydrophobic carbon electrodes are made from the carbon powder bonded with plastic materials such as poly tetrafluoro ethylene (PTFE). Carbon powder used as a support is light and has higher surface area. Electrode comprises of three-layer design as baking layer, gas diffusion layer and the active layer. The backing layer is wire screen, which is a good conductor and is used as a current collector; the backing layer should be highly permeable to gases, and in addition, it should be corrosion resistant, and highly conducting. The different materials, which are used as a backing layer, are metal screen, teflonized metal plaques, carbon cloth and carbon paper [96]. The diffusion layer is highly hydrophobic and contains gas feed channels, which supply reactants. Due to the hydrophobic nature of the diffusion layer, the electrolyte is prevented from penetrating deeper inside the electrode, thus keeping the pores free and allowing the free passage of gas to the reaction sites. The active layer is

less wet proofed than the diffusion layer (5-25%), thus ensuring the partially wetting of the carbon and electrocatalyst. In the catalyst layer three-phase zone is created where fuel, electrolyte and carbon supported electrocatalyst meet and the electrochemical reaction occurs at this interface where the active catalyst is present. The successful operation of a fuel cell needs a proper gas/electrolyte/solid three-phase interphase. The diffusion electrode with three-phase zone is shown in Fig.1.5. The following materials are used in the electrode preparation.

(a) *POLYTETRAFLUORO ETHYLENE (PTFE)*

It is a hydrophobic and chemically stables plastic material, which can be used as a binder for different types of carbon, to create a porous electrode structure [97]. In 1955, Du Pont de Nemours made PTFE commercially available under the trademark "TEFLON." Its use as a hydrophobic binder was first patented in 1960 for use in high temperature cells employing molten alkaline electrolyte. Electrodes can be made from two types of PTFE: as an aqueous suspension or a dry powder.

(b) CARBON MATERIALS

Variety of different carbons can be used in gas diffusion electrodes. These are Graphite, Carbon black, Acetylene black, Vulcan XC-72R, and Black Pearls 2000. Methods for comparing electrochemically active areas of different carbon powders have been developed [98].

The different criteria which should be satisfied by a reaction layer are: (a) feeding gas reactant to all catalyst sites to and from the current collector and (b) holding the electrolyte in reaction layer where active catalyst sites are present. The reactant gas dissolves at gas – liquid interfaces and these dissolved reactants are transferred to the

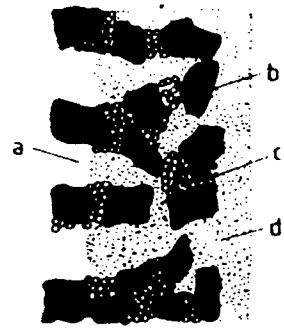

Fig. 1.5 Hydrophobic gas diffusion electrode. a) gas; b) carbon particle; c)wet proofing agent and d) electrolyte.

catalyst site and are reacted by diffusion [99]. The most popular catalyst support used in phosphoric acid fuel cell is Cabot Corporation's Vulcan XC-72R. This material is a conductive furnace black, and has very high conductivity and high specific surface area $250m^2/g$. The gas diffusion electrodes, prepared by using different electrocatalyst, can be characterized by using techniques, which helps to determine the relationship between the structural parameters and electrochemical performance [100]. The different techniques used are intrusion porosimetry, surface area analysis, scanning (SEM) and transmission (TEM) electron microscopy in conjuction with X-ray energy spectroscopy (XES). It is reported [101] that the surface area of support, which was used as graphite in preparation of electrodes, could be varied by grinding in a ball mill for varied grinding time. The influence of diffusion resistances on gas diffusion electrodes has been studied [102].

1.2.6.3.2 ELECTROLYTE IN ALKALINE FUEL CELL

The electrolyte used in fuel cell should have high specific conductivity, as it helps lowering the ohmic drop in solution between cathode and anode. The ionic current that is observed in the electrochemical reaction is due to the transport of the ions. The transference number close to unity helps to lower the polarization due to concentration changes of these ions.

Solutions of strong alkalis like potassium hydroxide or sodium hydroxides can be used as electrolyte in room temperature alkaline fuel cell. Potassium hydroxide is preferred over sodium hydroxide because its conductivity and carbonate ion solubility are higher. The conduction in these electrolytes is due to OH^- ions. Concentrated solution of potassium hydroxide allows operating temperature above the boiling point of water. And it has been used up to 300^oC. Special modifications are to be made in the designing of the

cell to remove the reaction products, which are capable of diluting the electrolyte, especially the formation of water in the hydrogen- oxygen fuel cell, which dilutes the electrolyte. In many aqueous alkaline fuel cell systems with non circulating electrolyte, or with a circulating electrolyte, a matrix or a diaphragm is inserted in the electrolyte to separate anode from cathode [103]. The diaphragm is mostly made from chrysolite and matrices are made from potassium titanate.

1.2.6.3.3 ELECTROCATALYST IN ALKALINE FUEL CELL

Electrocatalysis in fuel cell can be defined as the heterogeneous catalysis of a charge transfer reaction across an electrode-electrolyte interface. Catalyst helps in increasing the rate of reaction by decreasing the activation energy barrier by making available an alternate reaction path. Based on Tafel equation the activation energy barrier can be lowered, by increasing the electric field strength across electrode-electrolyte interface and it is possible to increase the reaction rate in the forward direction by more than an order of magnitude by changing electric potential difference by 100mV.

For a material, to be a good fuel cell electrocatalyst, it should satisfy the following conditions.

* It should possess electronic conductivity. The electocatalyst on its support should be an electronic conductor. If the electrocatalyst is poor conductor or a semi-conductor it must be supported on or dispersed within a conducting materials such as carbon or graphite.

* It should not degrade in the fuel cell environment, especially under the difficult conditions at cathode, and should show suitable adsorption characteristics for

reactants and or reaction intermediate [104]. Surface of an electrocatalyst must be active for chemisorption compared to surface of simple oxide on an inert electrode.

1.2.6.4 CONSTRUCTION OF AN ALKALINE FUEL CELL

The following five basic needs are to be satisfied for successful construction of the fuel cell, which can be competitive power source in the market.

(a) Losses due to polarization and internal resistance should be small.

(b) Electrodes should be resistant to corrosion.

(c) The electrolyte should be invariant.

(d) Electrocatalyst used in the fuel cell should not be costly.

(e) Fuels used in fuel cell should be cheap.

The hydrogen-oxygen fuel cell with an aqueous electrolyte and the electrocatalyst such as platinum metals (Pt, Ir, Rh, Pd, Ru) or binary alloys [105] of platinum metals or restricted number of binary alloys of platinum metal with another metal, fulfill the conditions (a) and (b). But the price of a fuel cell with these electrocatalyst is high. Hence the applications of the fuel cells are restricted only to special projects where high price of fuel cell batteries with good reliability is required. In alkaline electrolytes, nickel can be considered to be the catalyst for anode and lithiated nickel oxide or silver for oxygen electrode. Efficiency, comparable to that in acid cells, with platinum has been achieved. Hence, it is expected that the alkaline fuel cell will find numerous applications as soon as the problem of hydrogen as fuel is solved. Electrochemical characterization has been reported by using various [106,108] types of half-cell assemblies. The different types of setup used are: (a) electrochemical cell used by Kannan, (b) electrochemical set up used by Kiros and Kroenberg, and (c) floating half cell used by Fielder.

1.3 CATALYTIC ACTIVITY

Since oxygen reduction reaction is said to proceed by a peroxide pathway, a good electrocatalyst should be available, which is capable of decomposing the peroxide formed in oxygen reduction reaction. The catalytic activity of catalyst can be evaluated by studying the decomposition of H_2O_2, wherein the volume of oxygen liberated is monitored as a function of time from which catalytic activity of the electrocatalyst is determined. Activation energy is calculated from the obtained data by using Arrehenius equation.

Catalytic activity of a catalyst can be studied by using a conventional gasometric technique. The apparatus used for experimental study of the decomposition reaction was suggested by Cota et al [109].

Various transition metal oxides have been studied for the kinetics and mechanistic study of oxygen reduction reaction. These experiments have confirmed the formation of peroxide, which is decomposed heterogeneously on the catalyst surface, and the reaction is found to be first order [110]. A number of methods are used to study the decomposition of H_2O_2 such as gasometric, open circuit potential decay method, steady state polarization method, etc. Gasometric method has been used commonly by many workers. Catalytic decomposition on co-precipitated Mn ferrospinels has been studied [111] to define the composition and microstructural factors influencing the catalytic activity. Promotion of catalytic activity of MnO_2 by decomposition of H_2O_2 has been reported [112]. It is found that lot of work has been reported for decomposition of H_2O_2 for MnO_2 samples. Kinetic and decomposition of H_2O_2 for MnO_2 samples are also studied [113] and suggested that the catalytic decomposition rate increases as the particle size decreases

emphasizing the importance of real surface area rather than B.E.T. surface area. Decomposition of concentrated H_2O_2 on silver has been studied [114] as a function of bulk temperature. The catalytic decomposition of MnO_2 of various crystal modification has been studied [115] and found that the order of the reaction is one. Topochemical aspects of the surface reactivity of the cobalt ferrites have been studied by some workers [116]. The intrinsic and microstructural factors influencing the catalytic activity for cobalt ferrites is studied by Goldstein et al [117] by using H_2O_2 decomposition reaction.

The heterogeneous rate constant for peroxide decomposition on the platinum-ruthenium catalyst has been determined by studying the slope of the log i_L vs time where i_L is the diffusion limiting current corresponding to the concentration of the peroxide at a given time [118].

The decomposition of hydrogen peroxide on Co_3O_4 is found to be a first order reaction. But Tseung et al [119] have studied this reaction on Co_3O_4 and have reported the order of the reaction to be 1.2 and not one [120].

1.4 ELECTOCATALYTIC ACTIVITY

It is very important that the activity of a newly prepared catalyst be assessed before its use in any electrochemical application. This is usually done by evaluating polarization curve (electrode polarization vs. logarithm of the current density to give a tafel plot) for the oxygen reduction reaction. Many reports are available on the reduction of oxygen on platinum in alkaline media [121]. Electrochemical irreversibility of the oxygen reduction reaction for conventional catalyst can be attributed to their inability to absorb oxygen in a single dissociative step. Single dissociative step involves the presence

of two electrons [122]. The common feature of many of the best electrocatalyst in alkaline electrolyte has been the presence of high paramagnetic susceptibility, which can be related to the presence of unpaired d-bands electrons per atom in noble metals.

L. Genes [123] studied the effect of the particle size on the catalytic activity for oxygen reduction reaction in alkaline solution. For effective oxygen reduction reaction to occur the paramagnetic electrons in the oxygen molecules should couple with those in the electrocatalyst to facilitate side on adsorption [124, 126]. When oxygen molecules absorb in this manner, the O-O bond will split on a surface with neighboring OH and -O groups via mechanism involving a chain of hydrogen bond. This is called pseudo-splitting mechanism suggested by U. R. Evans [127]. Although the oxygen reduction reaction on noble metals catalyst, such as platinum, usually occurs on the bare metal surface but it can also take place on an oxide-covered surface [128]. Of the various perovskites oxides investigated as oxygen reduction catalyst, strontium–doped lanthanum cobaltite, such as $La_{0.5}Sr_{0.5}CoO_3$ and $LaNiO_3$ have shown that on this material, oxygen reduces completely to hydroxyl with no peroxide formation [129]. Studies of oxygen reduction on $Nd_{0.5}Sr_{0.5}CoO_3$ in 45% KOH indicate that rate determining step of the reduction reaction is the absorption of oxygen [130].

In addition to the above mixed oxides, $BaFe_{1-x}Co_xO_{3-x}$ also has been reported to be useful as an oxygen reduction catalyst in alkaline fuel cell. For ferrites, such as $La_{1-x}FeO_{3-y}$, it has been found that the catalytic activity for oxygen reduction reaction in alkaline media is related to the fraction of vacancies and that the ferrites themselves undergo reduction concurrently with the reduction of oxygen [131]. The low temperature performance of perovskites for oxygen reduction reaction, for catalyst such as strontium

doped lanthanum cobaltite, is far lower than that obtained for platinum catalysts. At temperature above 170°C their performance start approaching that of platinum.

In addition to the perovskites another group of metal oxides namely the spinels has shown some promise as oxygen reduction catalysts in alkaline solution. As observed for perovskites, the crystals having spinel structure also show special conductivity and magnetic characteristic that helps in enhancing the activity of spinels in oxygen reduction reaction. Some of the cobalt, magnesium, iron, copper and aluminium spinels have been evaluated for the catalytic activity for oxygen reduction electrodes in concentrated KOH solution [132]. $NiCo_2O_4$ is stable in 5M KOH at potentials greater than 0.7V, but at 0.5V the spinel structure is completely destroyed by forming compounds such as Co_2O_3, NiO, CoO, $CoO.H_2O$, and NiOOH, none of which is active for oxygen reduction reaction [133]. It is observed that the electrochemical reduction of oxygen on cobalt, magnesium, cerium, and manganese cobaltite spinels in KOH solution proceeds by the intermediate formation of peroxide, before four-electron reduction to water [134]. The properties of the spinel type oxides have been elaborately reviewed by some workers [135]. The role of conductive transition metal oxides in the oxygen reduction reaction is studied by [136].

Studies on $MnCo_{3-x}O_4$ for its electrocatalytic activity have indicated the dependence of the reduction reaction in alkaline media on manganese content [137]. The electrochemical reduction of oxygen on $NixCo_{3-x}$ O_4 using a double channel electrode flow cell (DCEFC) has been reported by [138]. S. K. Tiwari [139] has studied the electrochemical reduction of oxygen in KOH for $LaNiO_3$ electrode, which is prepared through maleic acid precursor route, and has found the apparent electrocatalytic activity

of these electrodes to be 10 times higher than those reported for same electrodes obtained from other methods.

1.5 COBALT OXIDE SPINEL AS AN ELECTROCATALYST

The spinel comprises the class of hard, variously colored minerals consisting chiefly of mixed oxides of metals such as aluminium, magnesium, zinc and iron. Some translucent varieties such as the so-called ruby spinel are used as gemstones. Spinels can be classified as normal, inverse, and intermediate, depending on the A and B ions in the 8a and 16d positions. The formula for the typical spinel can be represented as XY_2O_4 (where X and Y are metals). The spinel unit lattice contains 8 XY_2O_4 units arranged in a fairly complex configuration in which the oxygen ions form face centered cubic structures containing tetragonal oxygen cages that are partly occupied by the metals X and Y. The crystalline lattice of the spinels is shown in Fig. 1.6. It has close packing of the O_2^- anions, 64 tetrahedral and 32 octahedral vacant lattice sites forming a unit cell. The bivalent and trivalent cations occupy eight tetrahedral positions 8a and 16 octahedral positions (16d), which are located in vacant lattice sites. The normal spinel–type compounds can be classified by their ionic packing factor defined as the ratio between the cation radius to the anion interstitial radius. The electronic conductivity and magnetic ordering of the spinel can be correlated with these parameters.

Examples of the normal spinels are $MgAl_2O_4$, Fe Al_2O_4, $CoAl_2O_4$, ZnV_2O_4 [140] Co_3O_4 [141]. Another type of spinel structure is the inverse spinel. This can be represented by the formula $X(YX)O_4$, in which the X position in the normal spinel are occupied by half the Y's of the inverse structure, with the remainder of the Y's and all

the X of the inverse structure occupying the Y position in the normal structure. Examples of the inverse spinel are $Fe^{III}(Fe^{II}Fe^{III})O_4$, $Fe^{II}(TiFe^{II})O_4$, $Cr(Fe^{II}Cr)O_4$ and $Zn(SnZn)O_4$.

Mixed valency spinel oxide exhibit electrical conductivity or semi conductivity, which helps them to be used directly as electrode material with electronic transfers taking place with very low activation energy between the cation of different valences by hopping process. If spinels have poor electrical conductivity, then they have to be mixed with high surface area carbon or graphite to increase the electrode conductivity. Spinel exhibit very low specific surface areas when synthesized by ceramic method at high temperature. They may achieve high surface areas when prepared at low temperatures, by using thermal decomposition of suitable precursors, reactive nebulization (spraying), freeze drying, or sol-gel type processes. The added advantage offered by spinel when prepared from aqueous solution at lower temperature is that they are more likely to retain the H_2O molecules and OH groups in the structure. Hence it is necessary to control this bulk and surface cationic properties, determining the electronic factor and real surface area which determines the geometric factor, which is necessary to get better intrinsic electrocatalytic activity.

1.5.1 COBALT OXIDE SPINEL

A typical unit cell for an ideal spinel structure [142] is shown in Fig 1.6(a). In this ideal cubic structure, the anions form cubic close packing in which the cations occupy partly the tetrahedral and partly octahedral voids. The unit cell contains 32 anions forming 64 tetrahedral and 32 octahedral interstices are taken by cations. Thus the unit

cell contains 8 formula units. The unit cell with perfect cubic close packing array corresponds to the formula $X_8Y_{16}O_{32}$. In the normal spinel structure the 8X ions occupy tetrahedral sites in the face centered cubic oxide lattice and the 16Y ions occupy octahedral site as indicated in Fig. 1.6(b) the tetrahedral and octahedral sites are generally referred to X and Y sites respectively. The spinel structure is fairly empty because only $^1/_8$ have the tetrahedral and ½ of the octahedral sites are occupied.

The spinel possesses interesting electrical properties ranging from insulators to metallic conductors. Due to ordering and orientation of the spin in the lattices spinal exhibit interesting variation in their magnetic properties. This kind of ordering of spin results in antiferromagnetic, ferromagnetic and ferrimagnetic spinels.

Cobalt oxide spinel is expected to be a normal spinel ($Co^{2+}[Co^{2+}Co^{3+}]O_4$ because (low spin) Co^{3+} gains more stabilization energy in octahedral site that Co^{2+} losses by going into the tetrahedral site[143]. It is said that Co_3O_4 and $NiCo_2O_4$ can be intrinsically semiconductors but the low temperature of decomposition and the hydrothermal condition of the spraying process produces heavily doped very conductive samples [144].

1.5.2 SYNTHESIS OF Co_3O_4 SPINEL

Several methods are known for the preparation of spinels, but the common procedure used is the ceramic technique [145]. In this method, the oxides of metals are used as the starting compounds. In order to homogenize the oxide mixtures and thereby promote the diffusions of ions during the spinel formation process, the initial compounds are pulverized and then subjected to prolong high temperature calcinations at 1273-1473K. Due to high temperature calcinations the surface area of the specimen is

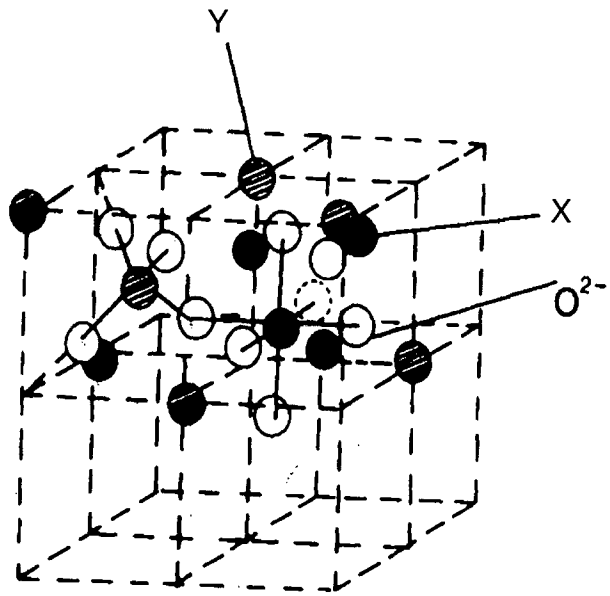

Fig. 1.6(a) Crystalline lattice of spinel

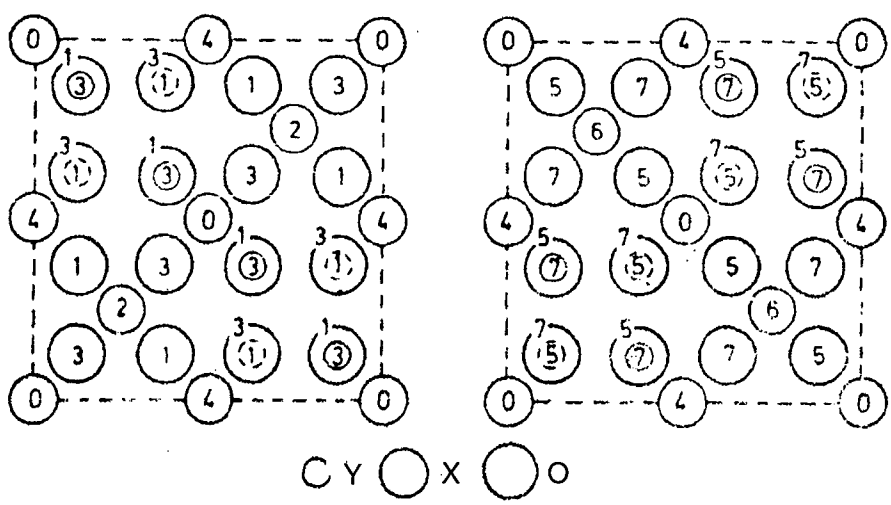

Fig. 1.6(b) crystalline lattice of XY_2O_4

considerably reduced, and consequently it is difficult and in certain cases altogether impossible to use them as catalysts.

The second method [146] consists in evaporating the solutions of nitrates of the corresponding metals and then decomposing the mixture thus obtained. In this method the calcinations temperature can be reduced to 573-673K.

The third method lies in the co-precipitation of hydroxides, oxalates of the corresponding metals followed by thermal decomposition of the precipitates. The main merit of this method is that the hydroxide or salts are mixed homogeneously in the coarse of precipitation. In this method the Co_3O_4 catalyst is prepared by precipitating $Co(OH)_2$ from mixed solution of $CoCl_2.H_2O$ and KOH then sintered at 573K for 5hrs [147].

Above two methods can be used [148] for preparing deposited catalyst, $NiCo_2O_4$, $MnCo_2O_4$ on carbon support.

Cryochemical synthesis of Ni-Co spinels [149] consists of spraying aqueous salt solution in liquid nitrogen evacuation and final decomposition in air or oxygen, which leads to a uniform mixture of the components.

Since the spinels are used in electrocatalysis, methods have been developed to synthesize them on carriers, on highly dispersed materials. Investigation of the formation of the spinel type oxides on carbon [150], graphite, carbon black has shown that this process is complicated. It depends both on the oxide to carrier ratio and to thermal synthesis condition. The main obstacle in the preparation of the deposited catalysts is that the carbon carrier exerts considerable influence on the oxide composition [151] in the course of thermal treatment, which in turn affects the combustion of the carrier. Specimens were found to burn during thermal synthesis of cobaltite on various carbon

supports in air at spinel formation temperature, i.e. 623-773K. When spinels are supported onto carbon materials, their specific surface area increases and electric resistance decreases. The surface of the cobaltite deposited on carbon black was found to increase from $14m^2g^{-1}$ to about $150m^2g^{-1}$ [152], while electric resistance decreased by about 10^4-10^5 times.

Several methods have been reported in the literature for the synthesis of Co_3O_4.

Co_3O_4 has been prepared [153] by thermal decomposition of cobalt nitrate at 523K for 20 hours [154]. The method used by Tseung et al [155] for preparation of Co_3O_4 involves co-precipitation of hydroxides. The precipitate obtained was filtered and dried at 573K for 5 hours. The Co_3O_4 obtained from this method is used for comparison purpose and they also synthesized Co_3O_4 by oxidizing and precipitating the dissolved Co^{2+} ions in 5NKOH solution using 20 $^{W}/_{o}$ H_2O_2 solution as oxidizing agent [156,157]. The Co_3O_4 is synthesized from hydroxides, obtained at room temperature by precipitation of the corresponding metal nitrates, with ammonia at pH = 9.Then the hydroxides are decomposed in air at 1273 K for 20 hr.[158].

The Co_3O_4 can also be prepared from its nitrate solutions (0.1M) by conventional aqueous precipitation with ammonia water. The pH was kept constant at 10.5, the precipitate was filtered, dried at 373K overnight, ground into fine powder, and air calcined at 773K for 4h. [159].

Thin films of Co_3O_4 on Ti support has been prepared by thermal decomposition [160], and also by spray pyrolysis technique between the temperature range 573-673 K [161].

1.5.3 CHARACTERIZATION AND PROPERTIES OF Co_3O_4

(a) ELECTROPHYSICAL PARAMETERS

The main electrophysical parameters of the oxides semiconducting systems are the electrical conductivity, electron work function, quantity and mobility of current carriers and the forbidden band width. And these parameters are quite sensitive to the chemical and structural composition of the oxide system and hence depend on the method and condition of oxide synthesis. The oxides of the transition element at the beginning of long periods have the n-type semiconductivity and those at the end have p-type semiconductivity. The oxides of CoO, NiO, $NiCo_2O_4$, Co_3O_4 and $MnCo_2O_4$ are p-type semiconductors [162].

The electrochemical and electrophysical characteristic of the large group of different oxides have been reported [163]. This oxide shows high electrical resistance. The electrical conductivity of simple oxides such as MnO, NiO, Co_2O_3 is of the order 10^{-6}–$10^{-4} m^{-1}$. The electrical conductivity of the spinel type cobaltite is somewhat higher. The conductivity of the Co_3O_4 is found to be 10^{-4}ohm cm^{-1} and that of $NiCo_2O_4$ is 10^{-2} ohm cm^{-1}. One method of reducing the electrical resistance is to deposit them on a conducting carrier such as carbon, carbon black, graphite or nickel [164].

On passing from simple oxides to spinel it is found that there is increase in the electrical conductivity, carrier concentration and carrier mobility and the electrochemical activity. The electrical conductivity and carrier concentration is found to change by 2-3 orders of magnitude in passing from oxides to spinel.

(b) CHEMICAL AND ELECTROCHEMICAL PROPERTIES

Chemical and electrochemical stability (change in the surface composition) plays an important role in practical application and in understanding the mechanism of electrochemical reactions occurring in spinel. Spinel type oxides [165] are comparatively stable in alkaline medium.

The chemical stability of the low temperature synthesis of Co_3O_4, the time variation of the structure and the composition of this spinel in KOH solution have been studied [166] with the aid of the operator technique.

The I.R. spectra of the initial (curve I Fig 1.7) have two characteristic absorption at 570-670cm^{-1}, which may be possibly attributed to the vibrations of the $Co^{III}O_6$ and $Co^{II}O_4$ polyhedra [167]. When Co_3O_4 comes in contact with alkaline solution, an absorption band appears in the region 400-500cm^{-1} and the intensities of the bands at 570-670cm^{-1} changes (curve II). This is related with the formation of simple cobalt oxide [168] Co_2O_3 and CoO due to partial decomposition of the spinel in the surface layer.

From this data it follows that the amount of Co_3O_4 spinels in the surface layer of the solid phase decreases with the increasing amount of cobalt ions in the electrolyte. The maximum variation of the catalyst surface composition takes place in the initial period. Thereafter the catalyst undergoes slight changes, and the amount of cobalt, which passes into the solution decreases. Higher electrolyte temperature accelerates the destruction of Co_3O_4; increase alkali concentration also leads to the decrease in the spinel stability.

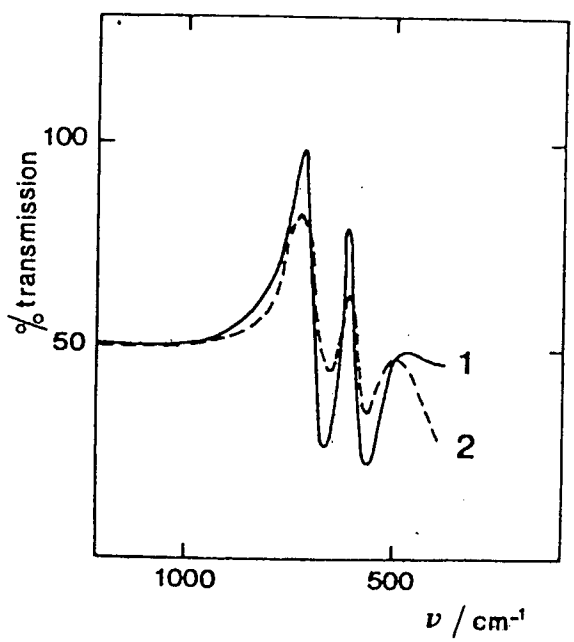

Fig. 1.7 The IR spectra of the initial curve1 and curve 2 of Co_3O_4.

1.6 SCOPE OF THE PRESENT INVESTIGATION

To make it possible to use the fuel cells for the terrestrial applications it is necessary to improve the performance of the air electrode by using non expensive catalyst. Platinum till date finds wide application as the electrocatalyst in fuel cell, lot of efforts are being made to replace the noble metal with metal oxide such as perovskites, spinels, etc. though synthesis of mixed metal ferrites has been exhaustively studied, comparatively not much work has been reported in the use of cobalt oxide spinel in the fuel cell studies.

It was thought interesting to develop a novel precursor method for the synthesis of Co_3O_4 spinel. Such a synthesis, especially involving low temperature decomposition, which could be expected to yield oxide product with better surface area. Further, since there are reports indicating usefulness of Co_3O_4 spinel as electrocatalyst in fuel cell applications, it would be interesting to explore the possible use of these cobalt oxide samples as electrocatalyst in alkaline fuel cell as electrode material.

REFERENCES

1. a) G. D. Rai, *"Non Conventional Energy Sources"*. Khanna Publishers, (3rd edition) Delhi, 1994.

   b) H. S. Randhawa and Bharti, *chem. Edu.,* (1994) p.48.

2. S. P. Sukhatme, *"Solar Energy, Principles of thermal collection and storage.*
3. A. K. Shukla, *"Green cars: An Appraisal"* Eleventh T. Ramachar memorial lecture." I. I. Sc. (Bangalore) July 2000.
4. J. O'. M. Bockris and S. U. M. Khan, "A molecular Approach, "*Surface Electochemistry, A molecular level Approach*". Plenum, New York.(1993)
5. W. R. Grove, *Phil. Mag.*, 21 (1842) 417.
6. W. Ostwalds, *J. Electrochem.,* 1 (1894) 122.
7. F. T. Bacon, "Aspects of H_2-O_2 Fuel cell." Fuel Cell systems –II, Advances in Chem. Series 90, A. C. S. Washington, DC (1969).
8. K. V. Kordesch, *J. Electrochem. Soc.*, 125 (1978) 77C-91C.
9. H. Ewe, E. Justi and A. Schmidt, *Electrochim. Acta,* 19, (1974) 799.
10. A. J. Appleby and A. R. Foulies, *"Fuel Cell Handbook,"* Van Nostrand Reinold, New York (1989) 3-14.
11. H. A. Liebhafsky and E. J. Cairns, "Fuel cell and Fuel batteries, a guide to there *Research and development,*" John Wiley and Sons, New York. (1968).
12. H. R. Kunz, Proc. Of The Workshop on the Electrocatalysis of Fuel cell, May15-17 (1978).
13. J. Van, A. J. McEvoy and K. R. Thampi , *Electrochim. Acta,* 39, (1994) 1675.
14. Krumplet and M. Kumar, *J. Power Sources,* 29 (1990).
15. G. J. K. Acres and G. A. Hards, *Phil. Trans. R. Soc.* London A (1996).
16. K. V. Kordesch and G. R. Simader, *Chem. Rev.,* 95 (1995) 191-207.
17. G. J. K. Acres and G. A. Hards, *Phil. Trans. R. Soc. Lond. A* (1996) 354, 1671

18. A. K. Shukla, K. V. Ramesh and A.M. Kannan, *Proc. of Indian Acad. Sci. (Chem. sci.), Indian Academy of Sciences.* India (1986).

19. M. W. Breiter, "*Electrochemical Processes in Fuel cell*". Springer-Verlag 1969.

20. J. O' M. Bockris and S. U. M. Khan, *A molecular Approach, "Surface* Electrochemistry : Electrochemical conversion and storage of Energy Plenum press, New York p.861-920. (1993)

21. K. Kordesch and G. Simader, "*Fuel cell and their applications*." Federal republic of Germany, 1996.

22. K. Tomantscger, F. Mc clusky, L. Opporto, and L A. Reid *J. Power Sources,* 18 (1986) 317.

23. D. R. De Sena, E. R. Gonzalez, E. A. Ticianlli, *Electrochim. Acta,* 37, (1992) 1855.

24. K. V. Ramesh and A. K. Shukla, *J. Power Sources,* 15 (1985) 201-205.

25. H. R. Kunz, and G. A. Gruver, *J. Electrochem. Soc.*, 122 (1975) 1279.

26. J. Irwin, D. Fagg, J. Labrincha and F. B. Marques, *Cat. Today*, 38 (1997) 467-472.

27. K. V. Ramesh and A. K. Shukla, *J. Power Sources,* 36 (1991) 547-555.

28. A. J. Appleby and S. B. Nicholson, *J. Electroanal. Chem.,* 53 (1974) 105.

29. S. W. Smith, W. M. Vogel and S. Kepelner, *J. Electrochem. Soc.*, 129 (1982) 1668.

30. W. T. Grubbs, *Nature,* 198 (1969).

31. S. Srinivasan, E. A. Ticianlli, C. R. Derouin and A Redondo, *J. Power Sources,* (1988) 359-375

32. E. Ticianelli, C. R. Derouin, S. Srinivasan, , *J. Electroanal. Chem.,* 251 (1988) 275 – 295.

33. K. Prater, *J. Power Sources,* 29 (1990) .

34. K. Prater, *J. Power Sources,* 51 (1994) 129.

35. K. Prater, *J. Power Sources,* 29 (1990) 239.

36. K. Prater, *J. Power Sources,* 37 (1992) 181.

37. A. Aramata, I. Toyoshima, M. Enyo, *Electrochim. Acta,* 37, (1992) 1317.

38. F. Kadirgan, B. Beden, J. M. Leger, C. Lamy, *J. electroanal. Chem.* 142 (1982) 171.

39. S. Swathirajan and Y. M. Mikhail, *J. Electrochem. Soc.*, 138(5) (1991) 1321.

40. A. Hamnett and B. J. Kennedy, *Electrochim. Acta,* 33, (1988) 1613

41. J. B. Goodenough, A. Hamnett, B. J. Kennedy, R. Manoharan, S. A. Weeks, *J. electroanal. Chem.* 240 (1988) 133.

42. J. Appleby, R. K. Sen, "Proc. Of The Workshop on the Electrocatalysis of Fuel *cell",* May15-17 (1978)

43. K. V. Kordesch and G. R. Simader, *Chem. Rev.,* 95 (1995).

44. K Juttner, *Electrochim. Acta,* 29 (1984) 1597-160

45. W. Vielstich, "Proc. Of The Workshop on the Electrocatalysis of Fuel Cell", May15-17 (1978).

46. K. Mund, G. Ritchter and F. Von Sturm, *"Proc. Of The Workshop on the* Electrocatalysis of Fuel cell", May15-17 (1978).

47. J. Giner, *Fuel Cell systems –II,* Advances in Chem. Series 90, A. C. S. Washington, DC (1969).

48. J. Heitaben, W. Vielstich, *Fuel Cell systems –II, Advances in Chem.* Series 90, A.C.S. Washington, DC (1969) 81

49. K. Strasser, *J. of power Sources*, 29 (1990) 149-166.

50. K. Kordesch, S. Jehangir and M. Schautz, *Electrochim. Acta,* 29, (1984), 1859-1596.

51. K. Kordecshand G. Simader, "*Fuel cell and their applications"* p. 55-71.

52. K. V. Kordesch and K. Tomantscger, *" Fuel Cell for Electric Vehicles,"* Electric Vehicle Exposition, Aug 25-29, 1880, Adelaide, Australia.

53. H. R. Kunj and G. A. Gruver, *J. Electrochem., Soc.*, 122 (1975) 1279-1287

54. E. Yeager, *Electrochim. Acta,* 29 (1984) 1527-1537.

55. M. Tarasevich, A. Sudkowshi and E. Yeager, "*Comprehensive treatise of Electrochemistry*" (eds.) B. E. Conway, J, O 'M Bockris, B. Yeager, S. Khan and R. E. White, New York: Plenum Press 7(1983) p. 301.

56. D. Fischer, *J. Appl. Electrochem.,* 14 (1984) 403.

57. P. F. Garcia, R. D.P. E. Bierstedt, F. B. and Fleppen, 1980, *J. Electrochem. Soc.*127, (1974).

58. Y. Matasumara, and E. Sato, *Electrochim. Acta,* 25 (1980) 585

59. R. Manoharan and A. K. Shukla, *Bull. Mater. Sci.,* 6 (1984) 259.

60. R. Manoharan and A. K. Shukla, *Bull. Mater.* Sci., 25 (1985) 585.

61. A. K. Shukla, R. Manoharan, J. B. Goodenough, A. Hamnett,and C. Palitiero, *J. Appl. Electrochem.,* 15 (1985) 774.

62. M. N. Tarasevich, and B. N. Effremov "*Electrodes of Conductive Mettalic Oxides*", Elsevier Scientific. Publishing comp., Amsterdam (1980). P.229.

63. A. M. Kannan, "*Preparation and Characterization of fuel cell electrodes*", Ph. D. Thesis, Indian Institute of Science, Bangalore (1986).

64. A. C. C. Tseung, B. S. Hobbs, *Electrochim. Acta*,17 (1972)1557

65. K. V. Ramesh, , "*Preparation and Characterization of fuel cell electrodes*", Ph. D. Thesis, Indian Institute of Science, Bangalore(1986).

66. Y. Matsumoto, H. Yoneyama and H. Tamura, *J. Electroanal. Chem.,* 83 (1977) 237-243.

67. I. Iliev, S. Ganburzev and A. Kaisheva, *J. Power Sources,* 17 (1986) 345-352

68. Y. Kiros, *J. Electrochem.Soc.*143, (1996) 2152.

69. J. Kivissari, J. Lamminen, M. J. Lampinen and Vitanen, *J. Electrochem. Soc.*, 32(1990) 233-241

70. Y. Kiros, and S. Schwartz, *J. Power Sources,* 36 (1991) 547.

71. V. S. Bagotskii, M. R. Tarasevich and V. Yu. Filinovski, *Electrokhimiya* 15 (1969) 1218.

72. M. Savy, *Electrochim. Acta,* 13 (1968) 1359.

73. K. V. Kordesch, "*Handbook of Fuel cell Technology*," Prentice hall, New Jersey, (1968) 361.

74. A. C. C. Tseung and H. L. Bevan, *J. electroanal. Chem.,* 45 (1973) 429.

75. H. L. Bevan and A. C. C. Tseung, *Electrochim. Acta,*19 (1974) 201.

76. E. I. Kurusheva, O. V. Moravskaya, V. V. Karonik, L. W. Eramia, N. A. Shumilova and V. S. Bagotskii, *Electrokhimiya* 11, (1975) 620.

77. R. K. H. Burshtein, M. R. Tarasevich, A. M. Khutornoi, V. S. Vilinskaya, F. Z. Sabiro, I. I. Estachov and G. L. Teplitskaya, *Electrokhimiya 11*, (1975) 1064.

78. M. R. Tarasevich, V. S. Vilinskaya, A. M. Khutornoi, R. K. H. Burshtein, F. V. Makordi and Yu. A. Tkach, *Electrokhimiya.*

79. N. I. Ryasintseva, E. I. Kurusheva, N. A. Shumilova, A. M. Trunov, *Electrokhimiya 10*, (1974) 822.

80. A. Damjanovic, A. Dey and J.O'M Bockris, *Electrochim. Acta,* 11(1966) 376.

81. R. Manoharan and A. K. Shukla, *J. Power Sources,* 10 (1983) 333.

82. K. Tammeveski, M. Arulepp, T. Tenno, C, Ferrater and J. Claret, *Electrochim. Acta,* 42 (1997) 2961-2967.

83. J. Fournier, G. Faubert, J. Y. Tilquin, T. Cote, D. Guay and J. P. Dodelet, *J. Electrochem. Soc.*144, (1997) 145-154.

84. L. Swette and N. Kackley, *J. Power Sources,* 29 (1990) 423-426.

85. Y. Kiros and S. Schwartz, *J. Power Sources,* 36 (1991) 547-555.

86. Y. Matsumoto, H. Yoneyama and H. Tamura, *J. electroanal. Chem.,* 83 (1977) 237-243

87. R. N. Singh, J. F. Koenig, G. poillerat, P. Chartier, *J. Electrochem.Soc.*137,

(1990) 1408-1415

88. A. M. Kannan, A. K. Shukla and S. Sathyanarayanan, *J. Power Sources,* 25 (1989)
89. I. Arulraj, *Solid State Ionics,* 68 (1994) 41-48.
90. Y. Matsumoto, H. Yoneyama and H. Tamura, *J. electroanal. Chem.,* 83 (1977) 237-243.
91. J. P. Singh and R. N. Singh, *Ind. J. Chem.* 39 A (2000) 819-825.
92. B. N. Effremov, M. R. Tarasevich, G. I. Zakharkin, and S. R. Zhukov, *Electrokhimiya 14*, (1978) 1304.
93. J. Perez, E. R. Gonzalez and E.A. Ticianelli, *Electrochim. Acta,* 44 (1998) 1329-1339.
94. K. Kordecsh and G. Simader, *"Fuel cell and their applications"*. P. 76, 95-88
95. K. Tomantschger and K. V. Kordesch, *J. Power Sources,* 25 (1989) 195-214
96. K. Tomantschger, K. V. Kordesch, F. McClusky, L. Oporto, and A.Reid and K. V. Kordesch, *J. Power Sources,* 18 (1986) 317-335.
97. S. Srinivasan, E. A. Ticianelli, C. R. Deruin and A. Redondo, *J. Power Sources,* 22 (1988) 359-375.
98. I. A. Kukushkina, G. V. Shteinberg, and A. V. Dribinskii, *Electrokhimiya*, 21 (1985) 1384-1387.
99. K. Kordesch, S. Jehangir and M. Schautz, *Electrochim. Acta,* 29 (1984) 1589.
100. K. Tomantschger and K. V. Kordesch, *J. Power Sources,* 25 (1989) 195-214.
101. A. D. S. Tantrum and A.C. C. Tseung, *Nature*, 221 (1969).
102. P. Bjornbom, *J. Electrochem.Soc.*137, (1990) 1408-1415
103. K. Stresser, *J. Power Sources,* 29 (1990) 149-166.
104. K. Kiros and S. Schwartz, *J. Power Sources,* 36 (1991) 547-555
105. K. Ramesh and A. K. Shukla, *J. Power Sources,* 19 (1981) 279-275.
106. R. Manoharan, *"Oxygen reducing carbon electrodes for alkaline fuel cells and*

metal air batteries", Ph. D. Thesis, Indian Institute of Science, Bangalore. (1984)

107. K. Kiros, *J. Power Sources,* 36 (1991) 547-555.
108. W. L. Fielder and J. Singer, Fuel cell
109. H. M. Cota, J. Kalan, M. Chin and F. J. Schoenweis, *Nature* (London) 203,1281 (1964).
110. H. Falcon and R. E. Carbonio, *J. Electroanal. Chem.,* 339 (1992) 69-83.
111. P. Lahiri and S. K. Sengupta, *"Catalysis Modern trends"*, N. M. Gupta, D. K. Chakrabarty, eds. 1995, Narosa Publishing House, New Delhi P. 301-304.
112. M. A. Hasan, M. I. Zaki, L. Pasupulety and K. Kumari, *Appl. Cata.* 181(1999) 171- 179.
113. M. W. Rophael, N. S. Petro and L. B. Khalil, *J. Power Sources,* 22 (1988) 149-161.
114. A. B. Heart & R. A. Ross, *J. Cata.* 2 (1963) 121- 126.
115. S. B. Kanungo, K. M. Parida and B. R. Sant, Electrochim. *Acta,* 26 (1981) 1157-1167.
116. G. Parravanno, *"Proceeding of the IVth International Congress on Catalysis"*, 1968 Moscow, P.149-165.
117. J. R. Goldstein and A. C. C. Tseung, *J. Cata.* 32 (1974) 452-465.
118. R. Venkatachalapathy, G. P. Davila and Jai Prakash, *Electrochem. Comm.*, 1(1999) 614-617.
119. J. R. Goldstein and A. C. C. Tseung, *J. Phys. Chem.,* 76 (1972) 3646.
120. S. Jiang, Z. G. Lin and A.C. C. Tseung, *J. Electrochem.Soc.*137, (1990) 759-764.
121. E. Yeager, *Electrochim. Acta,* 29, (1984), 1527-1537
122. M. R. Tarasevich, *Electrokhimiya* 9, (1973) 599.
123. A. J. Appleby, *"Comprehensive Treatise of electrochemistry,"* Vol. 7, B. E. Conway J. O' M Bockris, S. U. M. Khan and R.E. White, eds., Plenum, New York, (1983) 173.

124. Y. Matsumoto, H. Yoneyama and H. Tamura, *J. electroanal. Chem.,* 83 (1977) 237- 245.

125. R. Goldstein and A. C. C. Tseung, *Nature,* 222 (1969) 869.

126. H. L. Bevan and A. C. C. Tseung, *Electrochim. Acta,* 9 (1974) 201.

127. U. R. Evans, *Electrochim. Acta,* 14, (1969) 197.

128. A. Damjanovic and V. Brusic, Electrochim. *Acta,* 11 (1966) 376.

129. Y. Matsumoto, H. Manabe and E. Sato, *J. Electrochem. Soc.*127, (1980) 811.

130. K. L. K. Yeung and A. C. C. Tseung, *J. Electrochem. Soc.*125, (1978) 878.

131. S. Trassatti, "Electrodes of Conductive Metallic Oxides". (Elsevier Scientific Publishing comp.), Amsterdam, 1980.

132. J. E. Wynn and H. Knapp, *Proc. 24th Power Sources Conf.* 88 (1970).

133. A. C. C. Tseung and K. L. K. Yeung, *J. Electrochem. Soc.*125, (1978)1003-1005.

134. V. S. Vilinsakaya, N. G. Bulavina, V. Ya. Shepelev and R. Kh. Burshtein, *Electrokhimiya* 15 (1979) 932.

135. M. R. Tarasevich, V. S. Bagoskiiand B. N. Effremov, *Stud. Phys. Theor. Chem.*, 11(Electrodes of Conductive Metallic Oxides. Part A), 221 (1980).

136. S. Trassati and G. Lodi, *Stud. Phys. Theor. Chem.*, 11 (Electrodes of Conductive Metallic Oxides. Part A), 221 (1980).

137. E. Rios, J. l. Gautier, G. Poilerat and P. Chartier, *Electrochim. Acta,* 44(1998) 1491- 1497.

138. N. Heller-Ling, M. Prestat, J. –L. Gautier, J. – F. Koenig, G. Poillerat and P. Chartier, *Electrochim. Acta,* 42 (1997) 197- 202.

139. S. K. Tiwari, J. F. Koenig, G. Poilerat, P. Chartier, R. N. Singh, *J. Appl. Electrochem.* 28 (1998) 114-119.

140. Greenwood, "*Inorganic Solids*".

141. W. Rudorff and B. Reuter, *Z. Anorg. Chem.,* 253 (1947) 194.

142. W. L. Roth, *J. Phys. Chem.,* 25 (1964) 1.

143. D. Panayotov, M. Khristova, and D. Mehandjiev, *Appl. Catal.*, 34,49 (1987).

144. C. N. R. Rao, *"Chemical approaches to the synthesis of inorganic materials,"* 1994 Wiley Eastern Ltd, New Delhi.

145. S. Trassatti, "*Electrodes of Conductive Metallic Oxides*". (Elsevier Scintific Publishing comp.), Amsterdam, 1980 p.223.

146. S. Trassatti, "*Electrodes of Conductive Metallic Oxides*". (Elsevier Scintific Publishing comp.), Amsterdam,1980 p.224.

147. S. Trassatti, In: J. Lipkowskii, P.N. Ross, ed. "*Electrochemistry of Novel Materials*" VCH Publishers inc., (1994), pp. 2207-295

148. C. N. R. Rao, *"Chemical approaches to the synthesis of inorganic materials,"* 1994 Wiley Eastern Ltd, New Delhi, p. 14-17

149. S. Jiang, Z. G. Lin and A.C. C. Tseung, *J. Electrochem. Soc.*137, (1990) 759-764.

150. W. J. King and A.C. C. Tseung, Electrochim. *Acta,* 19 (1974) 485-491.

151 K. C. Patil, J. S. Budkuley and V. R. Pai Vernekar, *J. Inorg. Nucl. Chem.*, 41 (1979) 953.

152. K. C. Patil and M. A. Sekar, *International Journal of self-propagating high temperature synthesis*, 2, 3 (1994).

153. R. F. Savinell, R. L. Zeller III, and J. A. Adams, *J. Electrochem. Soc.*137, (1990) 489.

154. A. Restovic, G. Poilerat, P. Chartier, and, *Electrochim. Acta,* 40 (1995) 2669.

155. S. P. jiang, Z.G. Lin, and A.C. C. Tseung, *J. Electrochem. Soc.*137, (1990) 759-764.

156. G. Lin and A. C. C. Tseung, Extended Abstracts, *International Society of Electrochemistry, 35th meeting*, p. 63, Berkeley, C. A. 1984.

157. S. D. Teichner, *Adv. Catalysis*, 20,167 (1969).

158. J. P. Jacobs, A. Maltha, J. G. H. Reintjes, J. Drimal, V. Ponec and H. H.

Brongersma, *J. Of Cata. 147* (1994) 294-300.

159. B. L. Yang, S.F. Chan, W. S. Chang and Y. Z. Chen, *J. Cat.* 130 (1991) 52-61.

160. P. Nkeng, S. Marlier, J. F. Koenig, P. Chartier, G. Poillerat and J-L. Gautier *Electrochim. Acta,* 43 (1998) 893- 898.

161. R. N. Singh, J. F. Koenig, G. Poillerat, and P. Chartier, *J. Electrochem. Soc.*137, (1990) 759-764.

162. A. M. Trunov, V. A. Pressnov, M. V. Uminskii, O. F. Rakityanskaya, T. S. Bakutina and A. N. Kotseruba, *Electrokhimiya*, 11 (1975) 552.

163. D. M. Shub, A. N. Chemodanov and V. V. Shalaginov, *Electrokhimiya* 12 (1976) 595.

164. A. Rolla, A. Sadkowski, J. Wild and P. Zoltowski, *J. Power sources*, 5,(1980)189.

165. A. A. Domnikov, G. L. Reznikov and F. P. Puppets, *Electrokhimiya* 12 (1976) 1868.

166. W. J. King and A.C. C. Tseung, *Electrochim. Acta,* 19 (1974) 485-491.

167. B. N. Efremov, M. R. Tarasevich, G. I. Zakharkin and S. R. Zhukov *Electrokhimiya,* 14 (1978) 1971.

168. T. Kenjo and K. Kawatsu, *Electrochim. Acta,* 30 (1985) 229.

CHAPTER II

CHAPTER II

EXPERIMENTAL

INTRODUCTION

Transition metal oxides, especially the spinel type of oxides, represent an important class of versatile materials for electrocatalysis. They provide a unique opportunity to investigate the contribution of solid state chemistry to electrocatalytical reactivity. The usual method for the preparation of spinel involves ceramic technique in which oxides, hydroxides, nitrates, carbonates, oxalates are used as starting materials. Besides, spinels can also be prepared by combustion method, sol gel method, freeze-drying, spray drying method etc. [1].

In the present study, the precursor method was used in the synthesis of some samples of Co_3O_4 by using different routes. A brief description of the methods of the synthesis of these samples as well as the analytical procedures and the instrumental techniques employed in their characterization is presented in this chapter.

2.1 MATERIALS

The commercially available chemicals (Analar or equivalent grade) were used as such without purification. The chemicals that were used include hydrazine hydrate ($N_2H_4.H_2O$), nitrilotriacetic acid ($N(CH_2COOH)_3$), ammonium carbonate ($(NH_4)_2CO_3$), cobaltous carbonate ($CoCO_3$), cobalt nitrate hexahydrate $Co(NO_3).6H_2O$, cobalt chloride hexahydrate ($CoCl_2.6H_2O$), zinc sulphate heptahydrate ($ZnSO_4.7H_2O$), ethylene diamine

tetracetic acid-disodium salt, (EDTA), hydrochloric acid (HCl), potassium iodate (KIO_3), carbon tetrachloride (CCl_4) etc.

2.2 ANALYTICAL METHODS

The analytical methods used include the quantitative estimation of cobalt in the samples (combustion residues) and precursors, and hydrazine in precursors.

2.2.1 ESTIMATION OF COBALT

The cobalt content of the complexes and the combustion product was estimated by EDTA complexometric titrations, after decomposing the complex or dissolving the residue in 1:1 HCl (or HNO_3). A standard solution of 0.01M EDTA was prepared by directly weighing the disodium salt of EDTA (3.7225g in one liter of the solution) and dissolving it in the water. The solution was standardized by titrating it with standard zinc sulphate solution using Eriochrome Black T as an indicator [2].

A known weight of sample was separately heated with acid to dryness. The product was extracted with water (50 mL) and taken in a titration flask. The pH of the solution was adjusted (pH = 6) by adding hexamethyl tetramine, which acts as a buffer. A few drops of xylenol orange were added as an indicator and the resultant solution was titrated with 0.01M EDTA solutions until the colour changed from red to yellow [3].

1mL of 0.01M EDTA = 0.0005893g of Co

2.2.2 ESTIMATION OF HYDRAZINE

The conventional method of estimating hydrazine under Andrews's conditions [2] was used. About 40 mg of the sample was accurately weighed into a 250mL reagent

bottle. A mixture of 30mL of conc. HCl and 20mL of water was added to it followed by the addition of 5mL of chloroform or carbon tetrachloride. The solution was titrated with 0.025M KIO_3 slowly from the burette, with constant shaking of the stopper bottle between the additions, until the organic layer was just decolorized.

Hydrazine reacts with potassium iodate under the Andrews condition as follows:

$$IO_3^{-1} + N_2H_4 + 2H^+ + Cl^- = ICl + N_2 + 3H_2O$$

Thus,

1 ml of 0.025M KIO_3 == 0.0008313g N_2H_4

2.3 PHYSICO CHEMICAL TECHNIQUES

The materials in the form of combustion residues, prepared by the precursor method were characterized by employing Fourier Infra Red Spectroscopy, Simultaneous TGA – DTA, X-ray diffraction technique, B.E.T. liquid nitrogen adsorption and desorption method and Scanning Electron Microscopy.

2.3.1 INFRA RED SPECTROSCOPY

Infrared spectroscopy is a valuable tool for analyzing samples. The spectrum can be interpreted for the functional group present. Infra red instrumentation can be divided into two classes, namely, dispersive and non-dispersive. The dispersive type of spectrometer is similar to the UV-visible spectrophotometer. While the non-dispersive type has an inferometer in the place of a monochromator, which is then called as Fourier Infra-red spectrophotometer. The different components of the infrared instrument are

radiation source, optical system, detector, etc. The spectrum can be interpreted for the functional group present by matching the corresponding group frequency [4].

One of the instrumental methods used in the characterization of the Co_3O_4 sample was FTIR. Infrared spectroscopy is based on the fact that a molecule will have a number of fundamental rotational frequencies and each fundamental may be associated with the absorption of radiation of its own frequency. These absorption frequencies are obtained from the spectrum. FTIR provides simultaneous and instantaneous recording of the whole spectrum in the microwave and Infrared region of the electromagnetic radiation [5].

The infrared spectra of solid samples were recorded in the range of 4000 -400cm^{-1} by using Shimadzu DR 8031 instrument (Fig. 2.1). The spectra of the samples were obtained by dispersing them in KBr pellet. The observed infrared bands were analyzed by comparing with data reported by other workers [6].

2.3.2 X-RAY DIFFRACTION TECHNIQUE

For determination of crystal structure, the diffraction of X-rays by crystals is the most powerful method available at present. It is capable of providing accurate structural parameters of molecules present in the crystal structure.

The principle involved in the XRD technique is the one in which two parallel X-ray waves of particular wavelength strike parallel lattice planes of crystal. One of the waves is reflected by surface plane of the crystal in such a way that the angle of reflection is equal to the angle of incidence. The second wave penetrates the crystal and is reflected by lattice plane immediately below the surface plane [7]. If the two waves are in phase before reflection, they will continue to be in this phase after reflection. The extra distance

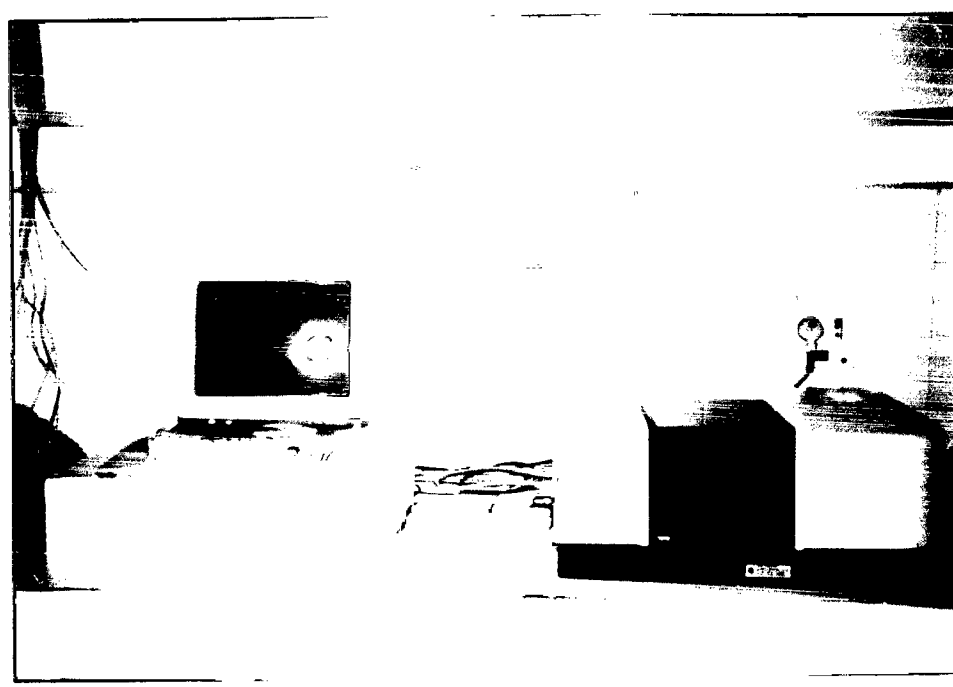

Fig. 2.1 Fourier Infra red spectrophotometer

(2dsinθ) that the second wave has to traverse is an integral multiple of the wave length. Hence one can say that the condition for constructive interference is

$$n\lambda = 2d\sin\theta \quad \ldots\ldots\ldots\ldots\ldots\ldots (1).$$

Where ' n' is an integer and 'd' is the spacing between successive planes, equation (1) is a Bragg condition for diffraction. The different components of the X-ray spectrophotometer are tube, collimator, and photographic plate on which radiation strikes.

The experimental method involves shining a monochromatic beam of X-rays at a known angle θ on one of the faces of crystal, and rotating the crystal about an axis parallel to the face and perpendicular to the beam.

Co_3O_4 samples prepared by precursor method were characterized by analyzing the powder by using CuK_α radiation, as per the requirements, filtered through the nickel or chromium X-ray diffractograms. The diffraction patterns were recorded on a Philips make diffractometer PW 3710 model available at Common Facility Center, Shivaji University, Kolhapur. The compounds were identified by comparing the observed interplanar d-spacing and relative peak intensities with those reported in the JCPDS data [8] file. Using d-values and relative intensities in the peaks did indexing for the sample. After obtaining the data, the different parameters such as a, and V as also the structures of the Co_3O_4 samples were determined.

2.3.3 SURFACE PROPERTIES

Surface characteristics of the catalyst samples were studied by measuring the surface area and porosity. The surface properties were measured by using an instrument of Quantachrome, NOVA 1200, in Catalysis Division, at NCL, Pune.

2.3.3.1. BET METHOD

The B.E.T. method is most widely used procedure for the determination of surface area of solid materials and involves the use of BET equation [9].

$$\frac{1}{W[(P_o-P)-1]} = \frac{1}{W_m C} + \frac{(C-1)}{W_m C} X \frac{P}{P_o} \quad \text{----------(2)}$$

Where 'W' is the weight of the gas adsorbed at a relative pressure P/P_o , 'P' is the equilibrium pressure, 'P_o' the saturated vapor pressure of the gas at the temperature of the adsorption, 'W_m' is the weight of the adsorbed gas at STP, 'C' is a constant related to the energy of adsorption in first adsorbed layer and its value is an indication of the magnitude of the adsorbent-adsorbate interactions. V_m the volume of gas at STP required to form monolayer in adsorption. Various quantities from the above equation like P, P_o, and V could be determined experimentally. W_m and C can be obtained by plotting $P/W(P_o-P)$ versus P/P_o , which is a straight line with slope $S_t = C-1/W_m C$. The specific surface area S in m^2/g of the solid can be calculated from the total surface area, S_t and the sample weight W.

$$S = S_t/W \quad \text{.....(3)}$$

2.3.3.2 POROSITY BY GAS ADSORPTION METHOD

The pores in the solid samples are normally characterized according to their sizes [10].

a) Pores with the opening exceeding $500A^{o}$ in diameter are called "macropores".

b) The term "micropores" describes a pores with diameter not exceeding $20A^{o}$.

c) Pores of intermediate sizes are called "mesopores"

Porosity of powders and other porous solids can be characterized by gas adsorption studies. The two common factors necessary for describing porosity are the determination of total pore volume and the pore size distribution. For evaluation of the porosity of most solid materials, nitrogen at 77K is used as a suitable adsorbate.

(A) TOTAL PORE VOLUME AND AVERAGE PORE RADIUS

The total pore volume is derived from the amount of vapor adsorbed at a relative pressure close to unity by assuming that the pores are then filled with liquid adsorbate.

$$V_{liq} = \frac{P_a V_{ads}.V_m}{RT} \qquad \ldots\ldots\ldots\ldots\ldots\ldots (4)$$

in which P_a and T are ambient pressure and temperature, and V_m is the molar volume of liquid adsorbate.

Assuming cylindrical pore geometry the average pore radius is given by the equation

$$\text{Av. pore radius} = \frac{2V_{liq}}{S} \quad \text{----------(5)}$$

S is BET surface area.

(B) PORE SIZE DISTRIBUTION (MESOPORE)

The distribution of the pore volume with respect to pore size is known as "pore size distribution". It is established, that the desorption isotherm is more appropriate than the adsorption isotherm for evaluating pore size distribution of an adsorbent.

$$r_k = \frac{-2\gamma V_m}{RT \ln (P/P_o)} \quad \text{----------(6)}$$

γ–Surface tension of the of the adsorbate at its boiling point(8.85ergs/cm^2 at 77K)

V_m is the molar volume of the adsorbate (34.7cm^3/mole), R=gas constant, r_k - Kelvin radius of the pore.

Surface area was also measured by conventional Zinc Ion Adsorption method developed by Kozawa [11].

2.3.4 THERMAL ANALYSIS

Thermal analysis is a group technique in which a physical property of a substance is measured as a function of temperature, whilst the substance is subjected to a controlled temperature (heating or cooling). This includes Differential Thermal Analysis (DTA), Thermogravimetry, (TGA), Derivative Thermogravimetric Analysis (DTG). Both TGA and DTA curves are effected by many factors like nature and shape of the material used as container, the sample weight and its history, the particle size, packing density of the

sample, sensitivity of the thermocouple and its location, the heating rate employed, the surrounding atmosphere etc [12].

2.3.4.1 DIFFERENTIAL THERMAL ANALYSIS (DTA)

The sample and the inert material are heated at a controlled heating rate and the temperature difference between them is continuously recorded as a function of furnace temperature. Substances undergoing a reaction are accompanied by change in enthalpy. This change brings in either increase in temperature of the sample (exothermic) with respect to the furnace temperature or decrease in temperature of the sample (endothermic) with respect to furnace temperature. This difference in temperature between sample and furnace temperature (also temperature of reference sample) appears either as positive difference (exothermic) or negative (endothermic). In the course of this study, all the experiments were carried out in nitrogen atmosphere and the heating rate employed was 10 ^{o}C/min.

2.3.4.2 THERMOGRAVIMETRIC ANALYSIS (TGA)

Here, the mass of a substance under consideration is measured as a function of temperature or time, whilst the substance is subjected to a controlled temperature (heating or cooling). Solid-state reaction occurring during the heating, involves loss in weight when gaseous products are formed or gain in weight during oxidation. Thus, the sample records loss in weight or gain in weight during heating.

2.3.4.3 DERIVATIVE THERMOGRAVIMETRY (DTG)

Derivative Thermogravimetry is an extension of thermogravimetry wherein the first differential of weight loss with respect to temperature is obtained. The peak temperature denotes the temperature at which the particular reaction has occurred. Area of this peak, is proportional to the total weight loss, which can be used to calculate important kinetic parameters.

Simultaneous DTA, TGA and DTG data for the samples was obtained by using Seiko instrument in SIL Division, National Chemical Laboratory, Pune. The samples were heated in nitrogen atmosphere (10mL/min) and the heating rate employed was 10^{o}C/min.

2.3.5 MICROSCOPY

The low energy (<50ev) secondary electrons emitted from the surface of the specimen, is the basis for different type of imaging. The beam is concentrated to small probe (20 A^{o} diameter), which is deflected across the specimen in a faster fashion using scanning coils. The secondary electrons can be detected above the specimen and an image, showing the intensity of the secondary electrons emitted from different parts of the specimen, can be displayed on CRT. This scanning image is useful for examining the morphology of a crystal surface. The particle size and surface morphology was determined by obtaining SEM data. The instrument used was JEOL JSM 5800 model from Instrumentation Centre, National Institute of Oceanography, Dona-Paula Goa. The instrument is shown in the Fig.2.2.

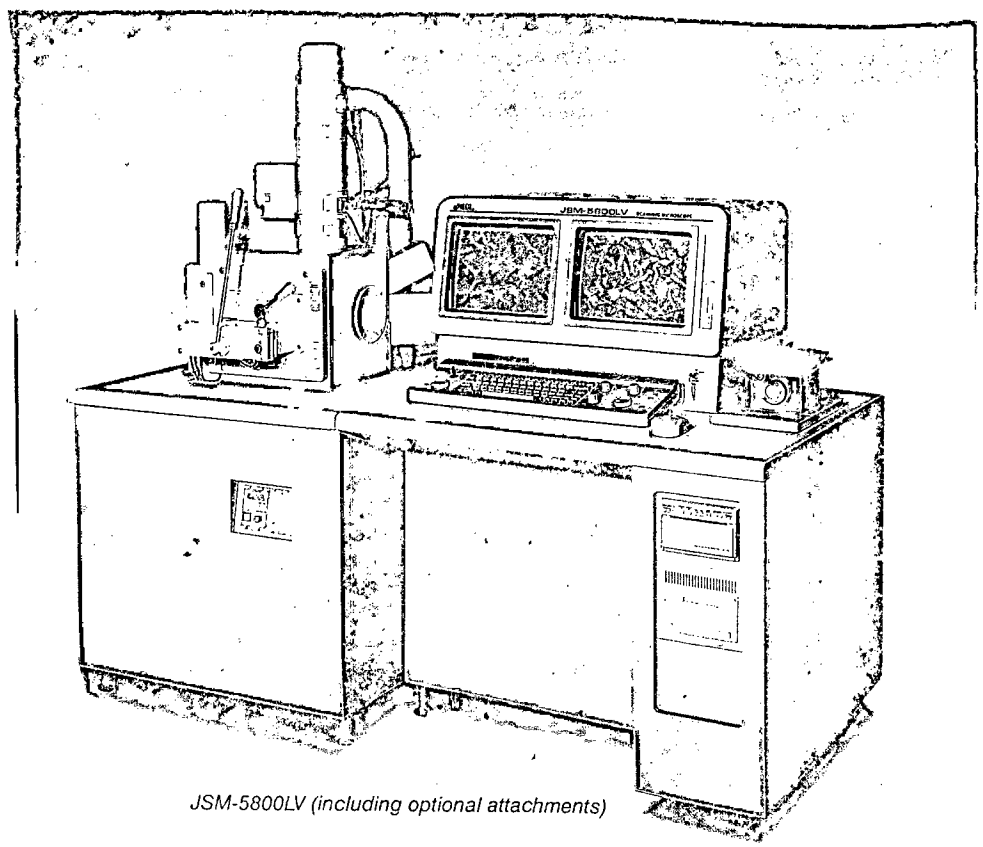

JSM-5800LV (including optional attachments)

Fig. 2.2 Scanning microscope 5800LV

2.4 CATALYTIC AND ELECTROCATALYTIC ACTIVITY

The catalytic and the electrocatalytic properties (activity) of the catalyst samples were studied, separately by the conventional H_2O_2 decomposition method and electrochemical measurements respectively.

2.4.1 STUDY OF GENERAL CATALYTIC ACTIVITY

One of the simplest methods of assessing the catalytic activity of solid samples is the experimental study of decomposition of hydrogen peroxide on the catalyst surface. The catalytic studies were carried out by using a gasometric set-up, as proposed by Cota et al [13], for the decomposition of hydrogen peroxide in the presence of a catalyst. The set up consists of stirrer, a two-neck flask, a burette, and a reservoir. In a typical experiment, accurately weighed sample of catalyst was taken into two-neck flask and to it 50mL of 6M KOH was added, followed by the addition of 5mL of 30 $^{W}/_{W}$ H_2O_2 into the flask. The volume of the oxygen gas liberated was monitored as a function of time, from the displacement of water in the burette [14]. The volume displaced is measured as a function of time using a stopwatch. The experimental set up is shown in Fig. 2.3.

2.4.2 ELECTROCHEMICAL METHODS

The electrochemical measurements were made by using a steady state galvanostatic technique. A schematic diagram of the cell used for the measurement of electrochemical perfomance parameter is shown in Fig. 2.4. The set-up is made up of plexiglass, since it does not react with acid and alkalis and at the same time it is transparent, The cell consists of rectangular plexiglass container with a lid that has

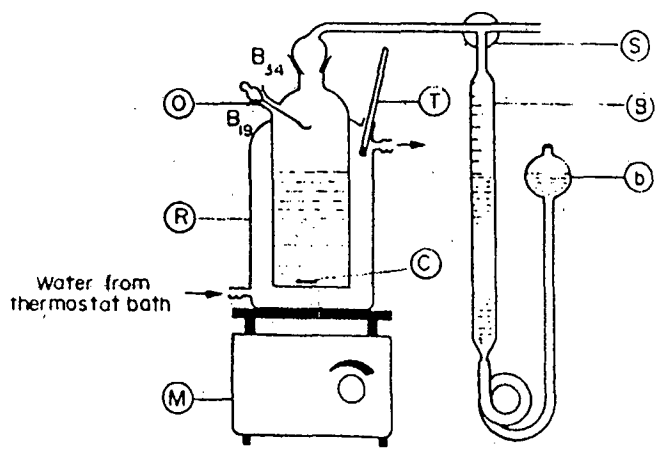

Fig 2.3 Apparatus used
for the study of decomposition
of H_2O_2 on CO_3O_4 catalyst.

b) Reservoir: c) Magnetic pellet: g) Burette: M) Magnetic stirrer: O) Syringe:
R) Thermostat bath: S) Stop cock: T) Thermometer.

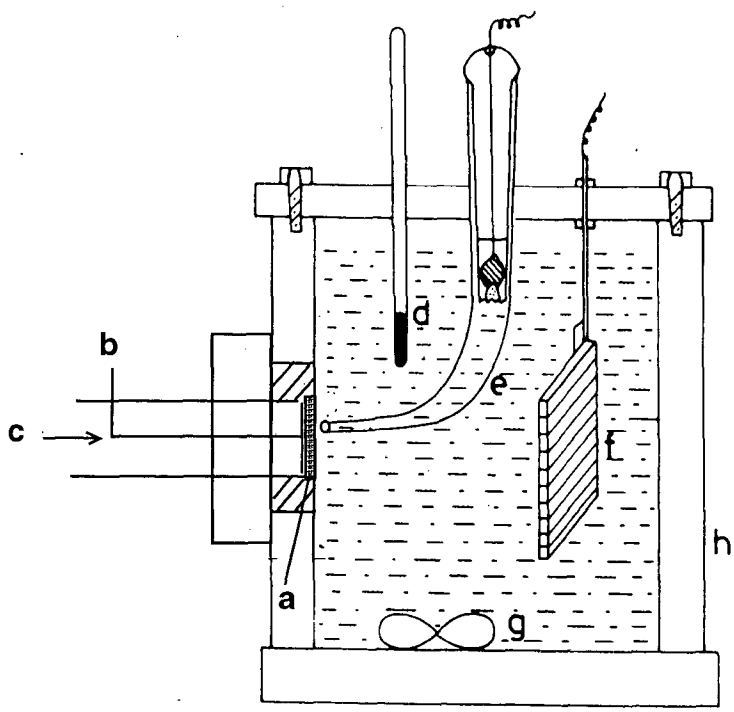

Fig. 2.4 The electrochemical cell assembly : a) working electrode; b) current collector; c) gas inlet; d) thermometer; e) reference electrode and lugin capillary; f) counter electrode; , g) magnetic stirrer and h) plexiglass container.

provision to hold a reference electrode, a lugin capillary, a high surface area flat bed counter electrode made from sintered nickel, and a thermometer [15].

The electrochemical cell assembly is made up of a) working electrode b) teflon screw c) gas inlet d) thermometer e) luggin capillary f) counter electrode g) plexiglass container and h) magnetic stirrer.

2.4.3 CYCLIC VOLTAMMETRY STUDIES

Cyclic voltammetry involves the measurement of current as a function of potential. The potential applied to an electrode (by means of potentiostat) is changed linearly with time in a repetitive manner. From cyclic voltammogram (i. e. a plot of current vs. potential) a typical current peak at a potential where reaction occurs is obtained.

The important parameters which can be obtained from cyclic voltammogram are anodic peak current $(i_p)_a$, The cathodic peak current $(i_p)_c$, the anodic peak potential $(E_p)_a$, The cathodic peak potential $(E_p)c$, and half peak potential $(E_{p/2})_c$.

The number of electron transferred in the electrode reactions for a reversible couple can be determined from the separation between the peak potentials [16].

$$(E_p)_a - (E_p)_c = 0.057/n$$

Cyclic voltammetry studies were performed for the working electrodes using the instrument EG and G Princeston model connected to an X-Y plotter at TIFR Bombay. The reference electrode used was Hg/HgO, OH^- and the counter electrode used was

sintered nickel plaque. The studies were carried out using 6M KOH using oxygen as a feed gas, and the scan rate used was between 20-350 mV/s [17].

REFERENCES

1. M. B. Tarasevich and B. Effromer, *"Electrodes of Conductive Metallic Oxides"*, Elsevier Scientific Publishing Co., Amsterdam, (1980).
2. J. Bassett, R. C. Denney, G. H. Jeffrey, and J. Mendham, *'Vogels Textbook of Quantitative Inorg. Analysis'*, E. L. B. Longman, (1979).
4. H. Willard, L. Merritt, J. Dean, and F. Settle, *"Instrumental Methods of Analysis"*, CBS Publishers and Distributors, New Delhi, (1986).
5. K. Nakamoto, *"Infra-red and Raman Spectra of Inorganic and Coordination Compounds"*, John Wiley and sons, New York, (1963).
6. Richard Nyquist and Ronald O. kagel, *"Infra-Red Spectra of Inorganic Compounds"*, Harcourt Brace Jovanovich Publishers, New York, (1971).
7. R. C. Mackenzie and B. D. Mitchell, *"Diffraction Analysis"*, Ed. R. C. Mackenzie, Academic, New York (1970).
8. JCPDS-International Center for Diffraction Data, PCPDFWIN v. 1.30 (1997)
9. S. Brunauer, P. Emmett, and E. Teller, *J. Ame. Chem. Soc.*, 60, 309 (1983)
10. K.S.W. Sing, D. H. Everett, R.A.W. Haul, L. Moscow, R.A. Pierotti, J. Rouquerol, and T. Siemieniewska, *Pure and Appl. Chem.*, 57, 4 (1985) 603.
11. A. Kozawa and T. Takai, *"Surface Electrochemistry; Advance methods and Concept"*, Ed. T. Takamura and A. Kozawa, Japan Scientific Soc. Press, Japan 1978.
12. K. Krawczyk, J. Petryk and K. Schmidt-Szalowski, *"Preparation of Catalysts VI"*, Elsevier Science B. V., G. Poncelet,(1995).
13. H. M.Cota, J. Katan, M. Chin and F.J. Schoenweis, *Nature* (London) 203,1281(1964).
14. S. P. Jiang, Z. G. Lin, and A. C. C. Tseung, *J. Electrochem.Soc.*,137, (1990) 759.

15. K. V. Ramesh, *" Preparation and Characterization of Fuel Cell Electrodes"*, Ph.D. Thesis, Indian Institute of Science, Bangalore (1986).

16. E. Gileadi, E. Kirowa – Eisner, and J. Penciner, *"Interfacial Electrochemistry an Experimental Approach"*. Addison-Wesley Publishing Company, Inc. Massachusetts, (1975).

17. R. Greef, R. Peat, L. M. Peter, D. Pletcher and J. Robinson, *"Instrumental Methods in Electrochemistry"*. Ellis Horwood, New york, (1985).

CHAPTER III

CHAPTER III

SYNTHESIS AND CHARACTERISATION OF Co_3O_4

INTRODUCTION

Transition metal oxides comprise a very important class of versatile materials for catalysis in general and electrocatalysis in particular. The widest class of non-metal substances investigated in electrocatalysis is the oxide systems. Among the transition metal oxides, those with the spinel structure are of great interest [1]. The binary systems of metal oxides having the composition AB_2O_4 are called spinels. Spinels are classified as normal, inverted and intermediate depending on the location of A and B ions.

The different advantages offered by these systems are: their easy preparation and availability, high activity, low cost, and satisfactory thermodynamic stability. Due to these advantages offered by the spinels, they find applications in various electrochemical systems. These compounds can be used as cathode or anode material in fuel cells, chlor-alkali and water electrolysis cells, air electrodes, generator and electro-synthesis electrodes, sensors or detectors. However these systems suffer from some drawbacks such as low specific surface area, and relatively high electrical resistance. Attempts are made to overcome these drawbacks by creating some new routes of synthesis for oxide electrocatalyst.

Several methods are known [2] for the preparation of spinels. Most commonly used is the ceramic technique, which involves the heating of their salts at very high

temperature (1000-1200°C). However, due to calcinations of the starting material at high temperature, the surface area of the sample is considerably reduced.

Another method used for the synthesis is the co-precipitation method wherein the precipitation of the hydroxides, oxalates etc. of the desired constituent metals is obtained, and then, it is followed by the thermal decomposition of the precipitates.

Among the different spinels, Co_3O_4 is considered as the most promising electrocatalyst in alkaline solutions because of its larger availability and lower cost compared to RuO_2 and also because of its good corrosion stability [3].

In the present investigation, a few novel methods for synthesis of Co_3O_4 were tried. The products obtained by these methods were characterized by conventional chemical and instrumental methods.

3.1 SYNTHESIS OF Co_3O_4

The spinel cobalt oxide (Co_3O_4) samples, investigated as electrocatalyst in this study, were synthesized by the precursor method. All the precursors used in the study were hydrazine based compounds. The advantages of hydrazine based precursors over the other precursors are [4,5]:

(i) very low ignition/decomposition temperatures (120-350°C),

(ii) auto catalytic decomposition/combustion, once ignited,

(iii) evolution of large amounts of gases such as NH_3, H_2O, CO_2 and N_2,

(iv) formation of ultrafine oxide materials having large surface area,

The Co_3O_4 samples were synthesized by different precursor routes as described below.

3.1.1 FROM COBALTOUS CARBONATE.

Stoichiometric quantity (5.947 g; 0.05m) of pink coloured the cobaltous carbonate of (A. R. grade) quality was taken and mixed with hydrazine hydrate (22.5mL; 0.15m). The mixture was thoroughly homogenized into a thick paste and kept overnight by closing the mouth of the beaker by using a paraffin film. The orange cream-colored precursor so obtained was dried in a desiccator. The precursor was characterized by chemical analysis for the cobalt and hydrazine content as explained in Chapter II.

Dry precursor was then decomposed in the following manner:

(I) A weighed quantity of the precursor was decomposed in a preheated silica crucible, **(CC-I)**.

(II) A weighed quantity of the precursor was decomposed in a preheated platinum crucible, **(CC-II)**.

(III) A weighed quantity of the precursor was photo catalytically decomposed (solar induced), in a platinum crucible, **(CC-III)**.

(IV) A weighed quantity of the precursor was photo catalytically decomposed (solar induced), in a silica crucible, **(CC-IV)**.

The decomposition residues so obtained were then used as such for characterization as described in Section 3.2.

3.1.2 FROM COBALT HYDRAZIDO CARBOXYLATE

The synthesis of hydrazido carboxylate was carried out by a known method [6-a]. It involves two steps as follows:

$$(NH_4)_2CO_3\,(S) + 2N_2H_4.H_2O\,(L) \longrightarrow (N_2H_5)_2CO_3 + 2H_2O + 2NH_3\uparrow$$

(a) To a weighed quantity of ammonium carbonate (9.2 g; 0.1m), hydrazine hydrate (11.0 mL; 0.2m) was added. The solution was initially stirred with a glass rod and then on a stirrer for 24 hours, keeping the mouth of the beaker partly open for NH_3 to escape, under this condition ammonium carbonate reacts with hydrazine hydrate to form a highly viscous colorless flowing liquid. The solution was stored in a tightly corked bottle.

$$(N_2H_5)_2CO_3 \longrightarrow N_2H_3COON_2H_5 + H_2O.$$

Aqueous cobalt chloride solution containing stoichiometric $CoCl_2.6H_2O$ (11.89g; 0.05m) was added to the syrupy liquid to obtain the cobalt hydrazido complex.

$$CoCl_2 + 2N_2H_3COON_2H_5 \longrightarrow Co(N_2H_3COO)_2.2.N_2H_4 + N_2H_5Cl + HCl$$

The amount of the ligand was maintained little high. The beaker was covered with watch glass and then placed in a water bath at 373K. After about 9 hours, a crystalline product separated out from the solution. This solution was then cooled and filtered to remove highly soluble N_2H_5Cl through the filtrate. Crystalline product was washed with minimum quantity of cold water and then ethanol. Dried product was then used for characterization to determine the Co and N_2H_4 contents (Chapter II).

The precursor was then decomposed in four different manners as given in 3.1.1 above and coded as **CH-I, CH-II, CH-III** and **CH-IV**.

3.1.3 FROM COBALT NITRILOTRIACETATE

Cobalt hydrazinium nitrilotriacetate salt was prepared by using the method described else where [6-b]. Aqueous suspension of cobaltous carbonate (5.947 g; 0.05m) was added to a weighed quantity of nitrilotriacetic acid (9.55 g; 0.05m) with constant

stirring for the desolution of the acid and to eliminate carbon dioxide it was then heated in a water bath for about 3 hours at 80°C. A known quantity of hydrazine hydrate (5.3 mL; 0.1m) was then gradually added to the mixture. The red crystals obtained were filtered in buckner funnel and weighed to find out the yield.

Reactions

$$CoCO_3 + N(CH_2COOH)_3 \longrightarrow CoH(CH_2COO)_3 + CO_2 + H_2O$$

$$CoH(CH_2COO)_3 + 2N_2H_4H_2O \longrightarrow (N_2H_5)Co(CH_2COO)_3.N_2H_4 + 2H_2O$$

The crystals were then powdered and decomposed in the same manner as described above (Section 3.1.1). The samples obtained on decomposition were coded as **CT-I, CT-II, CT-III and CT-IV** and used for characterization (Section 3.2).

3.1.4 FROM COBALT NITRATE

A known quantity of liquid hydrazine hydrate (10.5mL; 0.2m) and solid NTA (19.1g; 0.1m) were mixed until viscous liquid was formed. To this mixture an aqueous cobalt nitrate solution (18.3 g; 0.1m + 20ml of water) was added with constant stirring. And then the mixture was strongly heated in a porcelain dish on a burner (Budkuley et al – unpublished work), by covering the evaporating dish with an inverted funnel. The solid residue so obtained was weighed for yield and then used for characterization (Section 3.2). The sample obtained on decomposition was coded as **CN**.

3.2 CHARACTERIZATION OF COMBUSTION RESIDUES

Residues obtained after decomposition of various precursors and solution, as described in the earlier section were characterized by chemical and instrumental methods. A particular phase formation in the residue is necessary for its use as catalyst or electrocatalyst.

3.2.1 CHEMICAL ANALYSIS OF COMBUSTION RESIDUES

The cobalt oxide samples obtained as combustion residues from various methods, listed in the previous section, were characterized for their cobalt content by using EDTA complexometric method, which is discussed in detail in Chapter II. From the volume of the titrant EDTA solution, the percentage of cobalt in known amount of sample was determined [7]. Thus,

1.0ml of 0.01N EDTA = 0.0005893 g of cobalt

The theoretical percentage of cobalt in the product is given as:

$$\% \text{ Co} = \frac{\text{g of Co}}{\text{g of combustion residue}} \times 100$$

Percentage content of Co in different samples is given in Table 3.1. This data was used to fix the composition of the combustion residues.

3.2.2 SPECTRAL ANALYSIS OF COMBUSTION RESIDUE

Infra red spectra of N_2H_4 based compounds have been characterized by typical N-N and N-H stretching frequency and hence used to determine the nature of the hydrazine moiety in the precursor. Thus N-N of monodentate N_2H_4 occurs at 930 cm^{-1}, whereas

Table - 3.1 % yield on decomposition, Cobalt content, and metal–oxygen absorption frequencies in the residues obtained after decomposition of precursor by different methods

Sample code	% yield Expt.	% Cobalt Expt.	% Cobalt Calc.	M-O absorption frequencies cm^{-1}
CC-I	98.2	73.06	73.4%	570, 655
CC-II	98.52	73.60	73.4 %	575, 650
CC-III	98.62	73.66	73.4 %	560, 660
CC-IV	99.23	73.60	73.4 %	560, 670
CH-I	98.40	73.50	73.4 %	575, 620
CH-II	96.32	73.20	73.4 %	575, 660
CH-III	97.23	72.80	73.4 %	570, 660
CH-IV	99.30	73.0	73.4 %	575, 660
CN	98.0	73.8	73.4 %	560, 660
CT-I	98.53	73.60	73.4 %	560, 660
CT-II	96.55	72.50	73.4 %	560, 650
CT-III	98.30	73.0	73.4 %	560, 660
CT-IV	98.99	72.90	73.4 %	560, 660

bridged N_2H_4 occur at 960 cm^{-1} N-N of ionic N_2H_5 965 cm^{-1} and coordinated $N_2H_5^+$ 990 cm and finally N-N of N_2H_3COOH is seen at 990-1005 cm^{-1} [8].

Metal oxygen bond frequency in the infrared absorption spectrum for cobalt oxide samples (Fig. 3.3 to 3.5) was used to characterize the combustion residues [9].

3.2.3 THERMAL ANALYSIS OF COMBUSTION RESIDUES

Thermal analysis [10-a] of combustion residues was carried out by employing Seiko instrument and heating the samples in nitrogen atmosphere at 10^{o}/min. Initial loss of about 1.5% was seen in the TGA, whereas no peaks in the DTA was observed for this loss seen in the TGA [10-b]. The next step in TGA was observed in temperature range of 770-810 ^{o}C (Table 3.2) for most of the sample with about 6.5% loss in weight. A complementary exothermic peak (Fig. 3.9 to 3.11) was observed in the DTA in this temperature range identical patterns were observed for most of the samples [11].

3.2.4 X-RAY DIFFRACTION OF COMBUSTION RESIDUES

Table 3.3 gives the X-ray powder diffraction data (Fig. 3.6 to 3.8) of the combustion residues obtained from various precursors after decomposing in different methods. The d-values obtained for these samples were calculated from the diffraction patterns [12]. Indexing for the sample was done by using programmed method, PowdMult-an Interactive Powder Diffraction Interpretation and Indexing Programme version 2.3 developed by E. Wu, School of Physical Sciences Flinders University of South Australia, Bedford Park, S.A. 5042, Australia. The different parameters such as 'a'

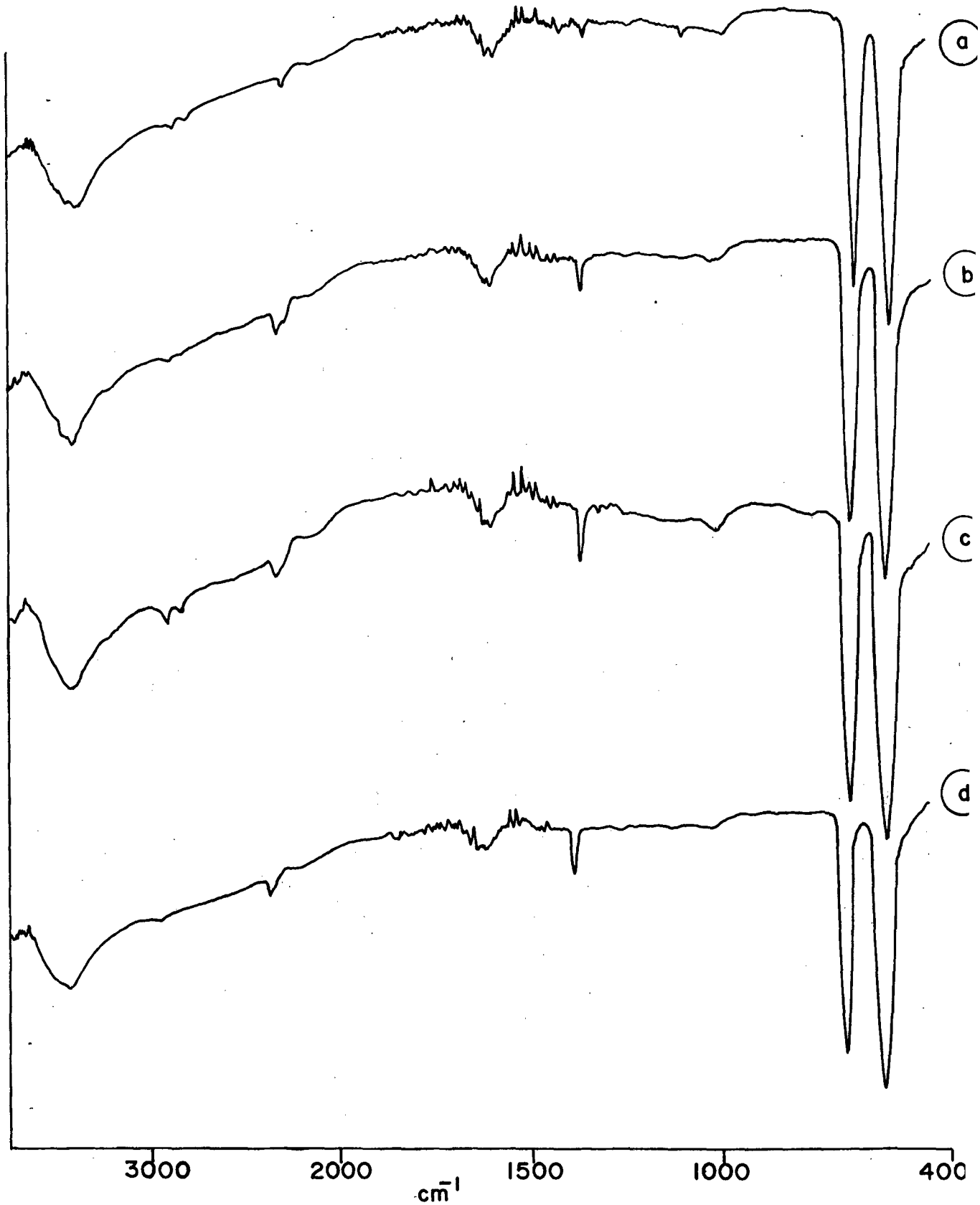

Fig. 3.1 Infra-red spectra of Co_3O_4 samples
a) CC-I b) CC-II c) CC-III d) CC-IV

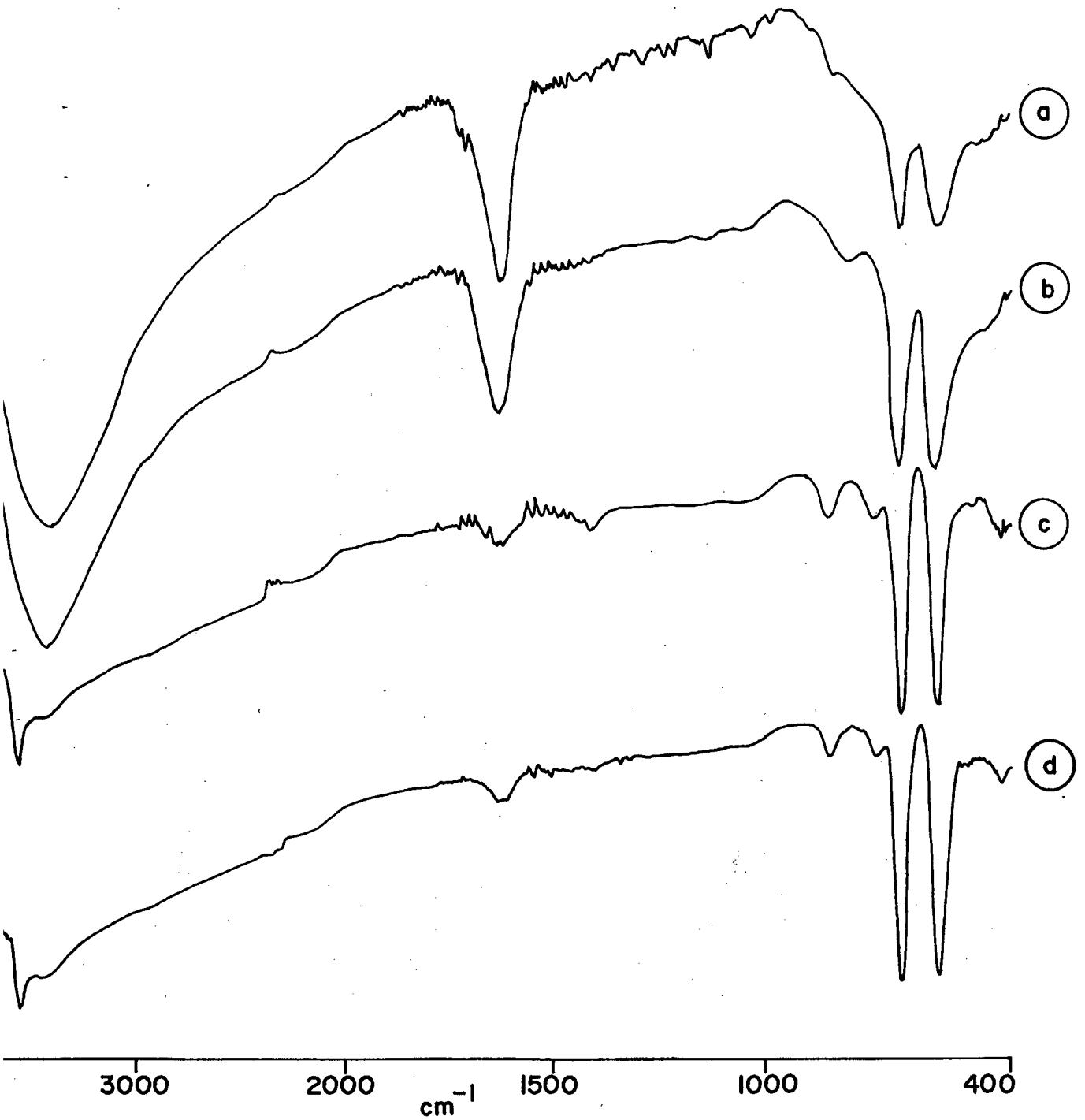

Fig. 3.2 Infra-red spectra of Co_3O_4 samples
a) CH-I b) CH-II c) CH-III d) CH-IV

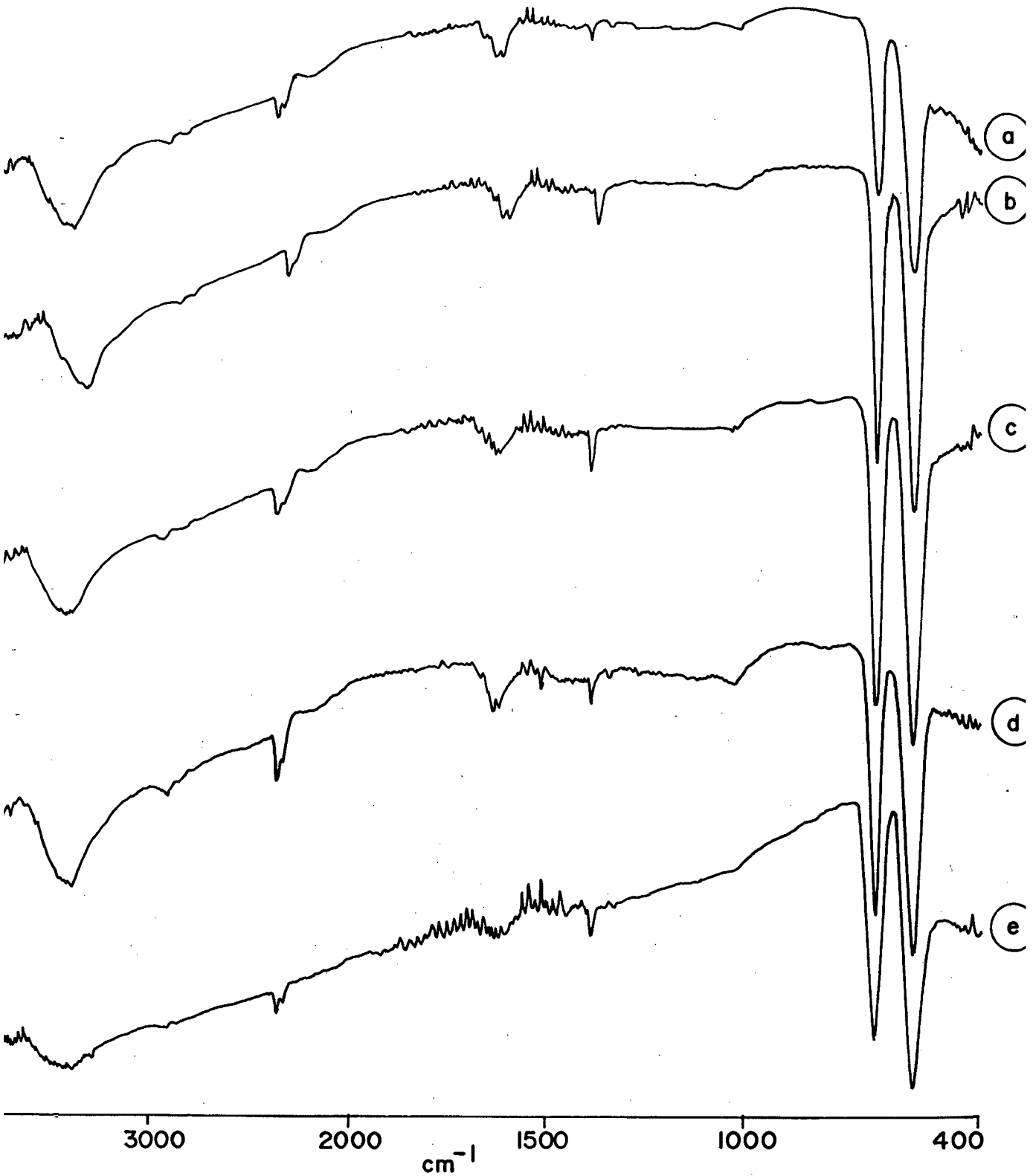

Fig. 3.3 Infra red spectra of Co_3O_4 samples
a) CT-I b) CT-II c) CT-III d) CT-IV e) CN

Table 3.2 DTA -TG data of Co_3O_4 samples

Sample code	Temp Range °C	Step	% loss in TGA		DTA peak temp °C	Reaction
			Theor.	Obsd.		
CC-I	50-150	1	2.2	1.11		
	750-820	2	6.5	6.48	820	$Co_3O_4 \rightarrow 3CoO + 1/2O_2$
CC-II	50-150	1	2.2	0.846		
	750-820	2	6.5	6.67	815	$Co_3O_4 \rightarrow 3CoO + 1/2\ O_2$
CC-III	50-150	1	2.2	1.83		
	750-820	2	6.5	6.38	815	$Co_3O_4 \rightarrow 3CoO + 1/2O_2$
CC-IV	50-150	1	2.2	2.09		
	750-820	2	6.5	6.72	815	$Co_3O_4 \rightarrow 3CoO + 1/2O_2$
CH-I	-	-	-	-	-	-
CH-II	-	-	-	-	-	-
CH-III	50-150	1	2.2	0.802		
	750-820	2	6.5	6.9	805	$Co_3O_4 \rightarrow 3CoO + 1/2O_2$
CH-IV	50-150	1	2.2	2.14		
	750-820	2	6.5	6.53	815	$Co_3O_4 \rightarrow 3CoO + 1/2O_2$
CN	50-150	1	2.2	0.39		
	750-820	2	6.5	6.78	815	$Co_3O_4 \rightarrow 3CoO + 1/2O_2$
CT-I	-	-	-	-	-	
	-	-	-	-	-	
CT-II	50-150	1	2.2	3.2		
	750-820	2	6.5	7.35	810	$Co_3O_4 \rightarrow 3CoO + 1/2O_2$
CT-III	50-150	1	2.2	-		
	750-820	2	6.5	6.60	795	$Co_3O_4 \rightarrow 3CoO + 1/2O_2$
CT-IV	50-150	1	2.2	2.14		
	750-820	2	6.5	6.64	820	$Co_3O_4 \rightarrow 3\ CoO + 1/2O_2$

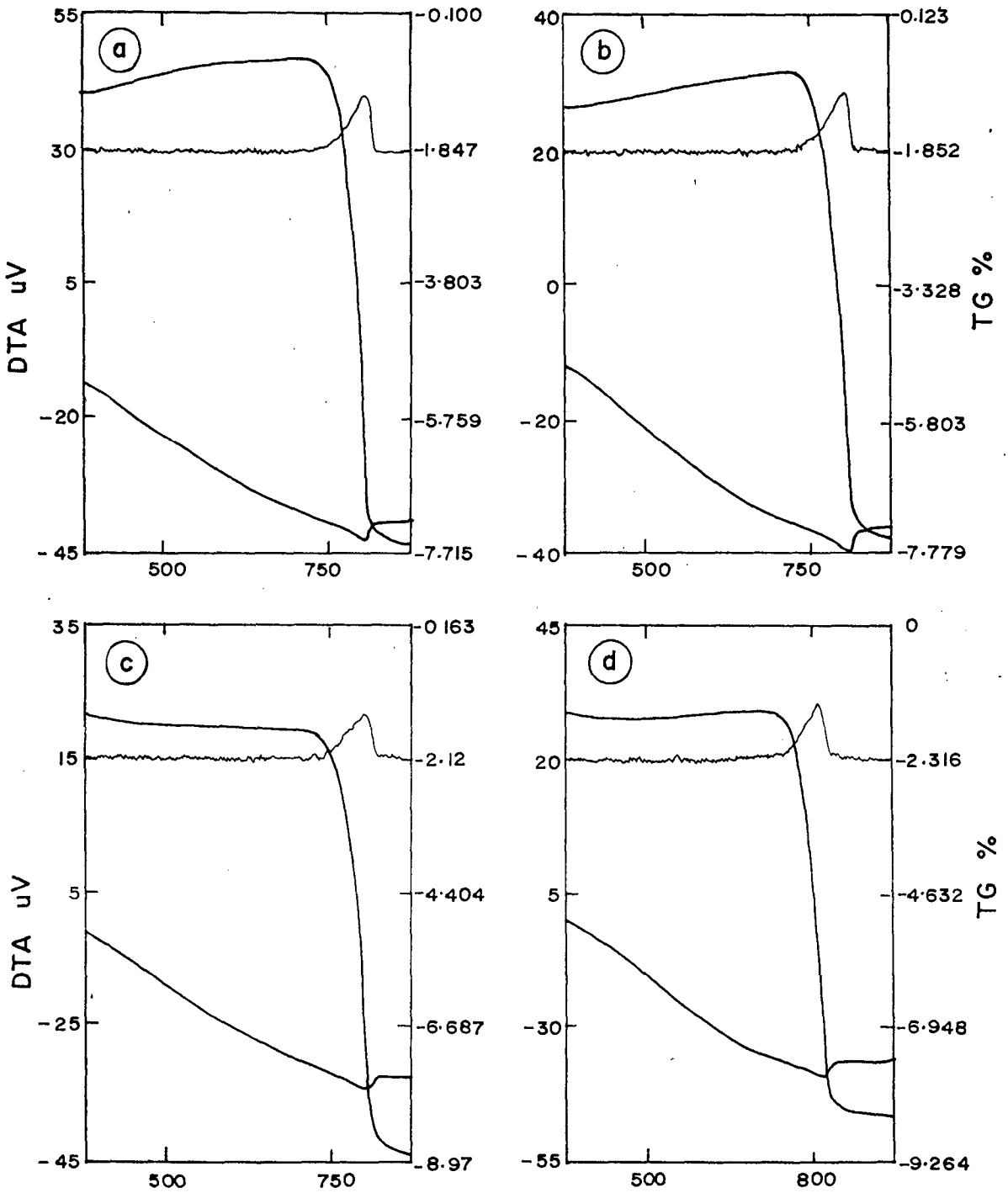

Fig. 3.4 Simultaneous TGA, DTA, DTG in N_2 of samples
a) CC-I b) CC-II c) CC-III d) CC-IV

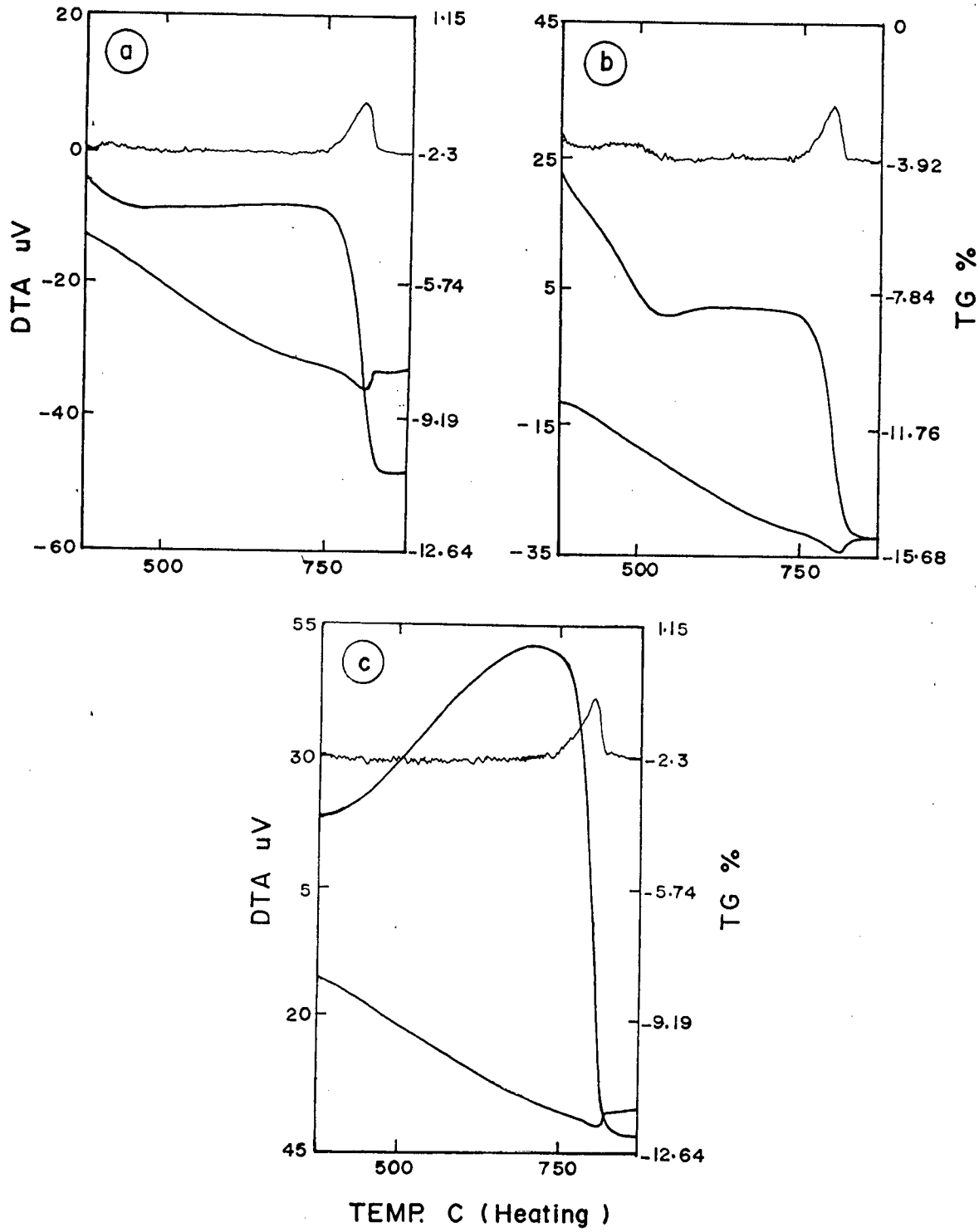

Fig. 3·5 Simultaneous TGA, DTA, DTG in N_2 of samples a) CH-III b) CH-IV c) CN

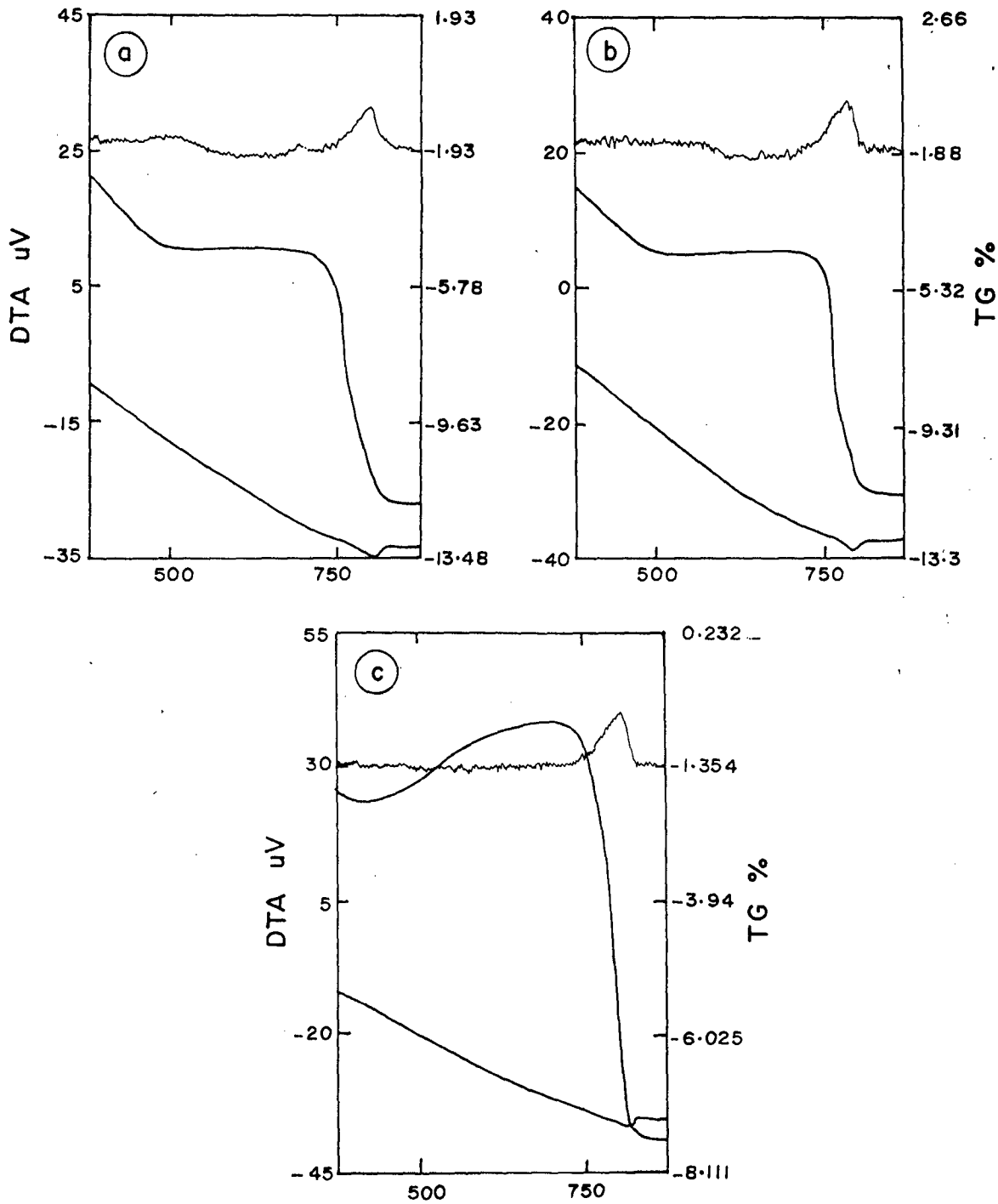

Fig. 3.6 Simultaneous TGA, DTA, DTG in N_2 of samples
a) CT-II b) CT-III c) CT-IV

Table 3.3 X-ray powder diffraction data of different Co_3O_4 samples [12] with CuKα

(A) Sample code: CC - I			λ=1.5405A
d-values	Relative Intensity	hkl	Other parameters
2.8497	26.1	220	a = 8.06A V = 523 Structure: Cubic
2.4320	100	311	
2.1610	7.4	321	
2.0205	11.7		
1.5530	62.4		
1.4275	39.6		

(B) Sample code: CC - II			λ=1.5405A
d-vales	Relative Intensity	hkl	Other parameters
4.07	19.5	-	a = 7.29A V = 387.42 Structure: Cubic
2.85	32.8	213	
2.43	100	311	
2.11	7.2	222	
2.0	19.5	320	
1.55	24.3	332	
1.43	47.4	510	

(C) Sample code: CC - III			λ=1.5405A
d-values	Relative Intensity	hkl	Other parameters
4.66	16.6	-	a = 8.05A V = 523.49 Structure: Cubic
2.86	22.2	213	
2.43	100	311	
2.01	16	400	
1.87	42.0	331	
1.65	6.2	422	
1.55	20.1	333	

Table 3.3(contd.)

(D) Sample code: CC – IV			λ=1.5405A
d-values	Relative Intensity	hkl	Other parameters
2.8497	16.0	220	a = 8.06 A V= 524 Structure: Cubic
2.4368	100	311	
2.0173	21.8	400	
1.5534	30.9	333	
1.4283	39.6	440	

(E) Sample code: CH - I			λ=1.5405A
d-values	Relative Intensity	hkl	Other parameters
2.99	35.2	-	a = 8.04A V = 579 Structure: Cubic
2.92	83.2	-	
2.81	24.5	-	
2.43	100.0	311	
2.31	25.6	222	
2.07	26.7	400	
1.57	27.8	570	

(F) Sample code: CH - II			λ=1.5405A
d-values	Relative Intensity	hkl	Other parameters
2.85	31.8	211	a = 6.98A V = 340 Structure: Cubic
2.44	100.0	311	
2.02	34.3	222	
1.69	8.6	420	
1.55	25.7	421	

Table 3.3(contd.)

(G) Sample code: CH - IV			λ=1.5405A
d-values	Relative Intensity	hkl	Other parameters
6.53	14	220	a = 8.05 A V = 523.4 Structure: Cubic
5.55	10.6	311	
2.86	20.7	222	
2.43	100.0		
2.31	18.6		
1.56	51.2		
1.42	42.3		

(H) Sample code: CN			λ=1.5405A
d-values	Relative Intensity	hkl	Other parameters
2.43	100.0	311	a = 7.29A V = 387 Structure: Cubic
2.12	56.8	213	
2.10	43.8	222	
1.54	19.9	332	
1.50	18.6	422	
1.42		510	

(I) Sample code: CT - I			λ=1.5405A
d-values	Relative Intensity	hkl	Other parameters
2.85	34.2	220	a = 8.06A V = 523 Structure: Cubic
2.44	100.0	311	
2.13	42.5	321	
1.55	21.1	333	
1.42	28.4	440	
1.27	11.6		

Table 3.3(contd.)

(J) Sample code: CT - II			λ=1.5405A
d-values	Relative Intensity	hkl	Other parameters
3.02	40.1		a = 8.059A
2.85	21.8	220	
2.43	100	311	V = 539
2.02	23.4	400	Structure: Cubic
1.55	32.1	333	
1.42	40.1	440	

(K) Sample code: CT - III			λ=1.5405A
d-values	Relative Intensity	hkl	Other parameters
			a = 8.106A
2.86	28.7	220	
2.43	100	311	V = 532.62
2.33	19.4	222	
1.55	36.8	333	Structure: Cubic
1.42	48.0	440	

(L) Sample code: CT - IV			λ=1.5405A
d-values	Relative Intensity	hkl	Other parameters
2.85	27.8	220	a = 8.04A
2.43	100	311	
2.01	25.0	400	V = 579.72
1.55	23.0	511	Structure: Cubic
1.42	23.0	440	

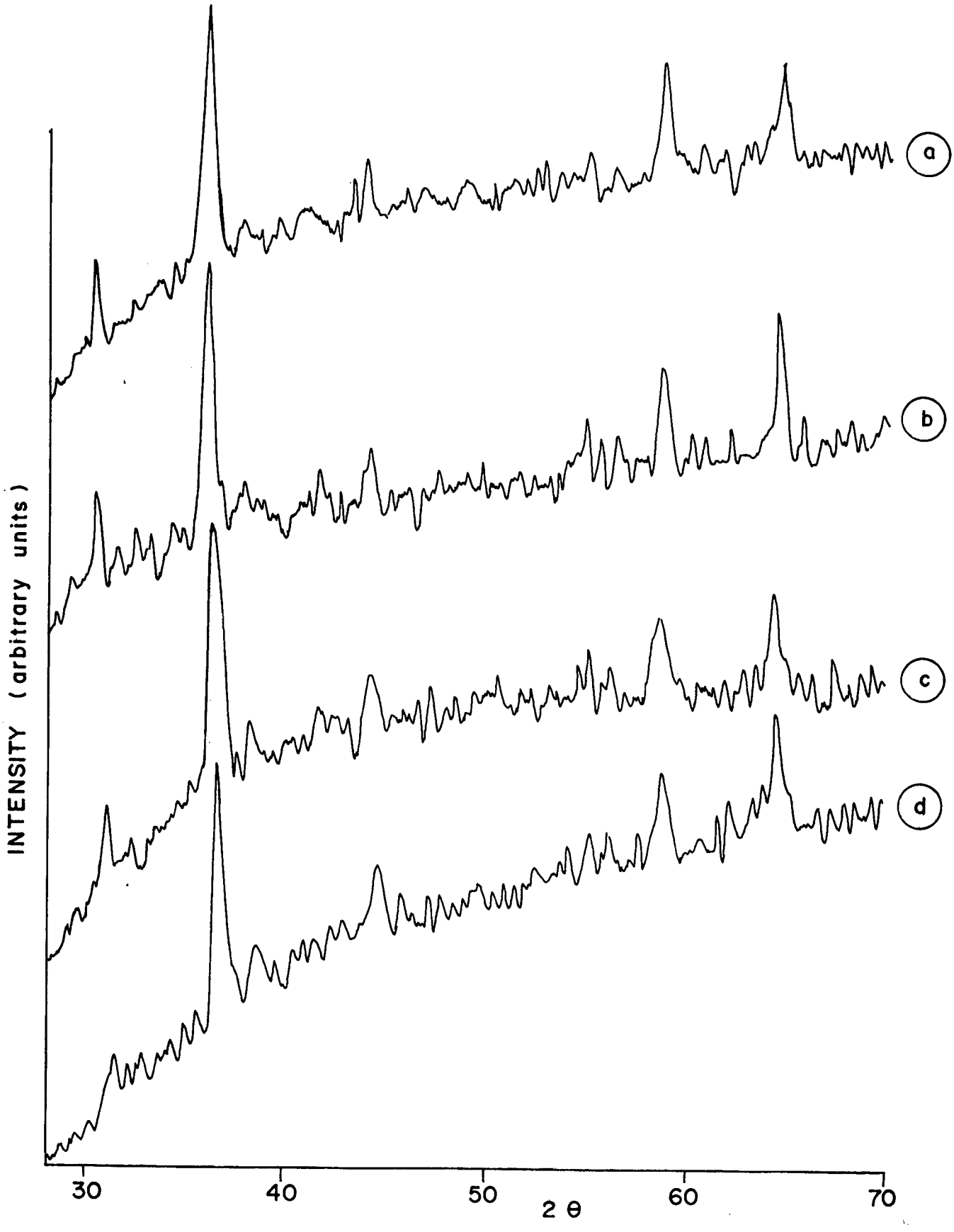

Fig. 3.7 X-Ray powder diffraction patterns of Co_3O_4 samples
a) CC-I b) CC-II c) CC-III d) CC-IV

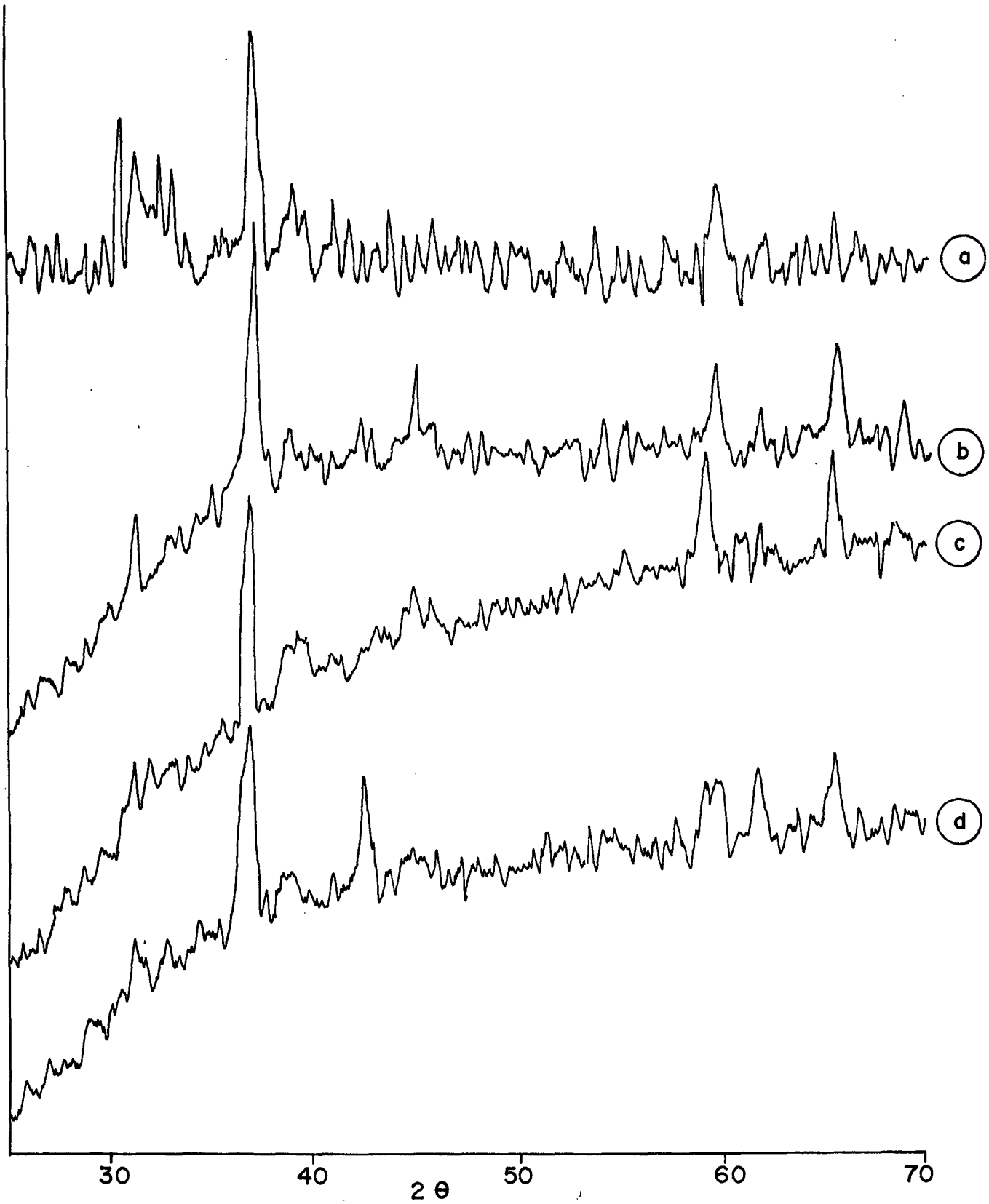

Fig. 3.8 X-Ray powder diffraction patterns of Co_3O_4 samples
a) CH-I b) CH-II c) CH-IV d) CN

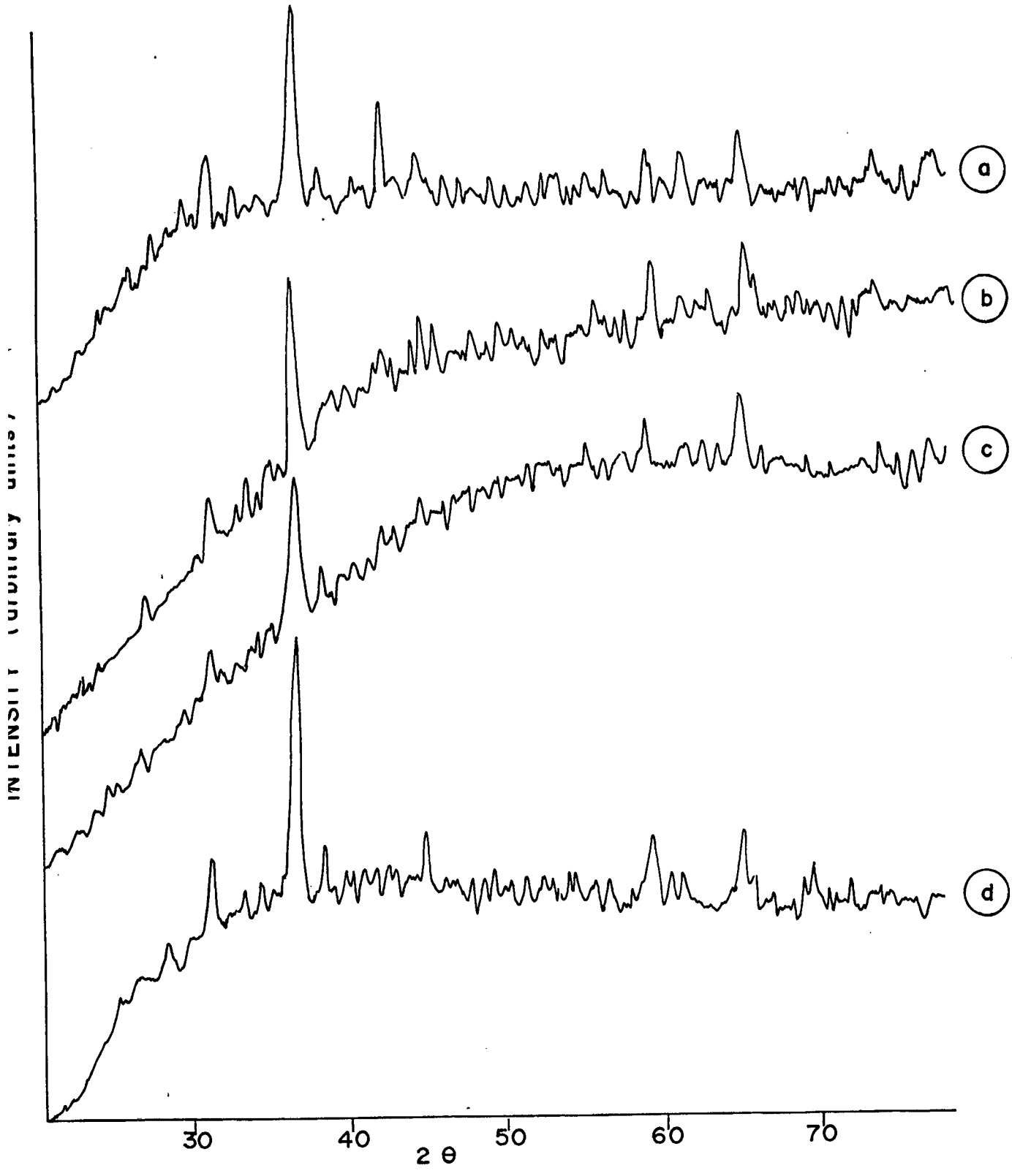

Fig. 3.9 X Ray powder diffraction patterns of Co_3O_4 samples
a) CT-I b) CT-II c) CT-III d) CT-IV

and 'v' were determined from the d-values and relative intensities. The average crystallite diameter was calculated by using Schrerrer's equation [15].

$$d = (0.9 \times \lambda) / (\beta \times \text{Cos}\ \theta)$$

where; λ = wave length for CuKα radiation,

β = width at half height, in radians,

θ = diffraction angle.

3.2.5 SURFACE AREA & POROSITY OF COMBUSTION RESIDUES

The B.E.T. surface area for different combustion residues is determined by using an instrument Nova 1200. All samples were activated around 300°C for 3 hours before adsorption was carried out. Nitrogen gas was used as an adsorbent. Pore size distributions of some residual samples were carried out. The surface area and pore size distribution of Co_3O_4 samples is shown in Table 3.4. The pore volume is found to be less than 500, and average pore diameter is found in range between 53.95-63.01A°, hence samples are found to be mesoporous in nature [16,17].

3.2.6. SEM OF THE COMBUSTION RESIDUES

Scanning Electron Microscopy was used to understand the morphology of the combustion residues. Micrographs of some of the samples are illustrated in Figs. 3.12 to 3.14. Particle size distribution of the samples can be determined from the SEM data.

Table - 3.4 Surface area and pore size distribution for different Co_3O_4 samples

Sample Code	B.E.T. surface area m^2/g	Total pore volume (cc/g)	Average pore dia. (A^0)	Pore volume (A^0) > 500
CC-I	142.9	-	-	-
CC-II	30.99	-	-	-
CC-III	37.29	0.05798	62.183	500.592
CC-IV	33.23	0.05082	61.18	498.181
CH-I	102	0.1381	53.95	478.816
CH-II	8.54	0.01346	63.01	457.430
CH-III	8.13	0.01180	56.35	459.131
CH-IV	109.47	-	-	-
CN	8.6	-	-	-
CT-I	8.793	0.01192	54.21	462.489
CT-II	15.36	0.0220	57.79	484.725
CT-III	8.13	-	-	-
CT-IV	7.13	-	-	-

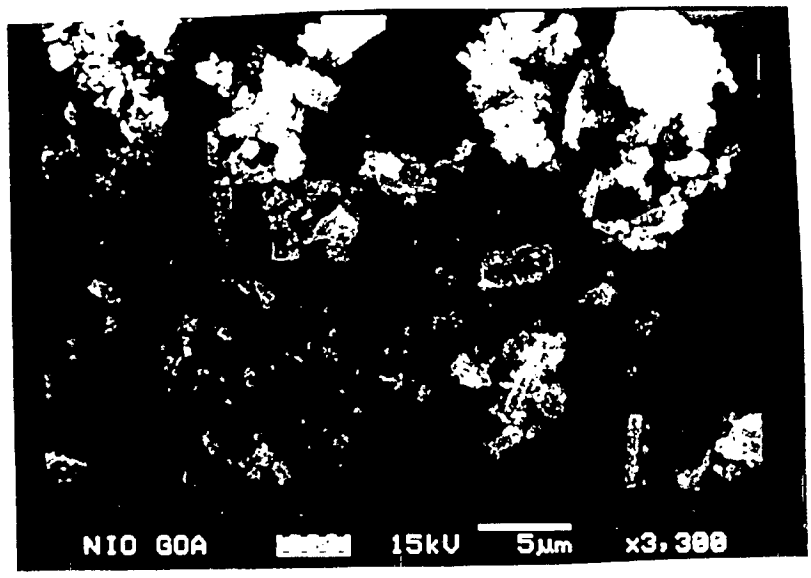

a)CC - I

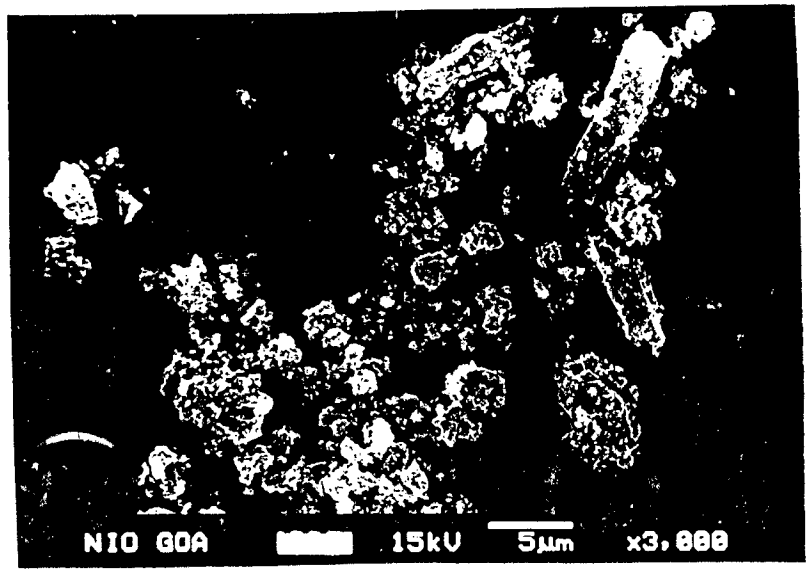

b)CC - II

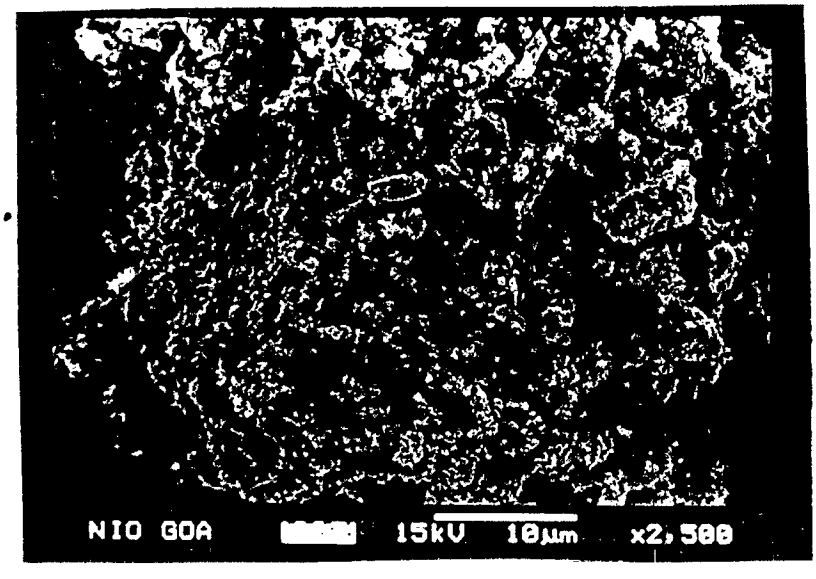

c)CC - III

Fig. 3.10 Scanning micrograph of CO_3O_4 sample
a)CC - I, b)CC - II and c)CC - III

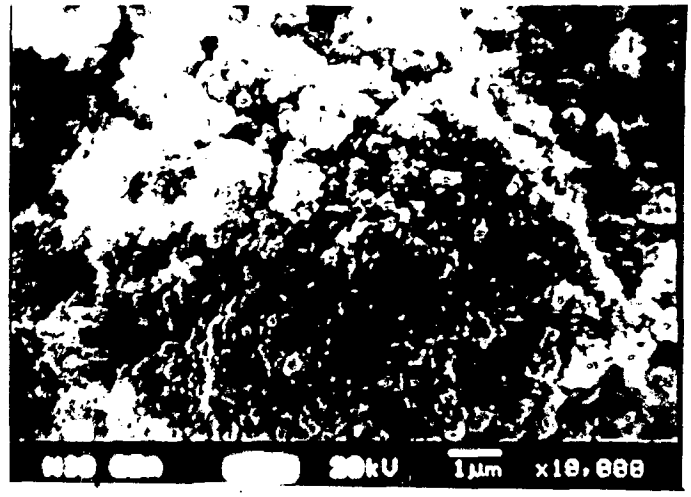

a)CT - I

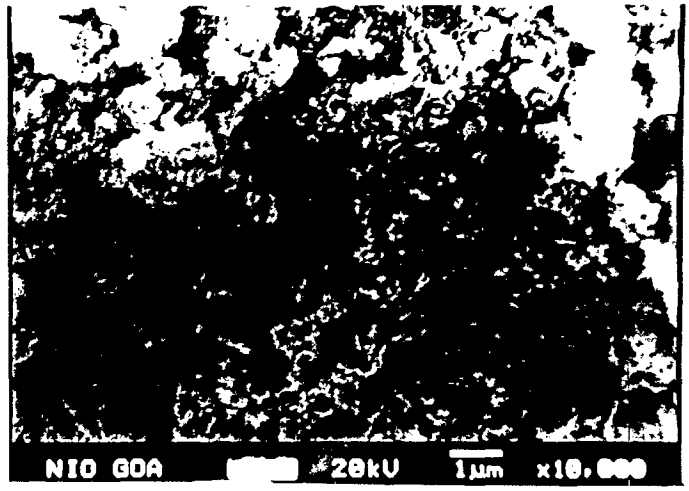

b)CT - II

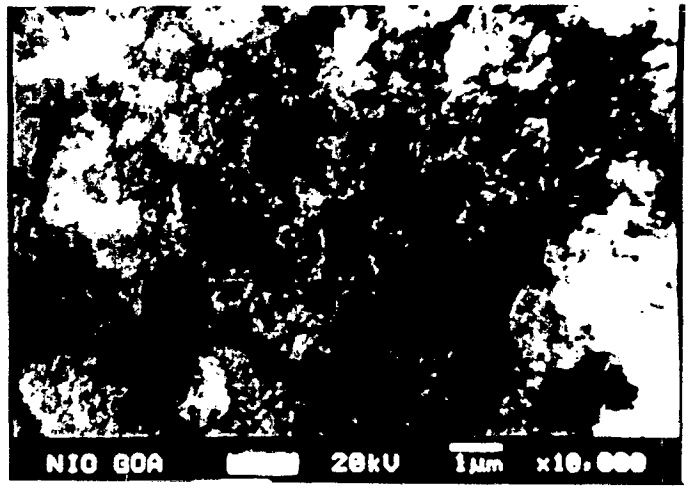

c)CT - III

Fig. 3.11 Scanning micrograph of CO_3O_4 sample
a)CT - I, b)CT - II and c)CT - III

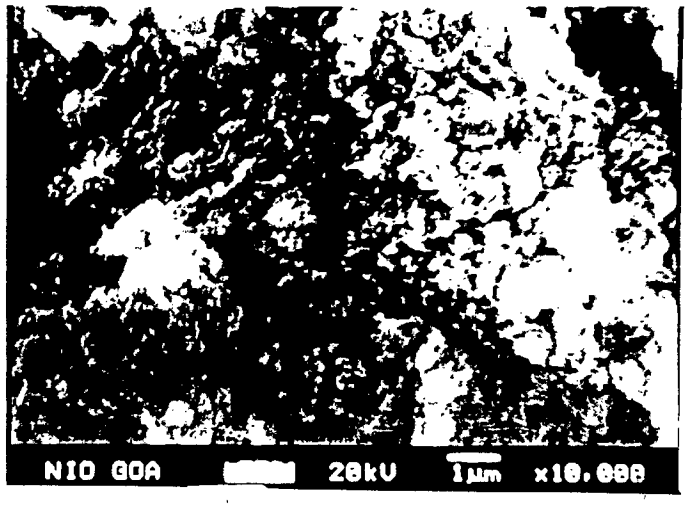

a)CC - IV

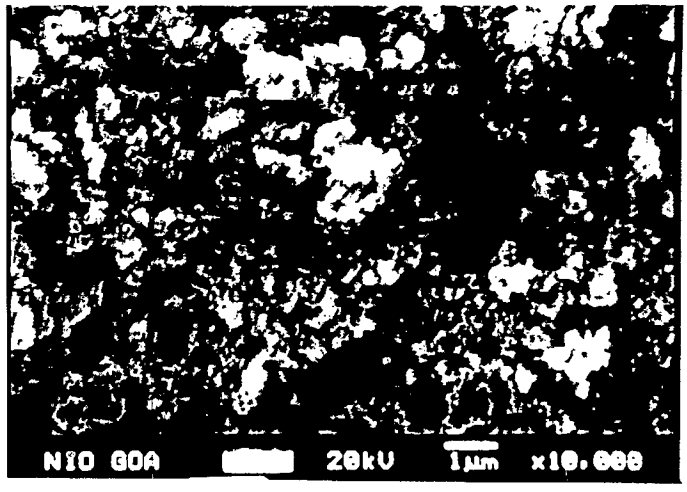

b)CH - I

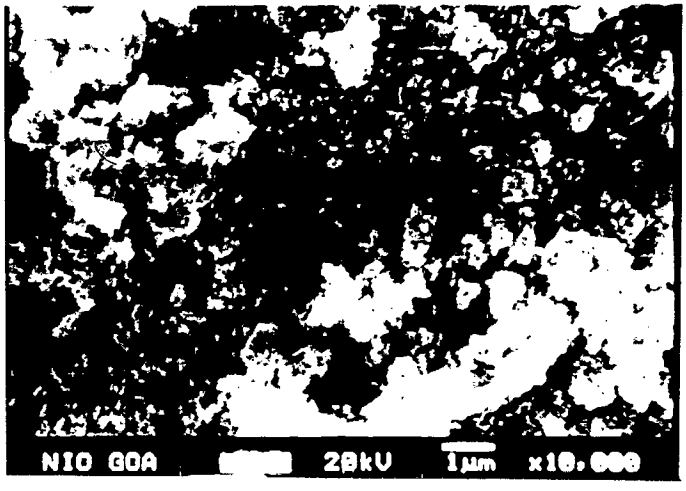

c)CN

Fig. 3.12 Scanning micrograph of CO_3O_4 sample
a)CC - IV, b)CH - I and c)CN

3.3 RESULTS AND DISCUSSION

Interpretation of the data obtained from the chemical and the instrumental analysis of the precursors and their combustion residues are given below.

3.3.1 PRECURSORS

Heterogeneous reaction (Section 3.1.1) between cobalt carbonate (solid) and hydrazine hydrate (liquid) appears to yield $CoCO_3.3N_2H_4$.

$$CoCO_3 + 3N_2H_4.H_2O \longrightarrow CoCO_3.3N_2H_4 + 3H_2O$$

The results of the chemical analysis of the product (% Co: obsd. 27.3, reqd. 27.42; % N_2H_4 : obsd. 43.08, reqd. 44.66) shows that there is good agreement between the observed and calculated values for the cobalt and hydrazine content, confirming the proposed formula for the precursor. N_2H_4 appears to coordinate to metal carbonate resulting in the peroxide linkage between two carbon atoms in the carbonate radical in the compound. The infrared spectrum of this compound (Fig.3.13) shows typical –O-O- absorption around 860 and 280, 380, 450 cm^{-1} as reported in the literature [18].

Formation of cobalt hydrazido carboxylate dihydrazinate, which was prepared by the method described elsewhere [6-a], was confirmed on the basis of chemical analysis as well as the IR spectroscopy.

Similarly, the product obtained, during the synthesis carried out as described in Section 3.1.3, was found to be hydrazinium cobalt nitrilotriacetate dihydrazinate, as evident from the chemical analysis (% Co: obsd. 18.10, reqd. 18.89; % N_2H_4: obsd. 22.06, reqd. 20.51). Infrared spectrum of the compound is almost superimposable to the one reported for the other divalent metals.

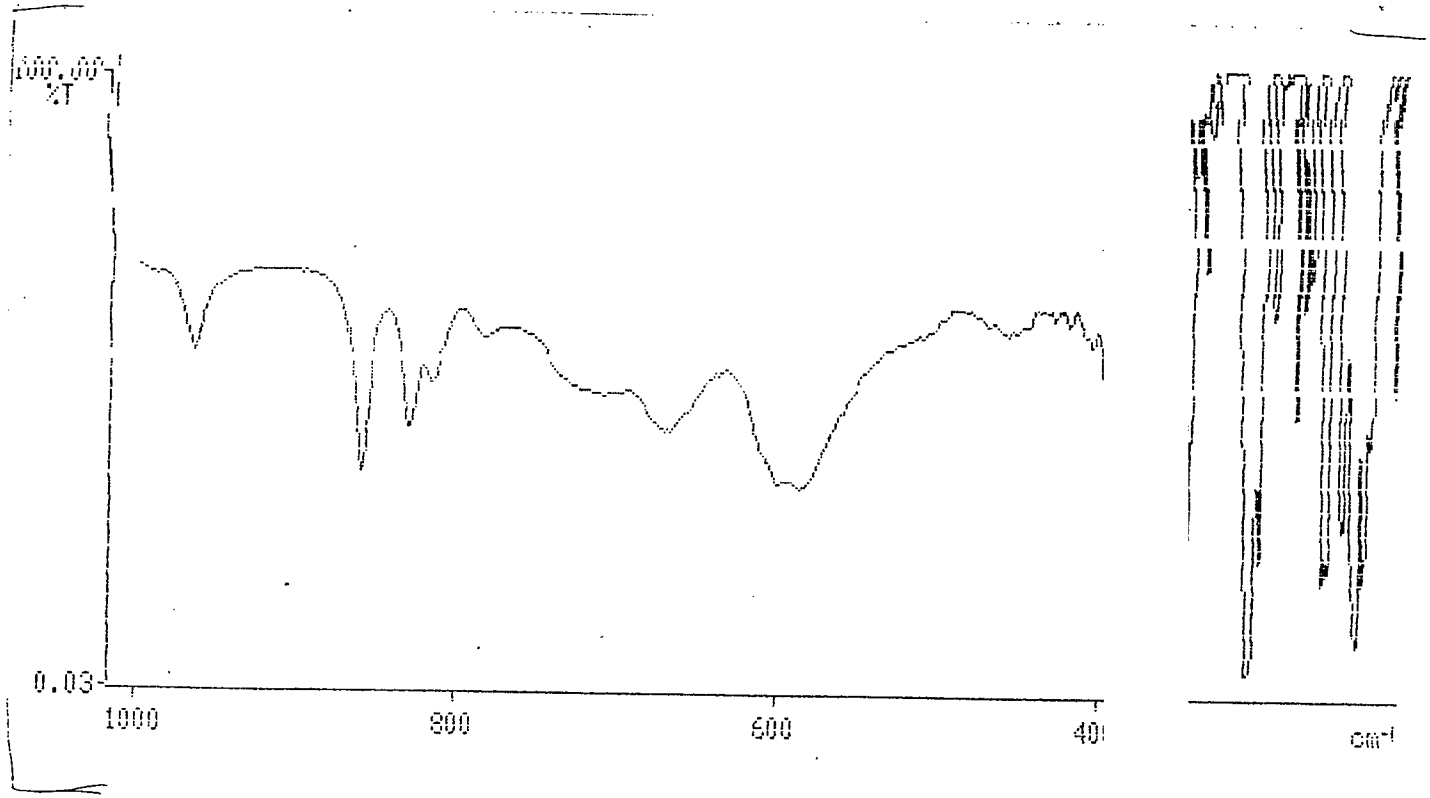

Fig. 3.13 Infra red spectrum of $CoCO_3N_2H$

In thermal analysis, all the precursors, whether carbonate based or hydrazido carboxylate based or nitrilotriacetate based, used in this investigation, when decomposed by heating at a constant heating rate of 10 degree per minute in nitrogen atmosphere, were found to yield Co_2O_3.

3.3.2 COMBUSTION RESIDUES

Irrespective of the method of decomposition (Section 3.1.1) of these precursors, mentioned above, the combustion residues were invariably found to be dark in colour, though vary in texture. Percentage of cobalt in the combustion residues was found to be very close (Table 3.1) to the theoretical value for Co in Co_3O_4, thus confirming the assigned formula for the residues.

Infrared spectra of all the samples (residues) are almost superimposable (Fig.3.1 to 3.3) with the metal-oxygen stretching frequencies in the samples appearing (Table3.1) at around 570 and 660 cm^{-1} and are in good agreement with the reported values for Co_3O_4.

Similarly, the X-ray powder patterns (Figs. 3.7 to 3.9) of different combustion residues are almost identical with the calculated d-values for 100% relative intensity being about 2.4 (Table 3.3). Indexing for the samples, which was done with the help of the programme mentioned in Section 3.2.4, indicates that these Co_3O_4 samples have cubic crystalline structure with 100% relative intensity appearing for 311 plane and the lattice parameter a = 8.06 (approx.). Structural parameters calculated from the X-ray diffraction data are given in Table 3.3.

Average crystallite diameter of the Co_3O_4 samples in the combustion residues was calculated by using the Scherrer's equation. The crystallite size determination was based

Table 3.5 Average Crystallite diameter of different Co_3O_4 sample Calculated from X-ray diffraction data by using Scherrer's equation [15].

Samples	Crystallite diameter
CC-I	63.02
CC-II	65.72
CC-III	86.64
CC-IV	49.65
CN	41.35
CH-I	41.35
CH-II	69.35
CH-III	-
CH-IV	34.07
CT-I	49.69
CT-II	63.02
CT-III	49.65
CT-IV	41.35

on 311 peak, which exhibited maximum height (Figs 3.7 to 3.9) for all the samples. The results are presented in Table 3.5, which indicate the formation of nano size particles for Co_3O_4 with the crystallite diameter within 1-100 nm.

This was further confirmed with the scanning electron micrographs (Figs 3.10 to 3.12) of the samples.Though Co_2O_3 was the final residue obtained in the thermal analysis of the precursors, during the decomposition of these precursors, either in a preheated crucible or solar induced, it was found that the combustion residue was invariably Co_3O_4 as is evident from the chemical analysis data or the instrumental analysis, namely infrared spectroscopy and X ray analysis.

Thermal analysis of the combustion residues was carried out by heating the samples at 10 ^{0}C/min in nitrogen atmosphere. Most of the samples were found to show about 1.4% weight loss in the TGA with no complementary peak observed in the DTA. This step, which was continuous as seen in the TGA, was observed in the temperature range 40-150 ^{0}C. This loss in the weight is probably due to the loss of small amount of moisture the samples might have absorbed.

The next step in the thermal analysis is observed in the temperature range of 760-820 ^{0}C, for all the samples (combustion residues). And the weight loss of about 6.5 % in the TGA in this temperature range, with a complementary peak in the DTA, could be assigned to the decomposition of Co_3O_4. Thus,

$$2Co_3O_4 \longrightarrow 6CoO + O_2$$

Theoretical percentage weight loss for the reaction, based on calculation, is 6.644%. Decomposition of Co_3O_4 is known [12] to occur, in this temperature range, to yield CoO.

REFERENCES

1. S. Trassatti, "*Electrodes of Conductive Metallic Oxides*", Elsevier Scientific Publishing comp., Amsterdam, (1980).
2. C. N. R. Rao, "*Chemical Approaches to the Synthesis of Inorganic Materials*," Wiley Eastern Ltd, New Delhi, (1994).
3. M. B. Tarasevich and B. Efremov, "*Electrodes of Conductive Metallic Oxides*", Elsevier Scientific Publishing comp., Amsterdam, (1980).
4. E. W. Schmidt, "*Hydrazine and its Derivatives*", John Wiley & Sons (1984).
5. K. C. Patil, and M. A. Sekar, *J. Self-propagating High Temperature Synthesis*, 2, 3 (1994).
6. a) K. C. Patil, J. S. Budkuley and V. R. Pai Vernekar, *J. Inorg. Nucl. Chem.*, 41 (1979) 953.

   b) J. S. Budkuley, and G. K. Naik, Thermochimica Acta, 320 (1998) 115-120.
7. J. Bassett, R. C. Denney, G. H. Jeffrey and J. Mendham, '*Vogels Textbook of Quantitative Inorg. Anal.* E. L. B. Longman, (1979) 324.
8. K. Nakamoto, "*Infra-red and Raman Spectra of Inorganic and Coordination Compounds"*, John Wiley & sons, New York, (1963).
9. Richard Nyquist and Ronald O.' Kagel, "*Infra-Red Spectra of Inorganic Compounds*", Harcourt Brace Jovanovich Publishers, New York, (1971).
10. (a) C. J. Keatch and D. Dollimore, *"An Introduction to Thermogravimetry"*, 2nd Edn., Heyden, London (1975).

    (b) P. V. Ravindran and A. K. Sundaram, *"Thermal Analysis manual"*, Ind.

Chem. Soc., Bombay (1979).

11. K. Krawczyk, J. Petryk and K. Schmidt-Szalowski, "*Preparation of Catalysts VI*', Elsevier Science B. V., G. Poncelet, (1995).

12. JCPDS-International Center for Diffraction Data, PCPDFWIN v. 1.30 (1997)

13. J. P. Singh and R. N. Singh, *Ind. J. Chem.* 39 A (2000) 819.

15. H. P. Klug and L. E. Alexander, *X-Ray Diffraction Procedures*, Wiley, New York (1962).

16. K.S.W. Sing, D. H. Everett, R.A.W. Haul, L. Moscow, R.A. Pierotti, J. Rouquerol and T. Siemieniewska, *Pure & Appl. Chem.*, 57, 4(1985) 603.

17. P. Lahiri and S. K. Sengupta, *"Catalysis Modern trends"*, N. M. Gupta, D. K. chakrabarty, eds.1995, Narosa Publishing house, New Delhi P. 301-304.

18. M. H. Grubelmann and A. F. Williams, *Struct. Bonding*, 55 (1983) 1.

CHAPTER I V

CHAPTER IV

CATALYTIC AND ELECTROCATALYTIC ACTIVITY

INTRODUCTION

The electrochemical reduction of oxygen is known to follow either of the following pathways in alkaline solution.

1. ***Direct 4-electron pathway***

$$O_2 + 4e^- + 2H_2O \longrightarrow 4OH^- \qquad E = 0.401V \qquad (1)$$

2. ***Indirect Peroxide pathway***

$$O_2 + H_2O + 2e^- \longrightarrow HO_2^- + OH^- \qquad E = -0.065V \qquad (2)$$

Indirect peroxide mechanism involves the intermediate formation of peroxide HO_2^-. The efficiency of oxygen reduction therefore depends on the removal of the peroxide intermediate as fast as it is formed. Hence it is desirable that the active catalyst compound has a high H_2O_2 decomposition activity to ensure facile reduction kinetics. This chapter is therefore divided into the following subsection.

4.1 Heterogeneous decomposition of H_2O_2

4.2 Electrocatalytic Activity

4.3 CV studies

4.4 Results and Discussion

(Correlation of electrochemical activity with chemical and structural feature of the catalyst.)

4.1 DECOMPOSITION OF H_2O_2 ON Co_3O_4

4.1.1 PRINCIPLES

On metal oxides of variable valences, the catalytic decomposition of hydrogen peroxide proceeds by a mechanism where oxidation and reduction of the catalyst occurs.

The reaction mechanism of decomposition of hydrogen peroxide is said to proceed through following two pathways [1].

(1) A redox pathway where electron transfer occurs on the surface of the catalysts and two free radicals H^+ and HO_2^- are formed.

(2) Chain reaction pathways where the further reaction of free radicals occur.

Some of the conclusions drawn on the basis of the experiments performed for the semiconductive oxides are as follows:

Metal oxides composites and pure oxides of mixed valences are found to be more active catalyst then simple monovalent metal oxides.

The rate-determining step in decomposition of hydrogen peroxide is the removal of electron.

* The rate of the reaction depends on catalyst surface area.
* The experimentally obtained activation energy is a very important parameter for rate of reaction.
* For studying the decomposition of H_2O_2, gasometry is a preferred method over titrimetry.

The role played by the transition metal oxides in the decomposition of the intermediate H_2O_2 formed during oxygen reduction reaction as an electrocatalyst is

found to be heterogeneous However, it has been found out [2] that this assumption is not correct for Co_3O_4/graphite electrodes. According to this report the decomposition of H_2O_2 formed as an intermediate decomposes by participation of dissolved Co^{2+} ion in the form of the dicobaltite ion $HCoO_2^-$ in concentrated alkaline solution.

4.1.2 EXPERIMENTAL

Co_3O_4 samples prepared by different methods as explained in chapter III were used for studying their general catalytic and electrocatalytic properties. Decomposition of H_2O_2 in presence of the catalyst in alkaline (KOH) medium was monitored gasometrically. Using these samples with carbon support, similar experiments were carried out since the electrocatalytic properties were to be investigated, later on with this support.

The decomposition reaction of H_2O_2 on different Co_3O_4 samples was monitored by conventional gasometric technique proposed by Cota et al [3] and shown in Fig. 4.1 shows the gasometric apparatus used for the study of H_2O_2 decomposition reaction. (30% W: W) H_2O_2 was used for this purpose. The concentration of H_2O_2 was determined by titration with standard 0.1N $KMnO_4$ solution in acidic media. And is found to be 1.3N. 6N KOH was prepared in de-ionized water and taken along with 0.025g of the catalyst sample in a reaction vessel. 2.5mL of 1.3N H_2O_2 was then mixed and the volume of oxygen liberated was measured in a burette at room temperature. The experiment was repeated for all the samples, each at three different temperatures.

Different Co_3O_4 samples, on carbon support, were also used to study the catalytic activity in the decomposition of H_2O_2. The Co_3O_4 samples were mixed with

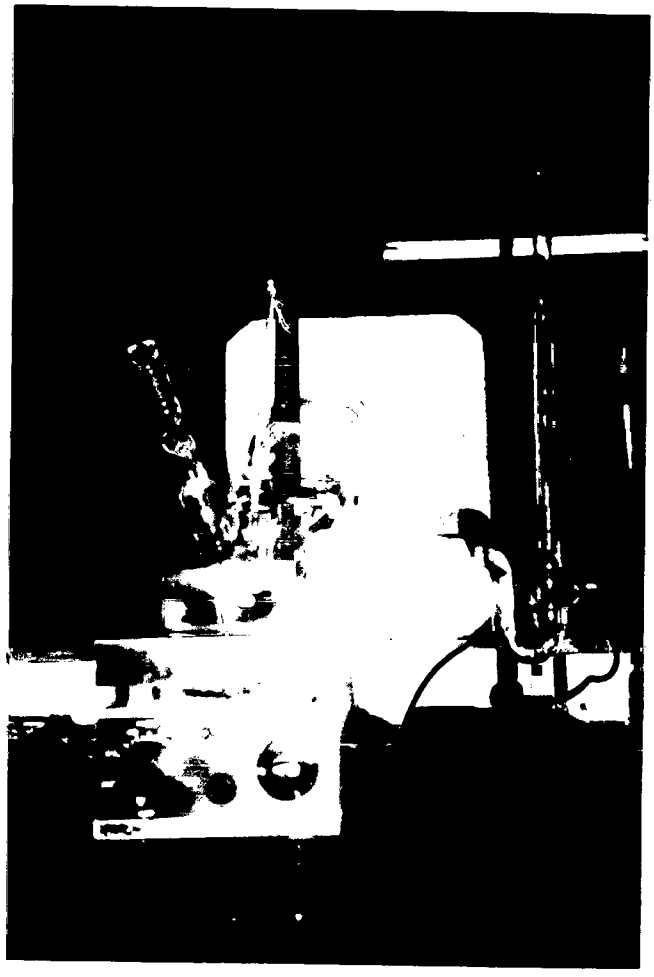

Fig. 4.1 Gasometric apparatus used for the study of H_2O_2 decomposition reaction

Vulcan carbon in two different ways, so as to monitor the changes occurring in the activity by changing the mixing conditions of the catalyst with carbon.

1. By using the precursor in presence of carbon and then decomposing the same.
2. By manually grinding the catalyst with Vulcan carbon in pestle and mortar.

Preparative conditions for catalyst samples on carbon support are tabulated in Table 4.1

4.1.3 OBSERVATION

Observed values for the volume of water displaced at different time interval in the kinetic (gasometric) study of the H_2O_2 decomposition were found to fit well in the first order formula. The different values obtained for the rate constants of the reaction, both by calculation and graphically are given in the Table 4.2 a and b. Comparison of catalytic activity of various Co_3O_4 catalysts, as illustrated by plotting a graph of (V_{max}-V) mL vs. t mins at an initial conc. of 0.135N of H_2O_2, gives the knowledge of the influence of catalyst sample on the rate of decomposition. Fig 4.2 shows the plot of (Vmax-V) mL vs. t min and Fig 4.3 shows the plot of log [Vmax/Vmax-V] vs. time in mins. The decomposition reactions of H_2O_2 on different Co_3O_4 samples are studied in temperature range between 298-328K. The concentration of peroxide was maintained at 0.135M. Fig 4.4 shows the Arrehenius plots using rate constants vs. 1/T. The Arrehenius activation energies, Ea values were calculated from the slopes obtained from the plot of rate constants vs. 1/T. The different values of Ea obtained for different Co_3O_4 samples are shown in the Table- 4.2

Table no. 4.1 Method of preparation of different 20% Co_3O_4/C & 20% Pt/C

Sr. no.	Sample 20%	Method of preparation	Decomposition	Mode of prepn.
1 1st	CC-I (P) Co_3O_4/C	0.230g of $CoCO_3$ + 0.620Vc + 0.099g of HH, stirred on a stirrer, for 24 hrs.	Decomposed in preheated silica crucible on burner.	Precursor
2	CC-I (G) Co_3O_4/C	0.0399g of Co_3O_4 (CC-I) + 0.156g of Vc	Grinded	Grinding
3	CC-II (P) Co_3O_4/C	0.230g of $CoCO_3$ + 0.620Vc + 0.099g of HH, stirred on a stirrer, for 24 hrs.	Decomposed in preheated platinum Crucible on burner	Precursor
4	CC-II (G) Co_3O_4/C	0.0399g of Co_3O_4 (CC-II) + 0.156g of Vc	Grinded	Grinding
5	CC-III (P) Co_3O_4/C	0.230g of $CoCO_3$ + 0.620Vc + 0.099g of HH, stirred on a stirrer, for 24 hrs.	Decomposed in preheated silica crucible in presence Of sunlight	Precursor
6	CC-III (G) Co_3O_4/C	0.0399g Co_3O_4 (CC-III)+ 0.156g of Vc	Grinded	Grinding
7	CC-IV (P) Co_3O_4/C	0.230g $CoCO_3$ + 0.620gVc + 0.099g HH, stirred on a stirrer, for 24 hrs.	Decomposed in preheated silica crucible in presence Of sunlight	Precursor
8	CC-IV (G) Co_3O_4/C	0.0399g Co_3O_4 (CC-IV)+ 0.156g of Vc	Grinded	Grinding
9 2nd	CH-I (G) Co_3O_4/C	0.0399g Co_3O_4 (CH-I)+ 0.156g of Vc	Grinded	Grinding
10 3rd	CN (P) Co_3O_4/C	0.287g$Co(NO_3)_2$+ water + 0.0319g VC + 0.100g HH + 0.371g NTA	Mixed in an evaporating dish & sintered on burner	Precursor
11	CN (G) Co_3O_4/C	0.0399g Co_3O_4 (CN) + 0.156g of Vc	Grinded	Grinding
12 4th	CT-I (P) Co_3O_4/C	0.068g Precursor (CT) + 0.0781gVc the two were mixed properly	Decomposed in preheated silica crucible on burner	Precursor
13	CT-I (G) Co_3O_4/C	0.0399g Co_3O_4 (CT-I) + 0.156g of Vc	Grinded	Grinding

14	CT-II (P) Co_3O_4/C	0.068g Precursor (CT) + 0.0781gVc the two were mixed properly	Decomposed in Preheated platinum Crucible on burner	Precursor
15	CT-II (G) Co_3O_4/C	0.0399g Co_3O_4 (CT-II) + 0.156g of Vc	Grinded	Grinding
16	CT-III (P) Co_3O_4/C	0.068g Precursor (CT) + 0.0781gVc the two were mixed properly	Decomposed in preheated platinum crucible in presence of sunlight	Precursor
17	CT-III (G) Co_3O_4/C	0.0399g Co_3O_4 (CT-III) + 0.156g of Vc	Grinded	Grinding
18	CT-IV (P) Co_3O_4/C	0.068g Precursor (CT) + 0.0781gVc the two were mixed properly	Decomposed in preheated silica crucible in presence of sunlight	Precursor
19	CT-IV (G) Co_3O_4/C	0.0399g Co_3O_4 (CT-IV) + 0.156g of Vc	Grinded	Grinding
20	Pt/C	Was prepared by using $Na_6Pt(SO_3)_4$ salt and vulcan carbon.	Was reduced with formic acid and dried in oven at 80°C.	

Table 4.2 Different kinetic parameters obtained from decomposition of Hydrogen Peroxide reaction

SAMPLES	Kc Sec^{-1}	KG Sec^{-1}	Eac Kcal	EaG Kcal	Ac	AG
	0.262	0.343				
CC-I	0.146	0.24	15.74	13.71	1.567	1.603
	2.2	2.07				
	0.048	0.042				
CC-I (P)	0.188	0.175	25.62	19.73	1.633	0.9843
	1.38	0.677				
	0.095	0.124				
CC-I (G)	0.17	0.218	7.18	7.59	0.3133	0.3491
	0.27	0.401				
	0.142	0.153				
CC-II	0.501	0.502	8.74	8.46	0.7079	0.7047
	0.507	0.512				
	0.077	0.105				
CC-II (P)	0.082	0.112	3.46	5.79	0.1253	0.1462
	0.126	0.146				
	0.079	0.119				
CC-II (G)	0.106	0.132	6.95	7.34	0.2153	0.2228
	0.210	0.241				
	0.213	0.24				
CC-III	0.353	0.429	4.34	2.49	0.4395	0.4102
	0.386	0.413				
	0.298	0.368				
CC-III (P)	0.757	0.849	3.57	4.49	0.7762	0.1112
	0.510	0.707				
	0.128	0.138				
CC-III (G)	0.150	0.354	2.97	3.88	0.1986	0.3126
	0.194	0.238				
	0.186	0.173				
CC-IV	0.410	0.384	6.45	7.15	0.5848	0.6266

	0.482	0.524				
	0.219	0.200				
CC-IV (P)	0.411	0.446	10.25	8.44	0.9616	0.7691
	0.938	0.646				
	0.101	0.108				
CC-IV (G)	0.135	0.218	6.9	7.82	0.3020	0.3936
	0.295	0.338				
	0.319	0.331				
CT	0.442	0.334	3.24	1.07	0.5546	0.3606
	0.516	0.361				
	0.118	0.13				
CT-I (P)	0.214	0.18	9.6	6.6	0.4898	0.3483
	0.442	0.33				
	0.12	0.148				
CT-I (G)	0.59	0.59	11.38	10.66	0.9642	0.9817
	0.658	0.658				
	0.233	0.311				
CT-II	0.744	0.963	6.65	5.44	0.8519	0.8778
	0.627	0.712				
	0.411	0.582				
CT-II (P)	0.513	0.641	6.89	4.73	1.091	1.12
	1.09	1.15				
	0.105	0.163				
CT-II (G)	0.203	0.253	6.1	6.9	0.3141	0.2897
	0.27	0.261				
	0.307	0.194				
CT-III	0.536	0.584	2.3	6.94	0.4989	0.7079
	0.425	0.529				
CT-III (P)	1.09	1.26	4.57	5.3	0.6486	0.7079
	1.49	2.0				
	0.167	0.17				
CT-III (G)	0.179	0.241	6.29	7.11	0.3855	0.4966

	0.401	0.477				
	0.214	0.214				
CT-IV	0.563	0.434	6.95	6.52	0.7534	0.5808
	0.586	0.485				
	0.125	0.141				
CT-IV (P)	0.134	0.154	2.5	2.45	0.228	0.284
	0.35	0.308				
	0.114	0.135				
CT-IV (G)	0.144	0.194	2.88	2.57	0.3327	0.3802
	0.3	0.329				
	0.135	0.141				
CN	0.335	0.399	9.81	10.35	0.6839	0.7328
	0.568	0.574				
	0.726	0.784				
CN (P)	1.5	1.46	3.35	2.75	1.409	1.39
	1.16	1.17				
	0.099	0.097				
CN (G)	0.116	0.145	2.95	2.95	0.1995	0.1841
	0.178	0.168				
	0.104	0.142				
CH	0.172	0.185	15.1	15.9	0.7586	0.6026
	0.747	0.598				
	0.135	0.141				
CH-I	0.353	0.396	11.05	10.06	0.6982	0.7396
	0.568	0.574				

4.1.4 RESULT AND DISCUSSION

Peroxide decomposition on Co_3O_4 samples appears to follow first order kinetics. It is found that the addition of high surface area Vulcan carbon to different Co_3O_4 samples prepared by precursor methods lowers the activation energy for most of the samples. Sample CC-III (G) and sample CT-IV (P) are found to exhibit lowest activation energy thus showing high catalytic activity.

4.2 ELECTROCATALYTIC ACTIVITY

4.2.1 GENERAL PRINCIPLE AND LITERATURE STATUS

Electrocatalysis is a science of minimizing the overpotential terms each given by Tafel equation.

$$|\eta| = \frac{2.303RT}{\alpha nF} \log \frac{i}{i_o} \qquad (3)$$

$$|\eta| = \frac{0.0591}{n\alpha} \log \frac{i}{i_o} \qquad (4)$$

Where 'i' is the current density corresponding to the overpotential 'η', 'i_o' is equilibrium or exchange current density. 'α' is transfer coefficient. 'n' is the number of electrons transferred in the electrode reaction. and $0.0591/n\alpha$ mV/dec is known as Tafel slope. In most cases $\alpha = 0.5$, when one electron process is the rate-determining step. and the expected Tafel slope is 120 mV/decade. Hence experimental determination of Tafel slopes throws some light on understanding the reaction mechanism. while the

magnitude of exchange current density 'i_o' gives the idea of facility of electrode reaction kinetics.

Different methods are employed for the determination of the electrode kinetic parameters, which includes Tafel slopes, exchange current densities and limiting current values from the steady-state potential data. Recently, a new simplified method has been presented to determine the kinetic parameter of gas diffusion electrodes for oxygen reduction reaction [4].

Accordingly the current potential behavior of gas diffusion electrodes is described by

$$E = E_{ocp} + 1/\alpha f \ln[i_{ocp}(i_{l.c}-|i|)/|i|i_{l.c}]-|i|R_u \qquad (5)$$

Where E = observed potential, E_{ocp} = open circuit potential, i_{ocp}= Current corresponding to E_{ocp}, i = observed cathodic current, $i_{l.c}$ = cathodic limiting current, α= cathodic transfer coefficient , R_u = uncompensated resistance, f = F/RT where F = Faraday constant, R = gas constant, T = temperature.

Equation (5) is sigmoidal in shape and possesses an inflection point at which the first derivative of potential with respect to the current, i.e. (dE/d|i|), is maximum and, hence the second derivative becomes zero. Then differentiating equation (5) w. r. t current i yield:

$$\frac{dE}{d|i|} = -\frac{1}{\alpha f}\frac{1}{|i|} - \frac{1}{\alpha f(i_{l.c}-|i|)} - R_u \qquad (6)$$

On further differentiation. equation (6) becomes

$$\frac{d^2E}{d|i|^2} = \frac{1}{\alpha f}\frac{1}{|i|^2} - \frac{1}{\alpha f}\frac{1}{(i_{l.c} - |i|)^2} \qquad (7)$$

At the inflection point. $i = i_{inf}$. $d^2E/d|i_{inf}|^2 = 0$ and hence:

$$\frac{1}{\alpha f |i_{inf}|^2} = \frac{1}{\alpha f}\frac{1}{(i_{l.c} - |i_{inf}|)^2} \qquad (8)$$

or.

$$i_{l.c} = 2|i_{inf}| \qquad (9)$$

Thus. the limiting current. $i_{l.c}$ can be obtained by determining the value of the current at the inflection point which corresponds to the maximum in the plot of dE/d|i| versus 1/|i|.

After obtaining limiting current $i_{l.c}$. the other kinetic parameters are obtained from eqn. (6) by recasting it in the following form:

$$\frac{dE}{d|i|} = -\frac{1}{\alpha f}\frac{i_{l.c}}{|i|(i_{l.c} - |i|)} - R_u \qquad (10)$$

The plot of dE/d|i| versus $i_{l.c}/|i|(i_{l.c} - |i|)$ leads to a straight line with an intercept $= -R_u$ and a slope $= -1/\alpha f$. The value of i_{ocp} is obtained by substituting the values of R_u. α, $i_{l.c}$ in eqn.(5). The current potential data obtained for Co_3O_4/C gas diffusion electrodes is plotted using [4]. The above mentioned all parameters are calculated from the experimental current potential data. the Fig. 4.5. 4.6 and 4.7 shows the plots for

determination of inflection point from which limiting current and other parameters are determined.

The following scheme is suggested for the reduction of oxygen on metal oxide electrodes [5].

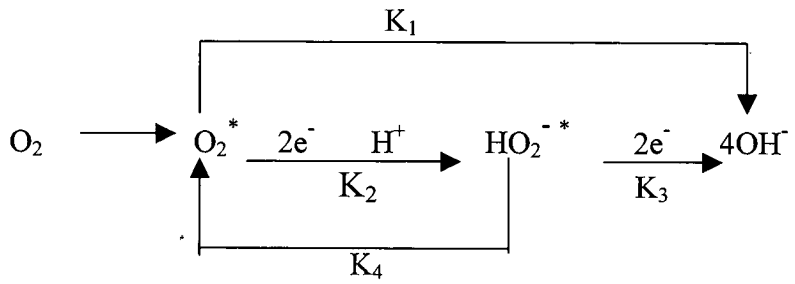

In the first step of the indirect path towards the HO_2^- as an intermediate, the chemical bond between the oxygen atoms of the molecule is not broken. The $4e^-$ reduction of oxygen in either acid or alkaline solution is of primary concern and are to its possible utilization in fuel cell and metal air batteries. On the basis of its high theoretical equilibrium potential of 1.23 volt vs. NHE. The majority of research on this reaction is centered in the use of noble metal electrode due to their relative stability in acidic and alkaline solution. The major efforts have been centered on the use of noble metals distribution as carbon electrodes, since carbon also has high stability both in acidic and alkaline solutions.

In order to develop cheaper catalysts, research has been concentrated on transition metal oxides such as pure or Li doped nickel oxides [6,7]. Nickel cobalt oxides [8,9] and cobalt iron oxides [10]. Also porphyrins and phthalocyanines showed high activity for oxygen reduction, but the activity is found to decrease with time due to

the slow dissolution of the transition metal from the complex into the solution [11,12]. It has been demonstrated that in cobalt spinels such as Co_3O_4 and $NiCo_2O_4$ [13,14] oxygen reduction mainly proceeds through $4e^-$ pathway while in their lower oxides (NiO, CoO, or their solid solutions Co_2O_3), it proceeds through $2x2e^-$ pathway, involving formation of HO_2^- without breaking the O-O bond [15,16]. Jiang et al [17] reported high catalytic activity and stability for Teflon bonded Co_3O_4/graphite electrodes owing to rapid dissociation of the peroxide intermediate through cobaltous ions present as dicobaltites $HCoO_2^-$. They proposed following reaction scheme

$$O_2 + H_2O + 2e^- \longrightarrow HO_2^- + OH^- \qquad (11)$$

$$Co_3O_4 \xrightarrow{\text{Strong alkali}} CoO + Co_2O_3 \qquad (12)$$

$$CoO + OH^- \longrightarrow HCoO_2^-{}_{(aq)} \qquad (13)$$

$$6\,HCoO_2^-{}_{(aq)} + 4HO_2^- \longrightarrow 2Co_3O_{4(S)} + 10OH^- + O_2 \qquad (14)$$

$$6\,HCoO_2^-{}_{(aq)} + 4HO_2^- \longrightarrow 2Co_2O_3 + 8OH^- + O_2 \qquad (15)$$

The HO_2^- is homogeneously decomposed by $HCoO_2^-$, even at very low concentration of $HCoO_2^-$ (~1ppm), while the transfer reaction of $HCoO_2^-$ in solution and Co^{3+} in the oxide lattice sites is heterogeneous. They reported Tafel slopes in the range 50-60 mV/decade at low overpotentials and 60-110 mV/decade at high overpotentials. Very recently Morales et al [18] have investigated sol-gel prepared pure and lead doped cobalt spinel type oxides Co_3O_4 and $PbCo_5O_x$ and found them to posses

high activity and good stability for electrocatalytic reduction of oxygen in alkaline medium.

The present investigation reports synthesis of cobalt oxide spinel though several new precursor routes and fabrication Teflon bonded carbon electrodes for evaluation of their electrocatalytic activity.

4.2.2 EXPERIMENTAL

(a) PREPARATION OF ELECTRODES

The electrode comprises of three layers. The electrodes are composed of nickel screen serving as a current collector and structural support for the electrode, the gas diffusion layer with its hydrophobic structure as an oxygen /air supplying zone, and an active catalyst layer as a reaction zone. PTFE provides hydrophobic and mechanical strength to the electrodes and is chemically inert. The materials constituting the construction of electrodes are as follows:

Active (catalyst) Layer	Catalyst on carbon PTFE	10-15%
Diffusion layer	Carbon PTFE	30-50%
Current collector	Nickel screen	-

Preparation of diffusion layer

The diffusion layer was prepared by taking 0.090g of Vulcan carbon sonicated with little water in ultrasonicator, 15% Teflon was added to the paste and after addition of cyclohexane, solution was again ultrasonicated. The diffusion layer was applied on the carbon cloth with the help of brush, the carbon cloth was dried in an oven, and again the diffusion layer was applied and dried. The procedure was repeated until the

required weight was obtained. The carbon cloth with diffusion layer is then sintered in furnace at 400°C for half an hour. The gas diffusion layer consists of gas supplying channel, it also helps in preventing the penetration of electrolyte and supports the active layer [19].

The electrode materials i. e. Co_3O_4 /C prepared in previous section is used for the preparation of electrodes. Table 4.1 shows the preparation of electrode samples. The catalyst loading was in the range of 7.45 $mgcm^{-2}$. Electrodes were made of carbon, binder and some kind of support. The carbon used in this work was Vulcan Carbon XC-72 (Cabot Corp.), PTFE was used as a binder. And a nickel screen was used as a support.

There are many methods of preparation of electrodes reported in literature such as pressing, rolling, screen-printing, spraying and tapecasting. In this work double layer Teflon bonded gas diffusion electrodes were prepared by pressing using method [20].

The electrodes were prepared by mixing Vulcan carbon with PTFE and catalyst. Co_3O_4 /C was mixed with 15% PTFE, few drops of water was added the mixture was mixed properly and isopropyl alcohol was added to the mixture and the paste is pasted on the carbon cloth already containing diffusion layer. The electrodes were then pressed at 240 Kg/cm^2 and then sintered at 350°C for half an hour in furnace.

The electrodes were dried, sintered and mounted on the nickel mesh, which was spot-welded to the nickel wire. The electrode, which was supported on nickel mesh, was then used for testing in half-cell. Fig. 4.8 shows flow sheet diagram for electrode preparation.

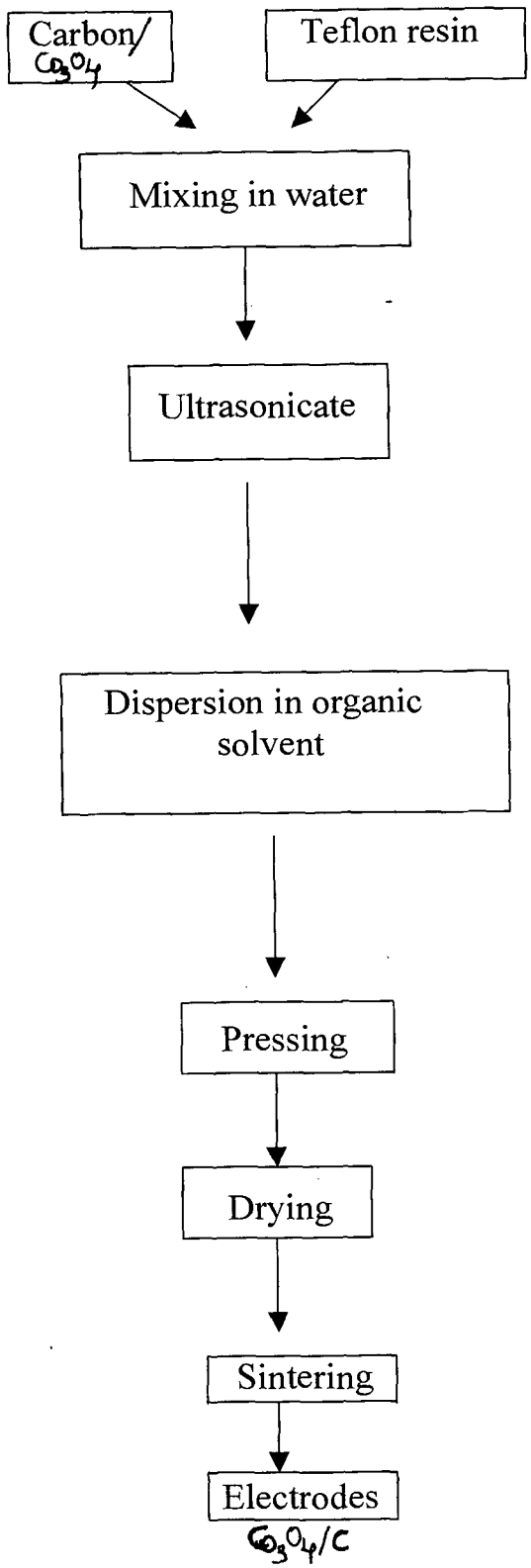

Fig. 4.8 Flow sheet for electrode preparation

(B) HALF CELL DESCRIPTION

The set up used for the electrochemical studies is shown in Fig. 4.9 The half-cell was used to obtain electrochemical measurements on the gas feed porous cathode where the electrodes were placed between the two walls of Plexiglas cell, which is then clamped with Teflon screw. The frontal view of the cell was exposed to electrolyte solution, and the other side of the electrode air/oxygen flowed to the electrode. Arrangements were made to control the flow of the air/oxygen passing towards the electrode as shown in the Fig. 4.9 The different parts constituting the half-cell are (a) Working electrode (b) Reference electrode (c) luggin capillary (d) counter electrode (e) thermometer (f) Teflon screw (g) gasket (h) magnetic pellet.

(C) POLARISATION

Steady state current potential curves for the Teflon bonded electrodes were obtained by galvanstatic polarization for the Teflon bonded electrodes obtained in 6MKOH at room temp. without IR correction. The electrode potentials were measured by using Hg/HgO, (KOH, 6mol L^{-1}) reference electrode attached with a lugin capillary to the working electrode having an area of 1.2 cm^2. The counter electrode was a nickel plaque placed in the same electrolyte. A thermometer was used to monitor the temperature. The electrolyte solution is constantly stirred, using a magnetic stirrer.

4.2.3 OBSERVATION

After the electrochemical measurements the data obtained is plotted as follows: Fig 4.10 shows the plot of Current density vs. Potential for CC (P) in presence of oxygen

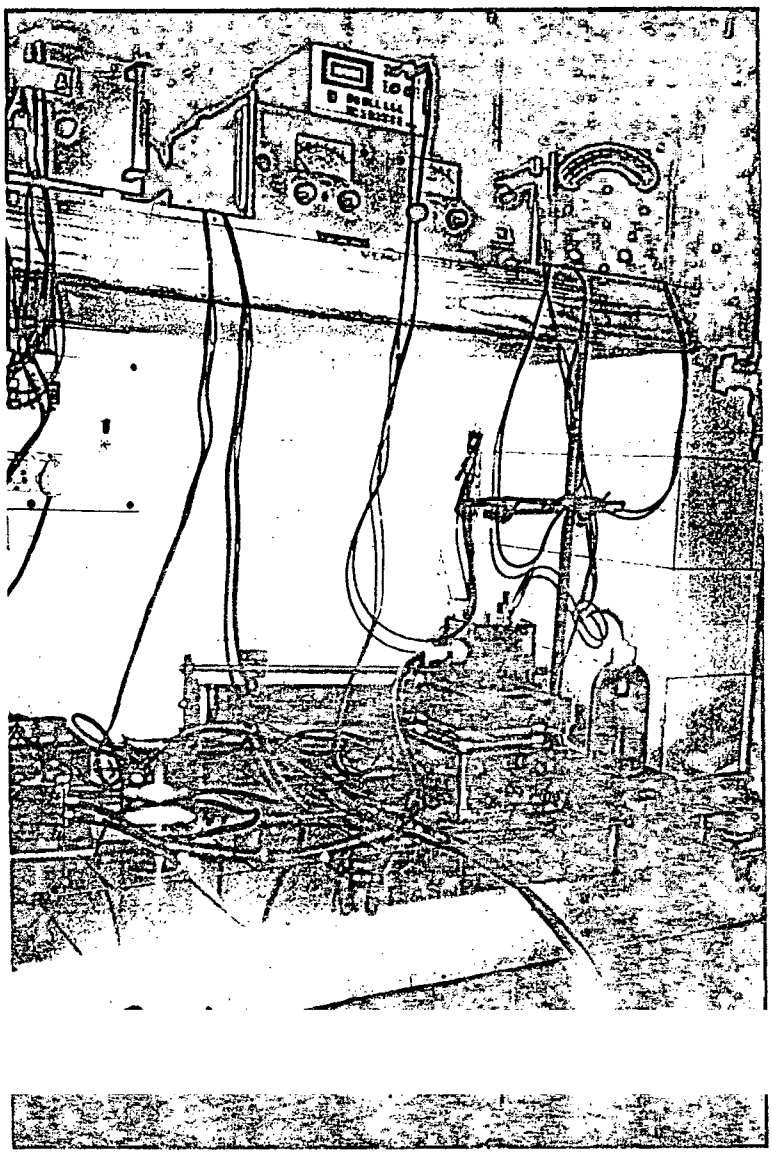

Fig. 4.9 Setup used for the electrochemical studies

Fig. 4.11 shows the plot of Current density vs. Potential for CC (P) method in presence of air. Fig 4.12 shows the plot of Current density vs. Potential for CC (G) in presence of oxygen. Fig 4.13 shows the plot of Current density vs. Potential for CN (P). CN (G). and method CH (G) in presence of oxygen. Fig 4.14 shows the plot of Current density vs. Potential for CT (P) method in presence of oxygen. Fig 4.15 shows the plot of Current density vs. Potential CT (G) method in presence of oxygen.

(In above all Figs. Plots the data obtained is compared with Pt/C and Vulcan carbon)

Fig 4.16 shows the plot of current density vs. CC samples in presence of oxygen. Fig 4.17 shows the plot of current density vs. CN. CH samples in presence of oxygen. Fig 4.18 shows the plot of current density vs. CT samples in presence of oxygen. Fig 4.19 shows the Tafel plots for CC (P). Fig. 4.20 Shows the Tafel plots for CC (G). and Fig.4.21 shows the Tafel plots for CN. CH. Fig. 4.22 Shows the Tafel plots for CT (P). Fig.4.23 shows the Tafel plots for CT (G) electrodes.

Fig 4.24 shows the plot of exchange current density vs. CC samples. Fig 4.25 shows the plot of exchange current density vs. CT samples. Fig 4.26 shows the plot of Transport hindrance of Co_3O_4 samples.

Table 4.3 (a) and (b) shows the different kinetic parameters obtained from steady state current potential data. such as exchange current density. Tafel slope. and Ru.

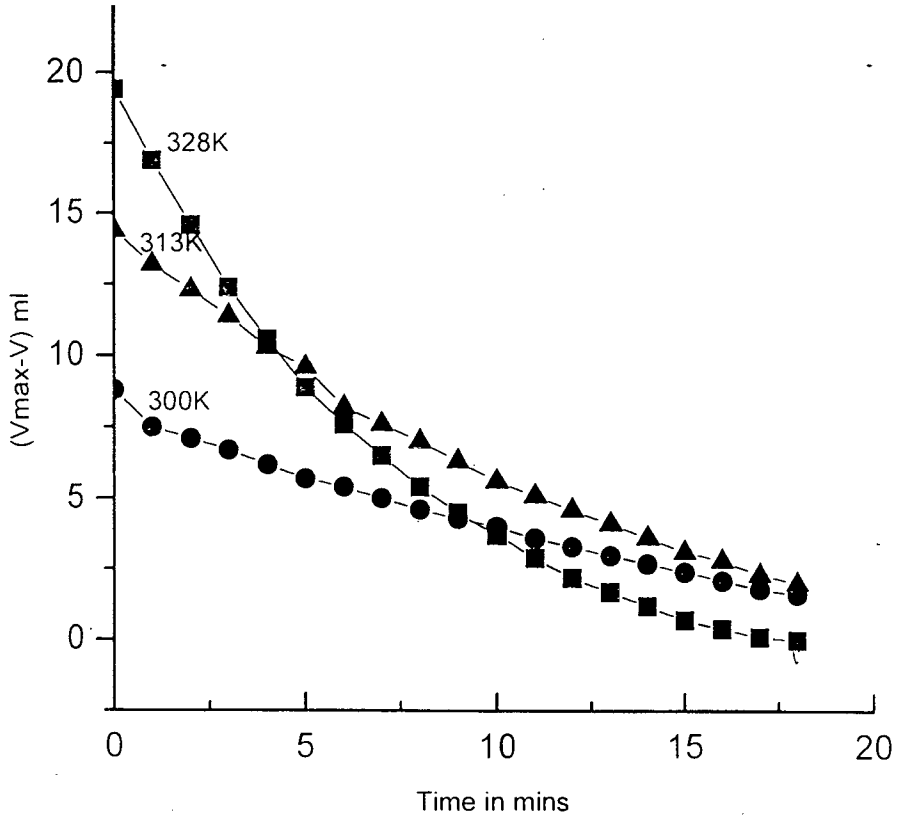

Fig.4.2 Plot of Vmax-V vs Time in mins

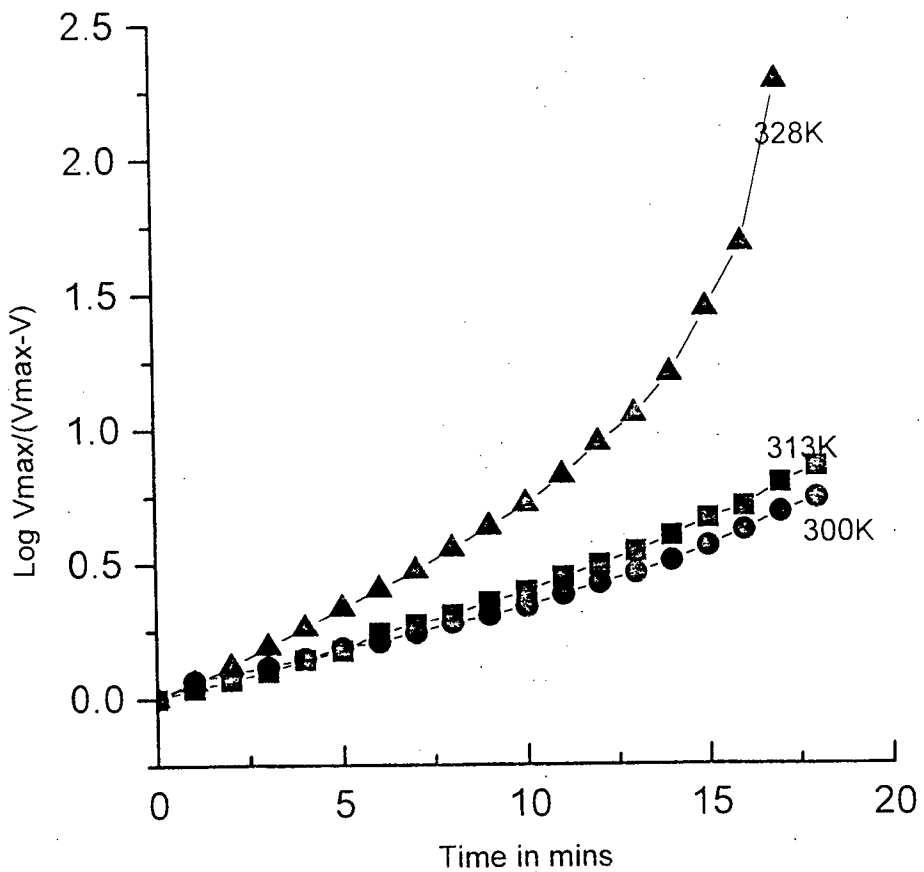

Fig. 4.3 Plot of Log Vmax/(Vmax-V) vs Time in mins

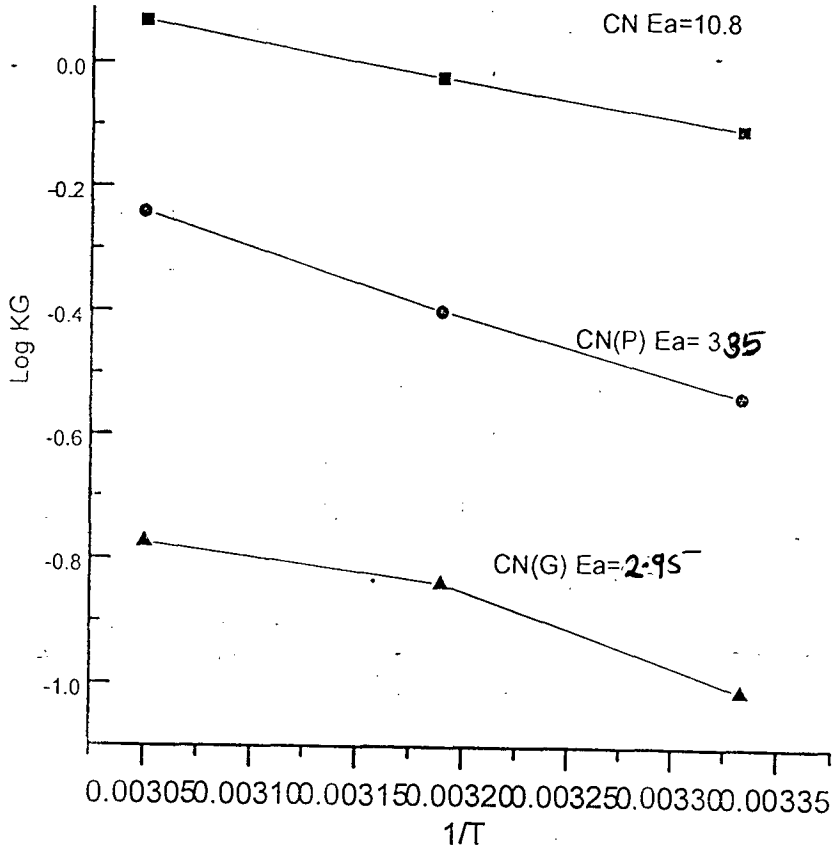

Fig.4.4 Arrehenius plot for sample CN, CN(P), CN(G)

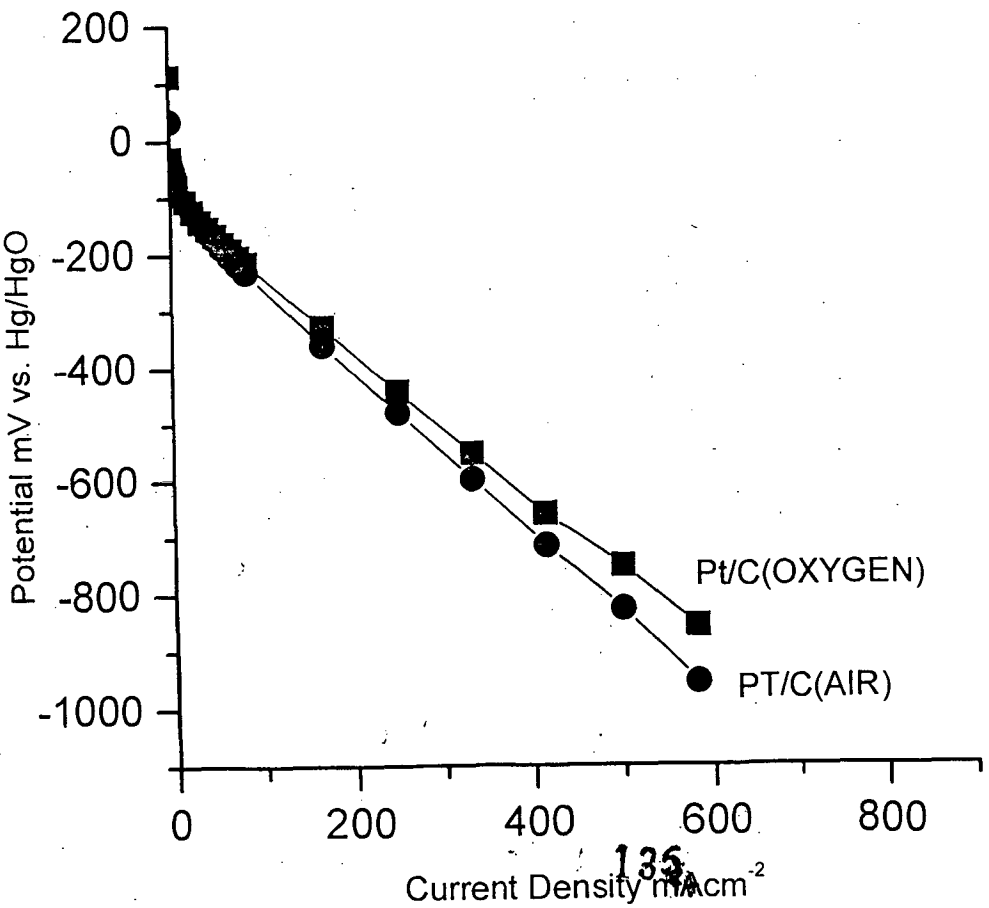

Fig. 4.5 Steady - state current Potential data for cathodic

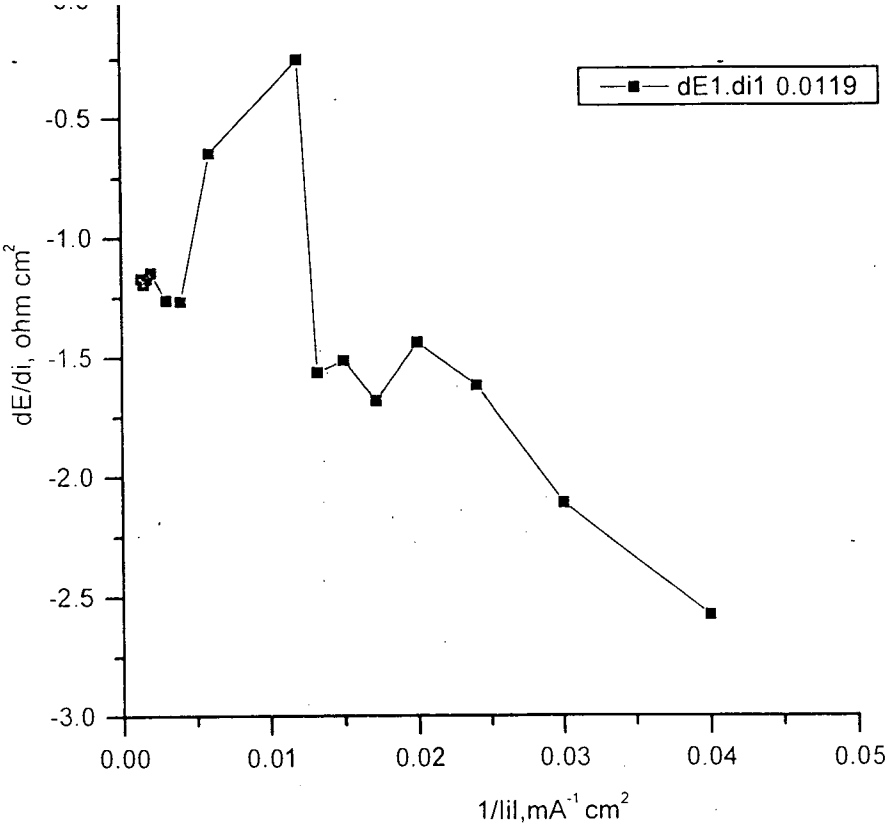

Fig.4.6 Plot of dE/diil vs. 1/iil for curve in Fig.4.5

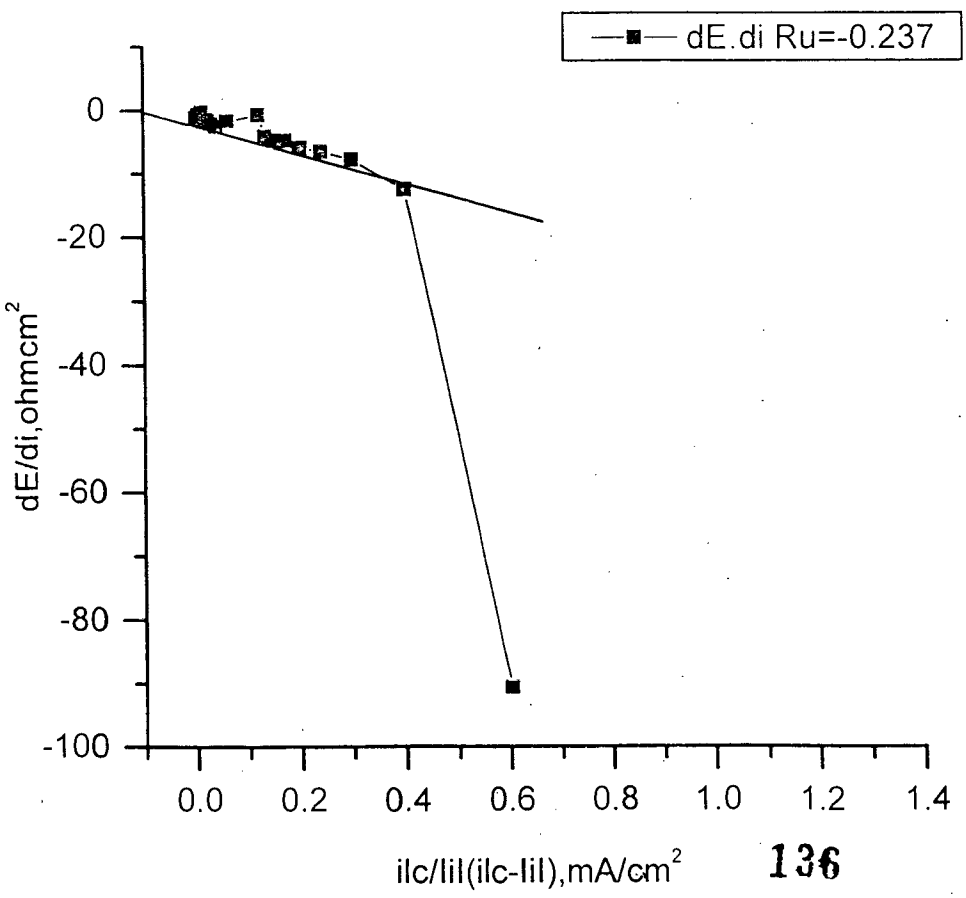

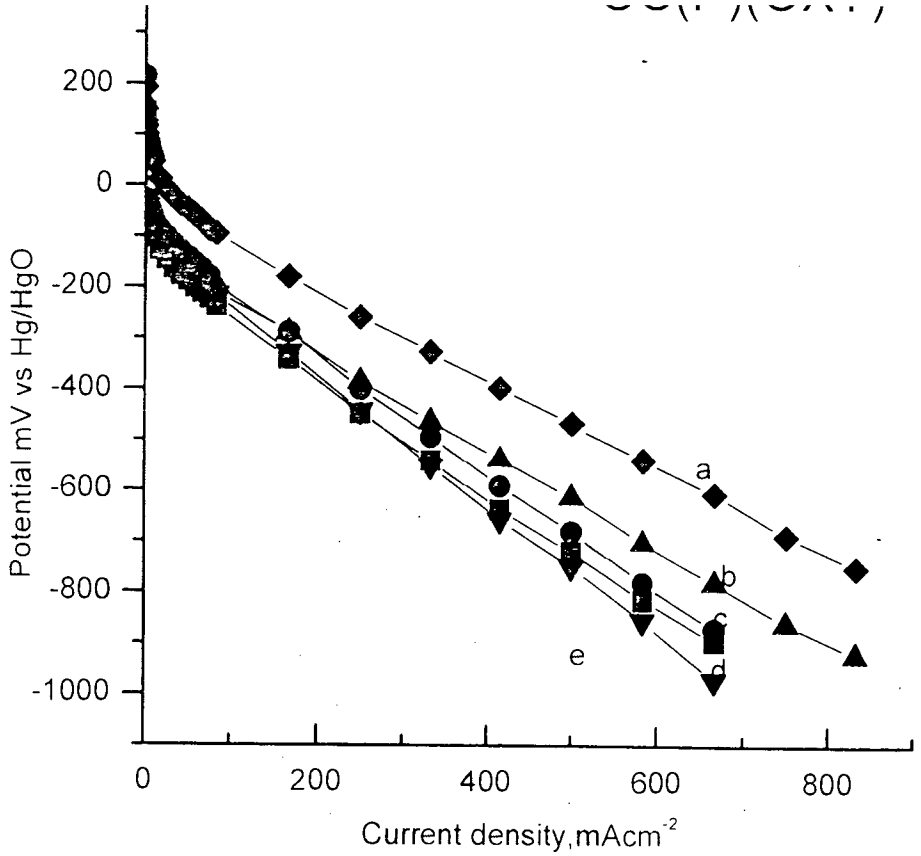

Fig. 4.10 Plot of potential vs. Current density,for(a)Pt/C,(b)CC-III, (C)CC-I,(d)CC-II,(e)CC-IV, samples in presence of Oxygen

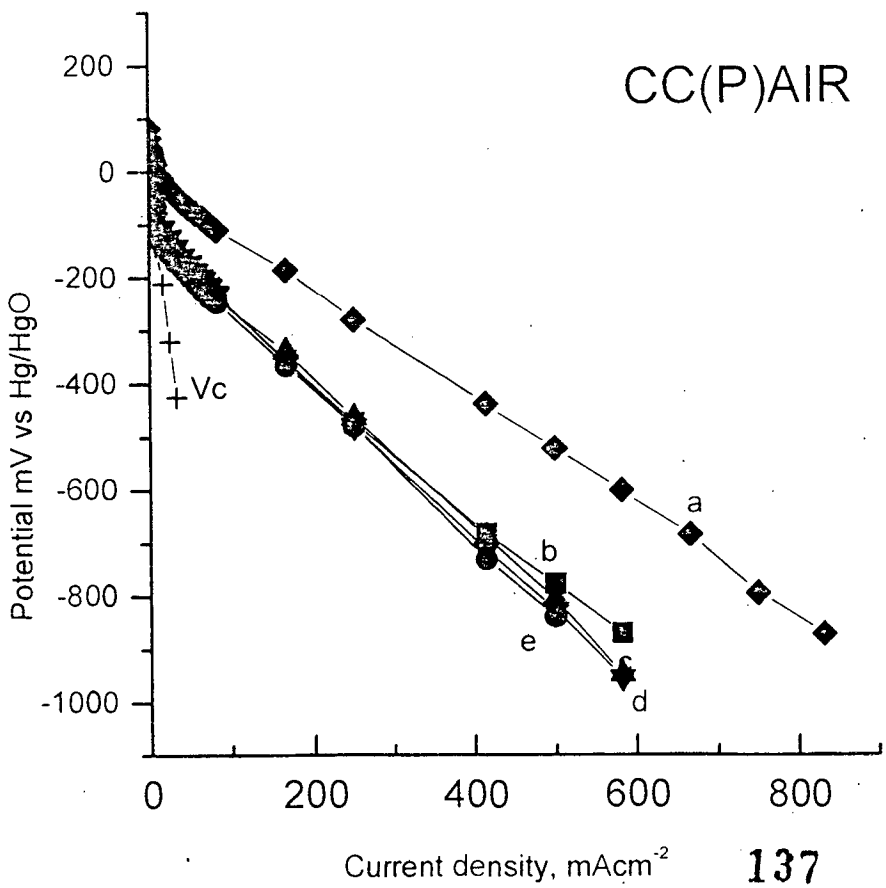

Fig. 4.11 Plot of Potential vs. Current density for (a) Pt/C (b) CC-I (c) CC-III (d)CC-IV (e) CC-II in presence of air

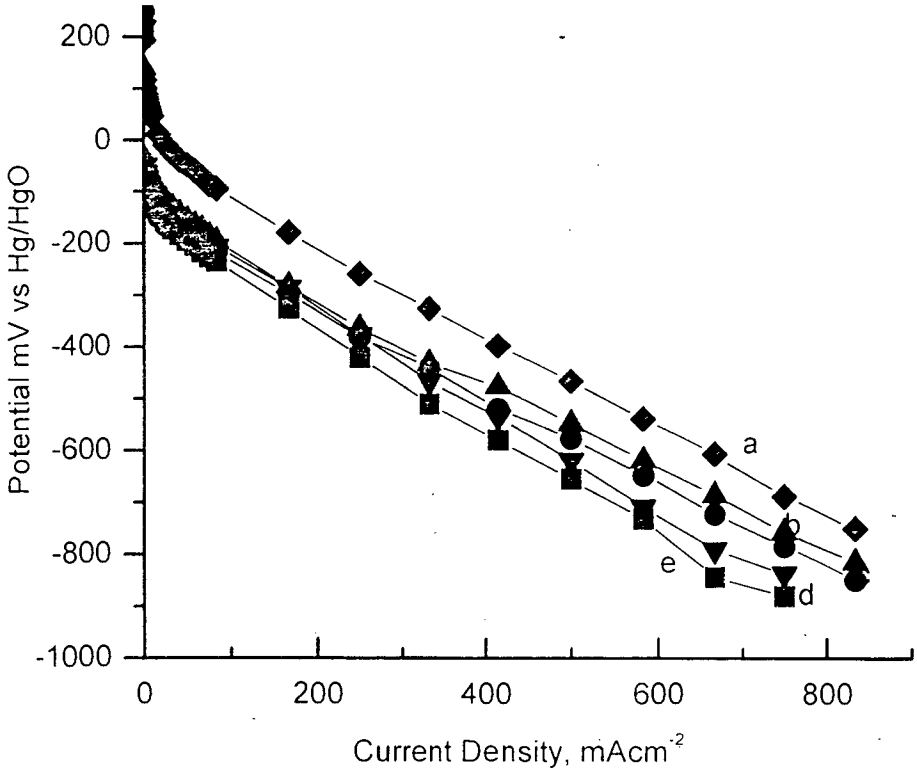

Fig. 4.12 Plot of potential vs current density for (a)Pt/C,(b)CC-III ,(C)CC-II,(d)CC-IV,(e)CC-I in presence of oxygen

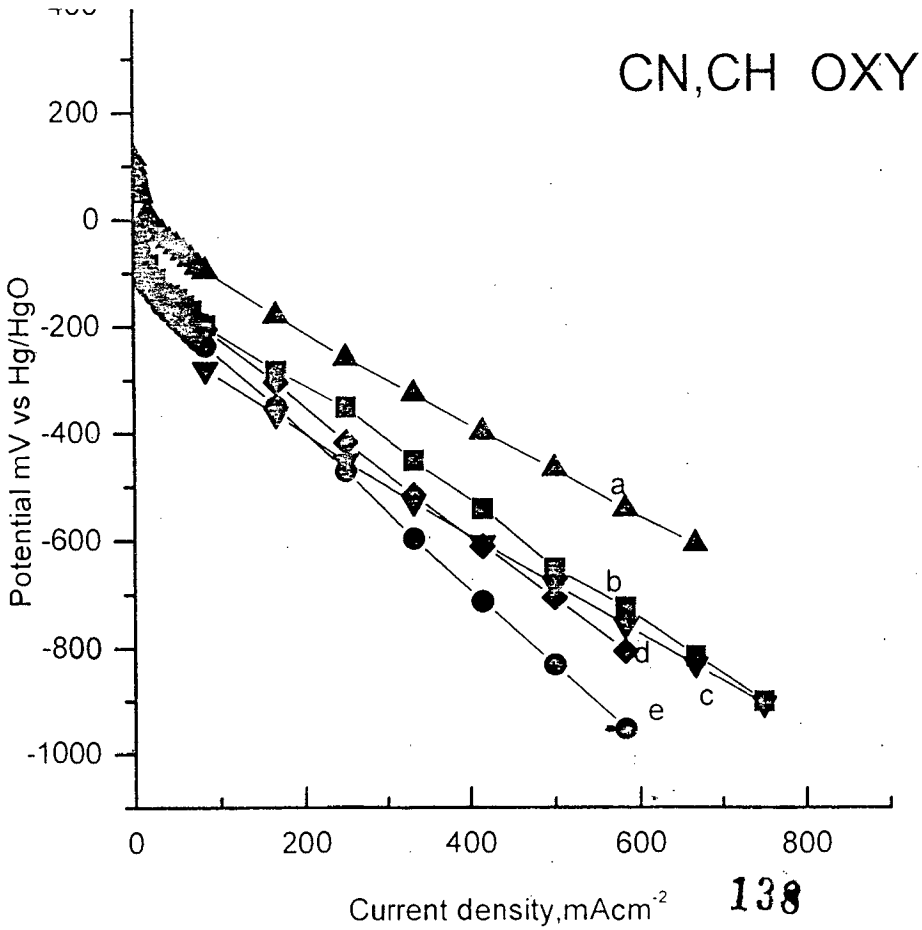

Fig 4.13 Plot of potential vs Current dnsity, for (a)Pt/C,(b) CN(G),

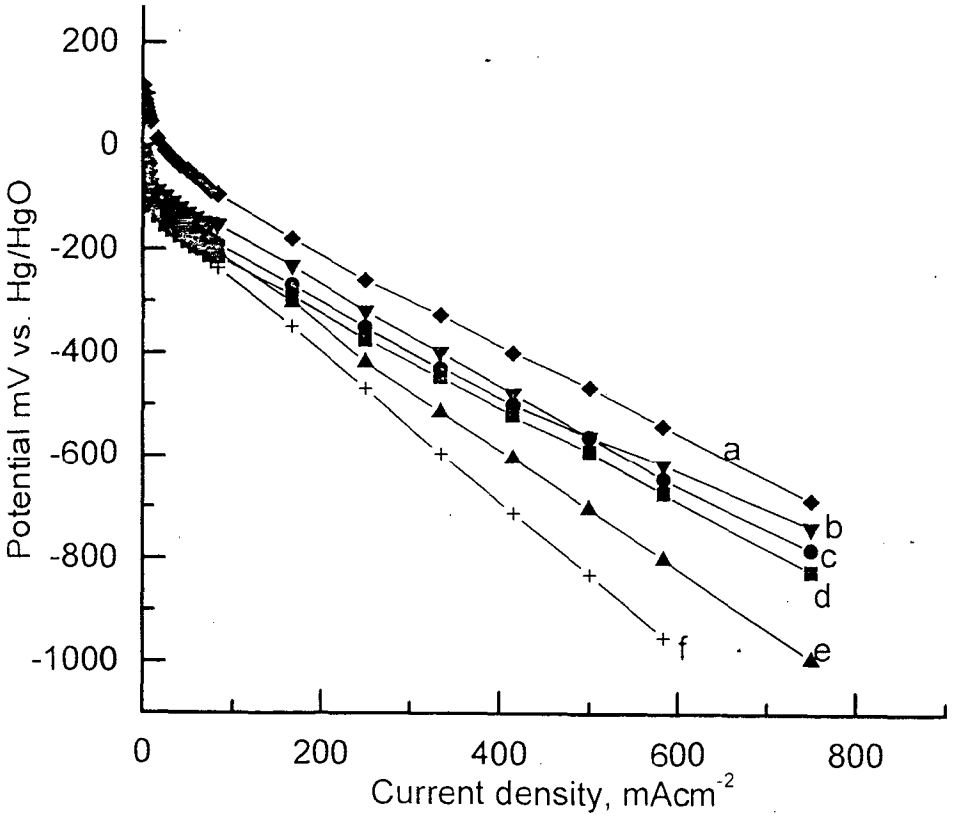

Fig. 14 Plot of potential vs. Current density for (a) Pt/C, (b) CT-IV, (c) CT-II, (d) CT-I, (e) CT-III, (f) Vc

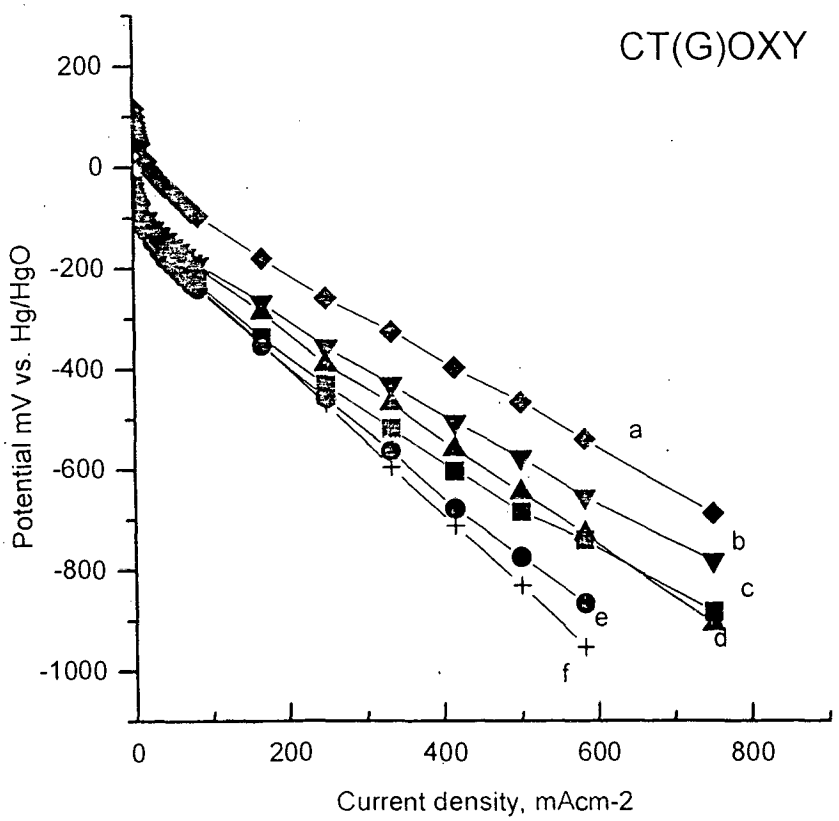

Fig. 15 Plot of Potential vs. Current density for (a) Pt/C, (b)CT-IV, (c) CT- III, (d) CT-II, (e) CT-I, (f) Vc

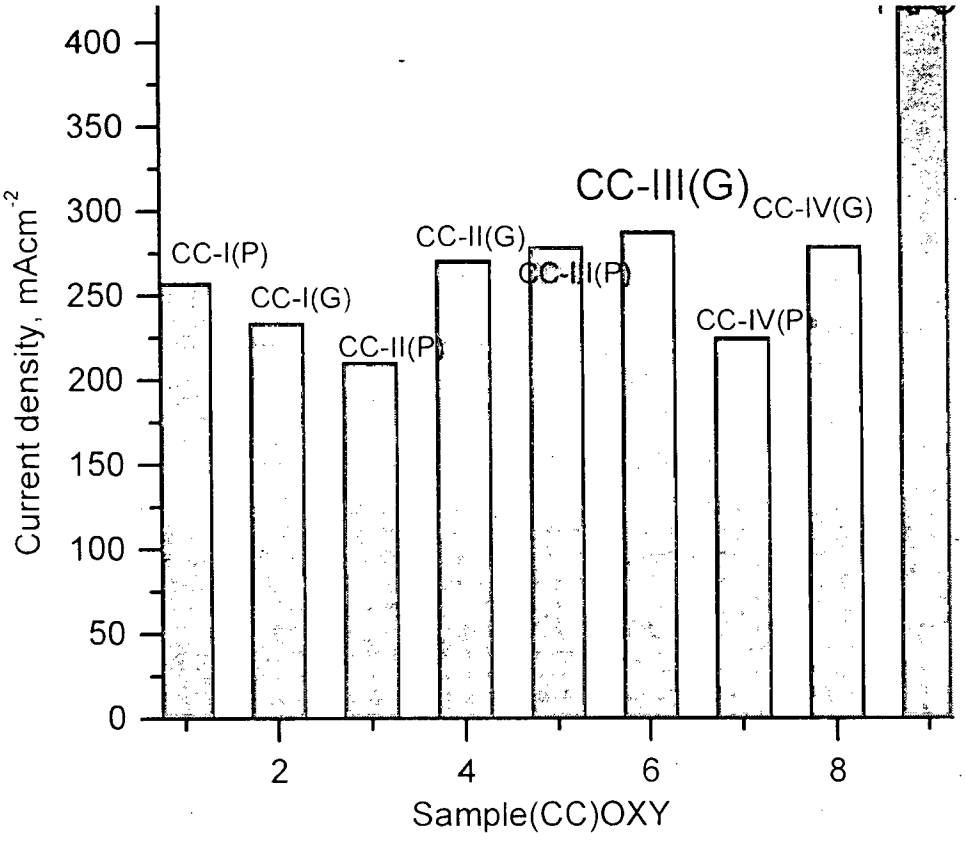

Fig4.16 Plot of Current density at i-400Potetnial for CC samples

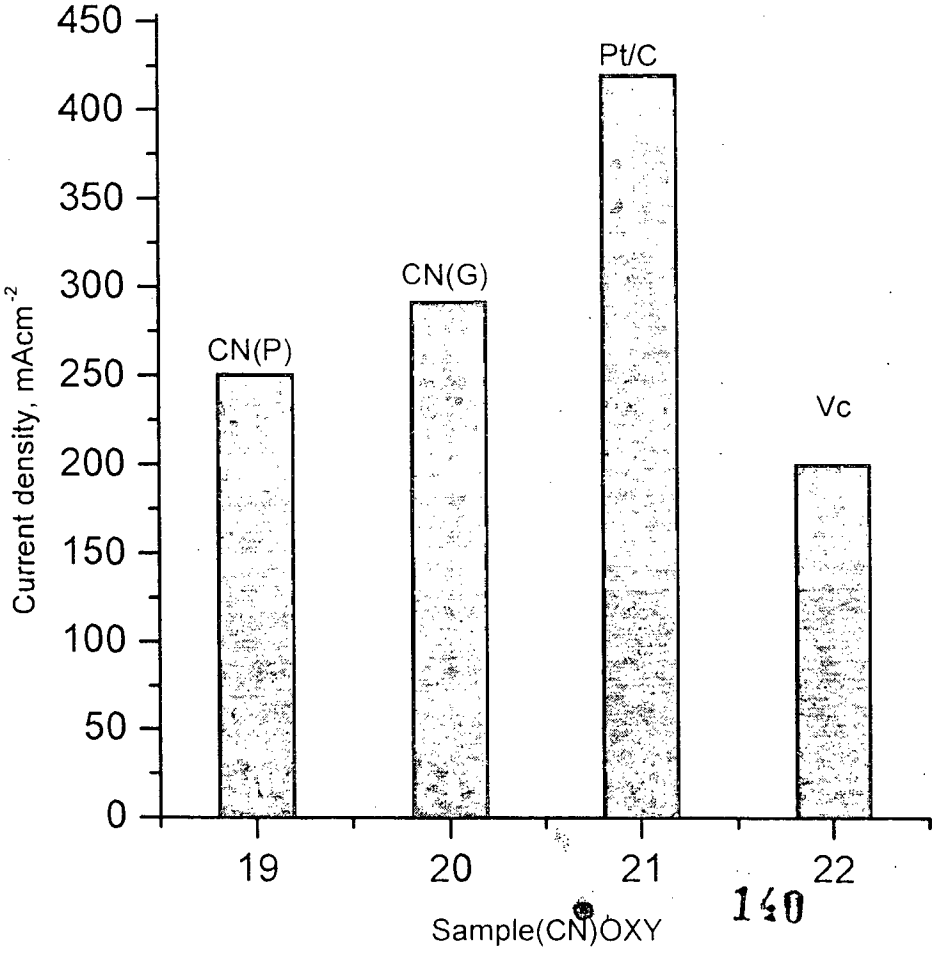

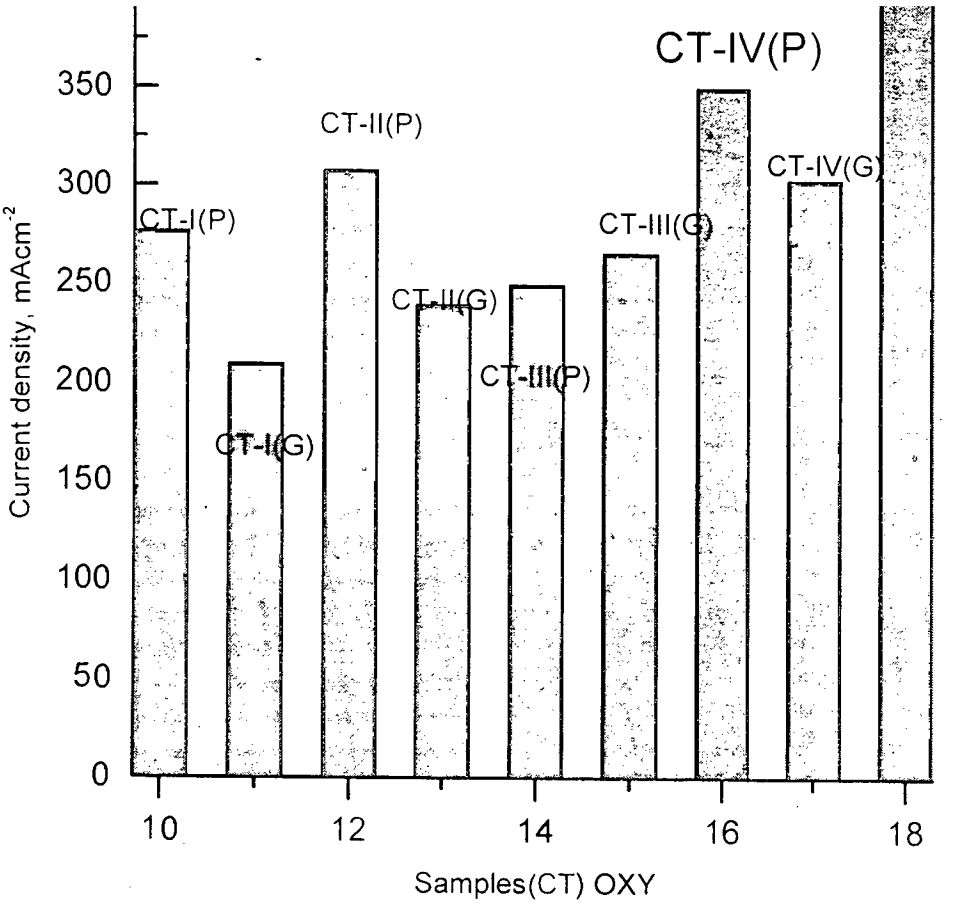

Fig4.18 Plot of Current density at i-400potential forCT Samples

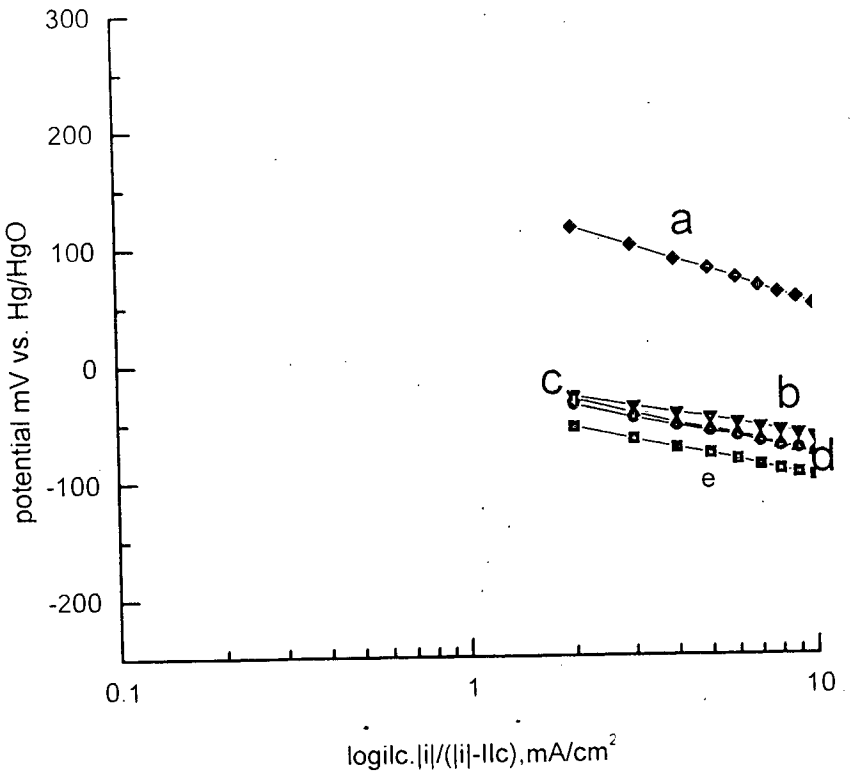

Fig 4.19 Tafel plots for CC(P) (a) Pt/C, (b) CC-I, (c) CC-III, (d) CC-IV, (e) CC-II

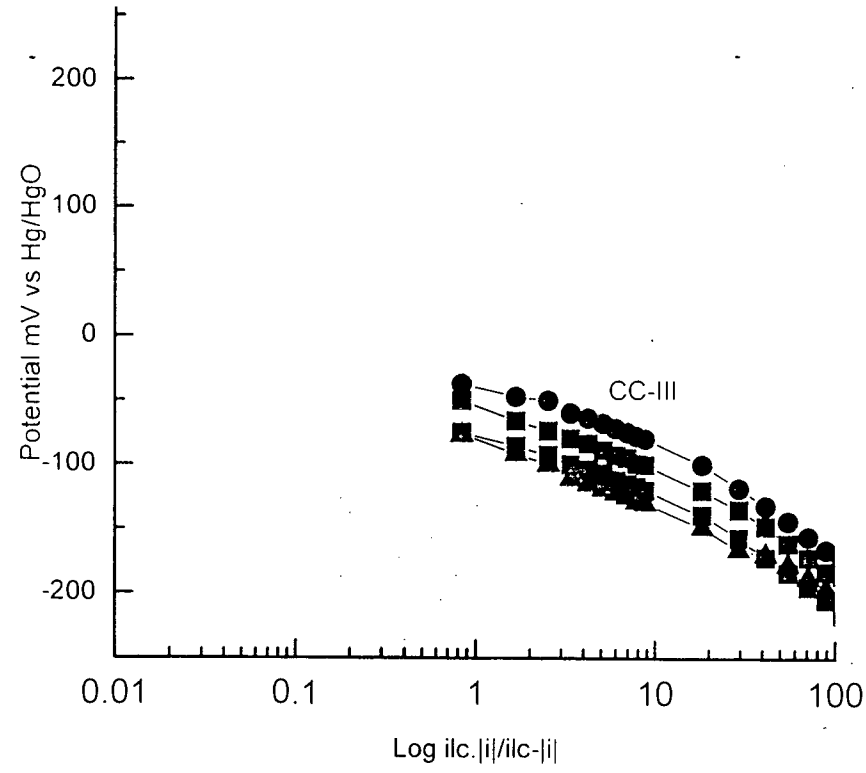

Fig 4.20 Tafel plots for CC(G), (a) CC-III, (b) CC-IV, (c) CC-I, (d) CC-II

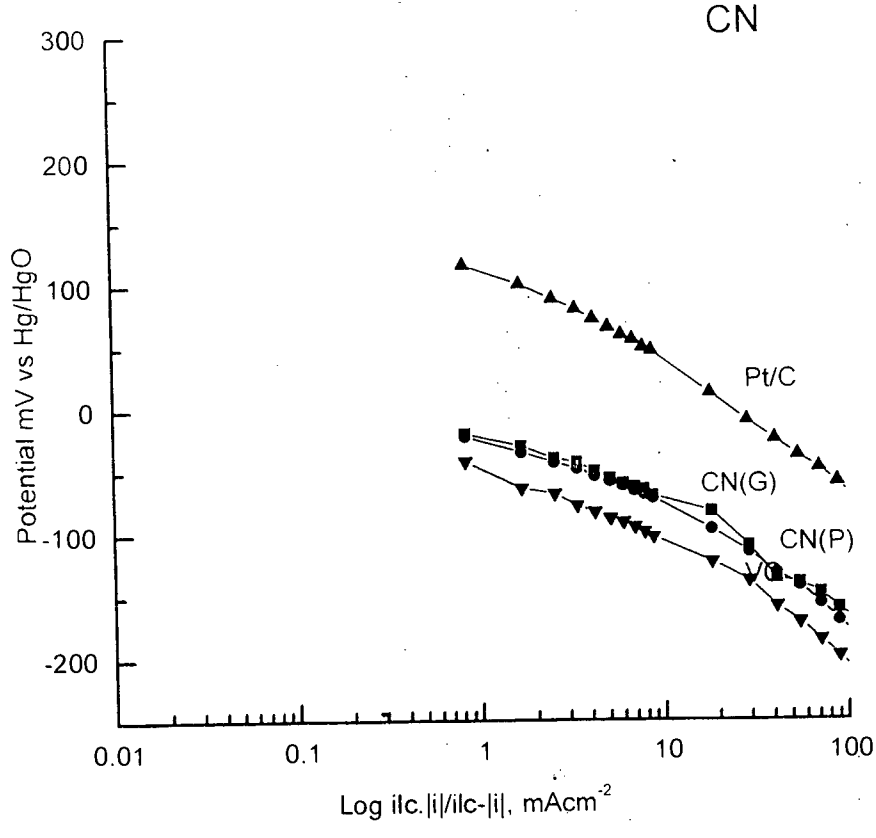

Fig 4.21 Tafel Plots for CN (a) Pt/C, (b)CN(G), (c)CN(P), (d)Vc

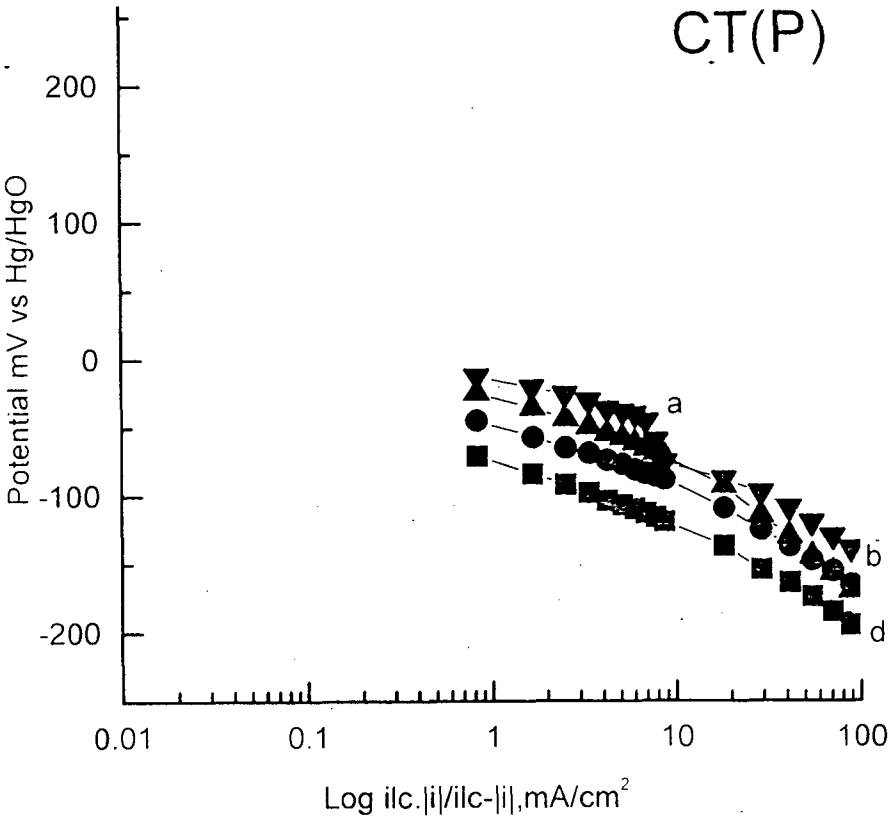

Fig 4.22 Tafel plots fot CT(P) a)CT-IV, b) CT-III c)CT-II, d)CT-I.

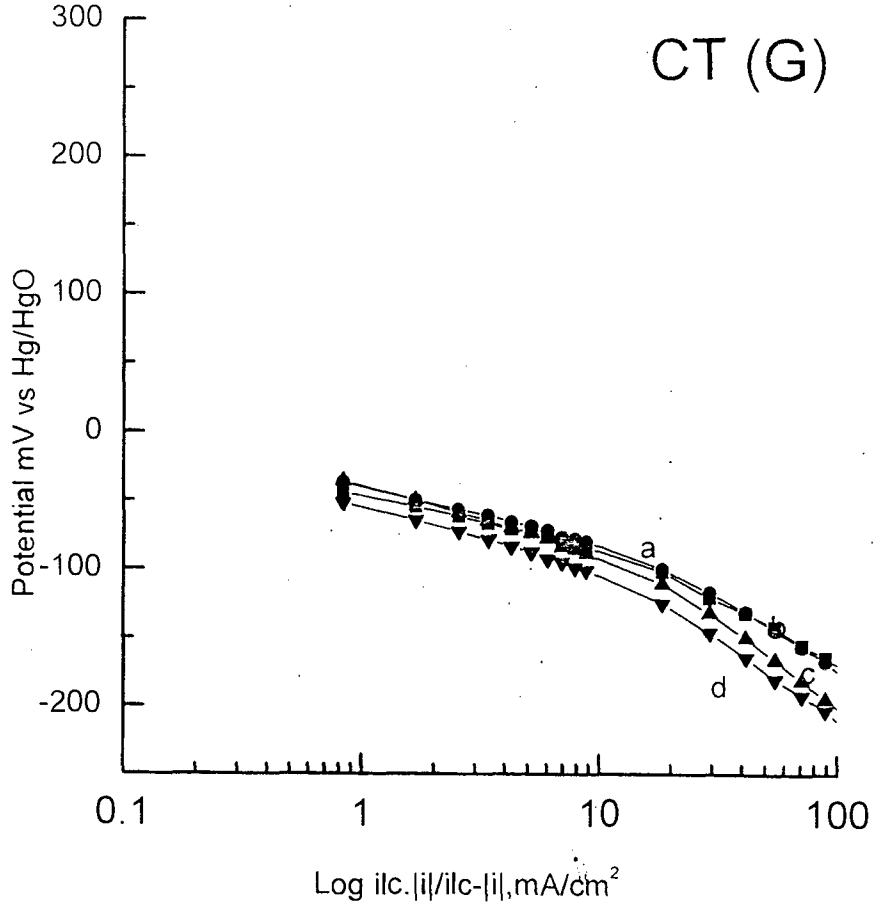

Fig.4.23 Tafel plots for CT(G), (a)CT-IV, (b)CT-III,

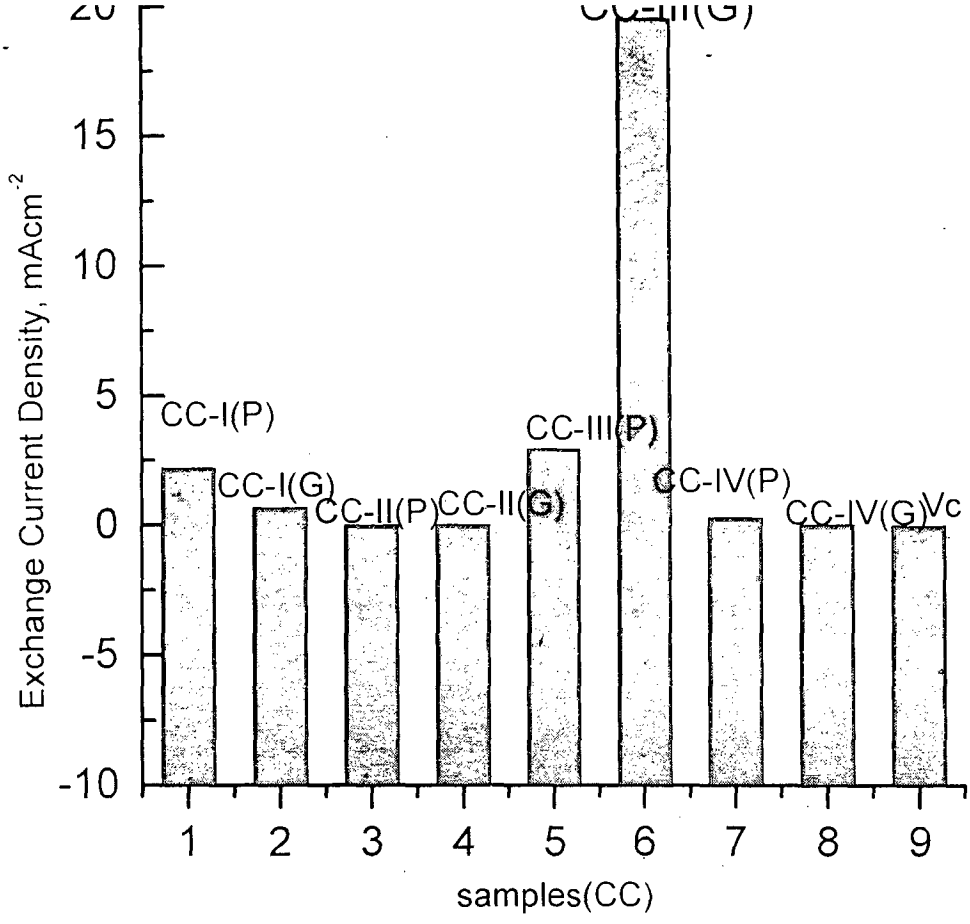

Fig.4.24Plot of exchange current density forCC samples in presence of oxygen

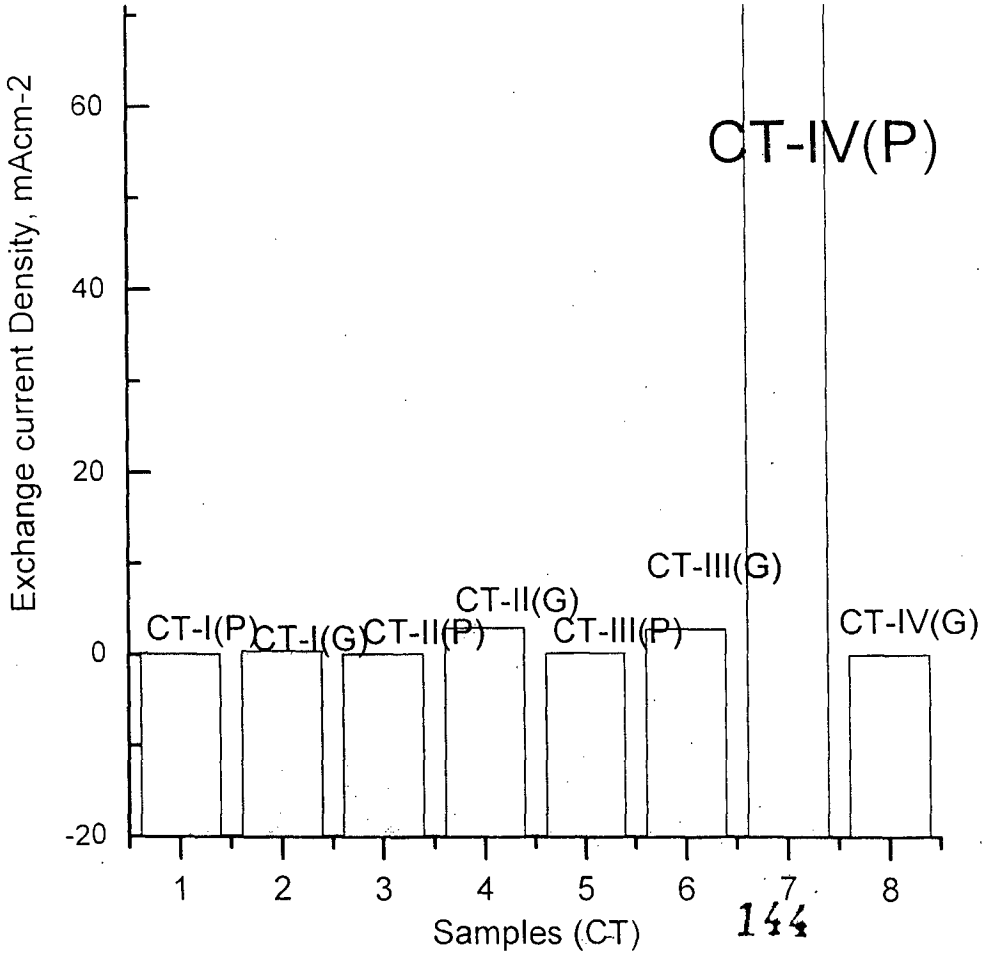

Fig.4.25 Plot of Exchange Current density for CT samples

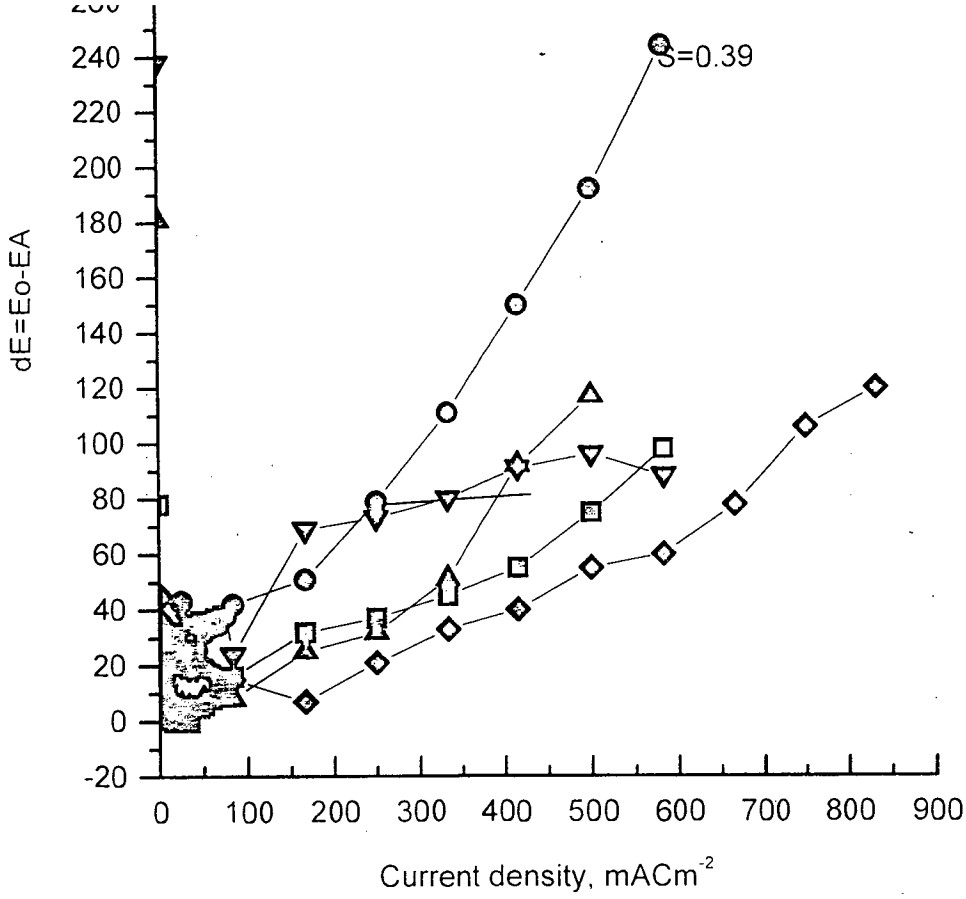

Fig 4.26 Transport hindrance plot for CC-P samples

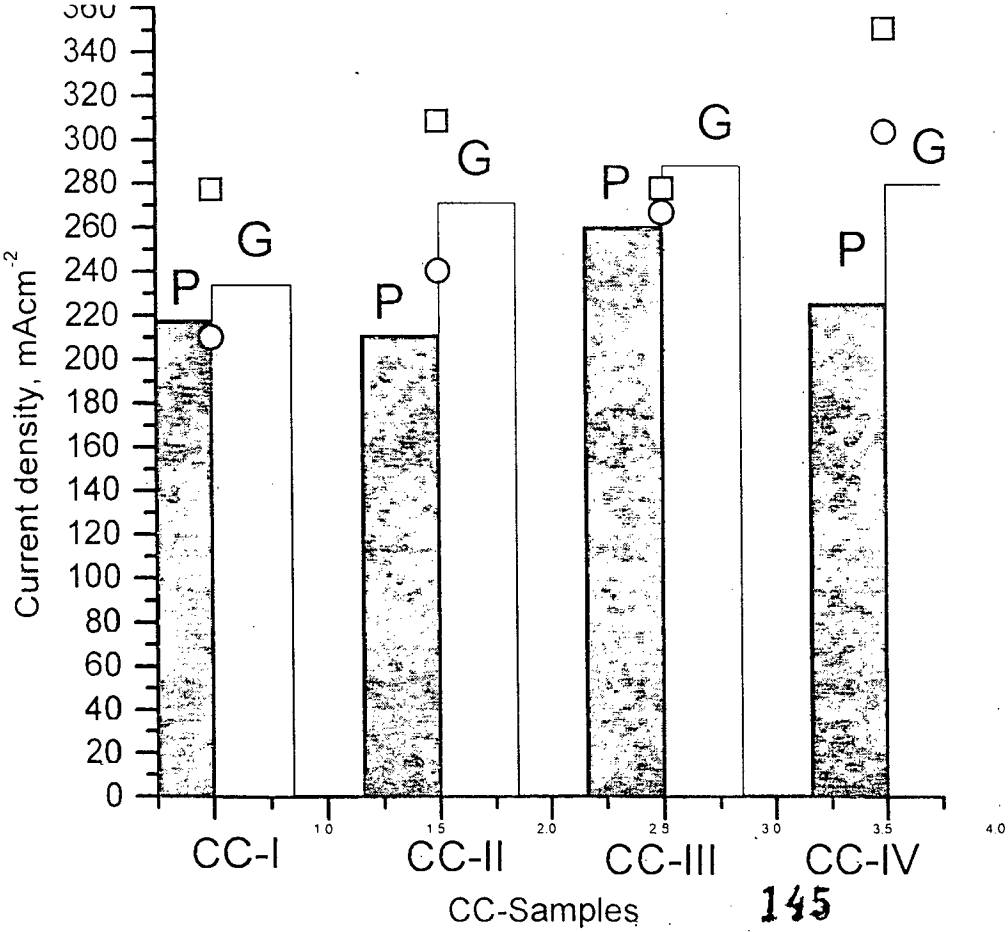

Fig 4.27 Comparison plot for CC samples

RESULTS AND DISCUSSION

4.1 POLARISATION STUDIES: The Various current potential (i-E) curves of the samples for oxygen reduction reaction are shown through Fig 4.10 - 4.15 both in presence of oxygen as well as air. The corresponding Tafel plots corrected for [4] are presented in Fig 4.19-4.23 from which Tafel slopes and exchange current densities were evaluated. It is generally recognized a good electrocatalyst should provide a current density of ~200 $mAcm^{-2}$ at overpotential of ~350 mV from the OCP [24]. Therefore as a measure of electrocatalytic activity of various samples the relative current densities are measured at an arbitrary potential of 400mV. These values along with other kinetic parameters obtained are presented in Table 4.3(a) and (b). The electrocatalytic activity in terms of i_{400} is discussed in relation to the method of preparation of the samples.

All the i-E curves of the samples sit between the carbon blank and platinum electrode. As expected the platinum shows the highest current of $420mA/cm^2$. Nevertheless the all the cobalt oxide samples showed current densities in the acceptable range of 200 ~$350mA/cm^2$, the highest value of $350mA/cm^2$ being not too much away from that of platinum. Also the exchange current densities i_o of the sample range from ~10^{-5} $mAcm^{-2}$ to ~10^{-8} mA/cm^2, which in fact is better than a very recent report of Morales et al [18] for the Co_3O_4 spinels prepared by sol-gel method and also evaluated in alkaline medium.

Herein, i_o values are considered as convenient parameters for comparing electrocatalytic activity of the various samples in relation to the method of preparation.

To begin with, a comparison is made within the CC- group sample i.e. those prepared by using $CoCO_3$ under various conditions. (Refer Table 4.1 or Fig 4.27).

(1) It is clear that the samples obtained by grinding showed generally higher catalytic activity than those obtained by precursor method i.e. the precursor deposited on the carbon support so that Co_3O_4 is produced in situ. This in situ decomposition in presence of hydrazine hydrate fuel being autocatalytic and exothermic, could have led to sintering of the catalyst particles, with the consequent reduction in surface area, and hence electrocatalytic activity.

(2) Further, comparison between CC-G samples in Fig 4.28 reveal that samples CC-I and CC-II has lower activity than CC-III or CC-IV samples. This implies that a better quality product is obtained when decomposition is carried out autocatalytically under sunlight reaction than obtaining the samples by direct decomposition on the burner.

(ii) Again CC-II(G) showed higher activity than CC-(IG) this implies that the decomposition on platinum crucible gives a better product than when obtained by decomposing in a silica crucible. As platinum can exert a catalytic effect during decomposition, it appears that catalyzed decomposition gives better product than non-catalyzed decomposition. Similar conclusion can be drawn with respect to current density values for CC-III(G) and CC-IV(G) samples.

3(i) Fig 4.29 gives the comparison across the CT samples. It is immediately interesting to note that the trend observed in CT samples is practically in reverse order that seen in CC samples. While the precursor derived samples had lower activity in the

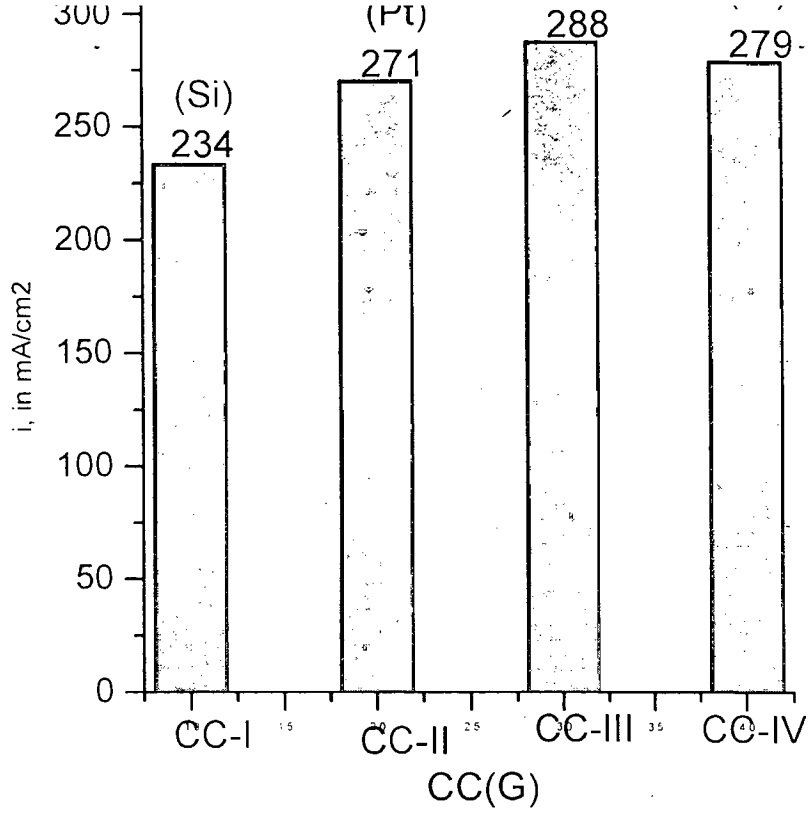

Fig.4.28 Comparison between CC(G) samples

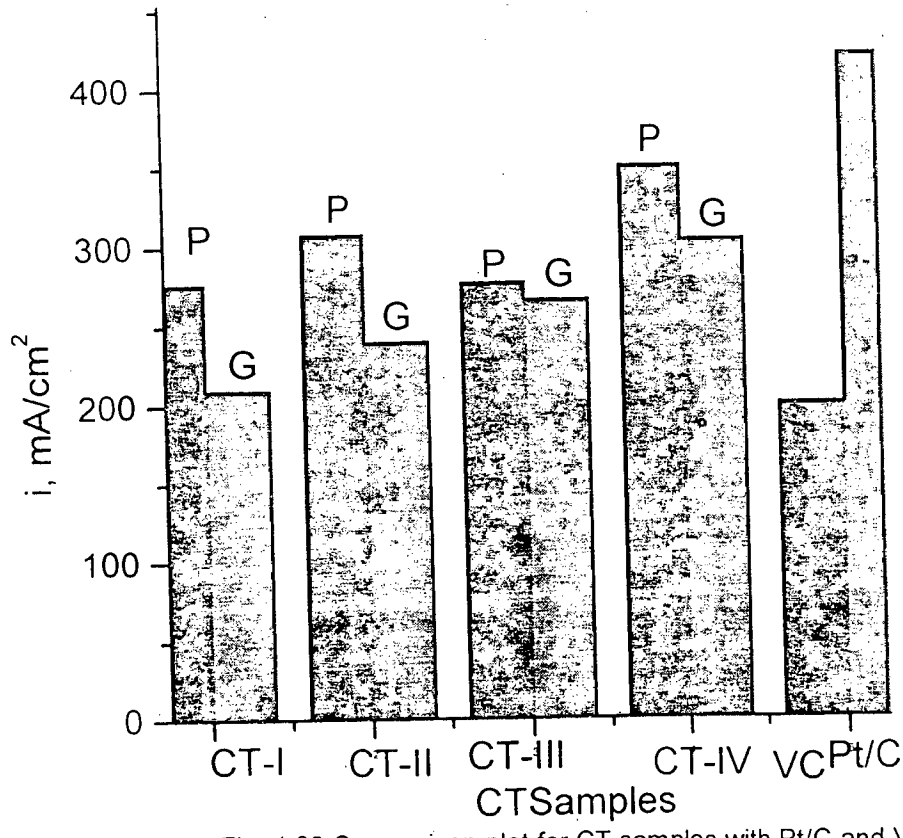

Fig. 4.29 Comparison plot for CT samples with Pt/C and VC

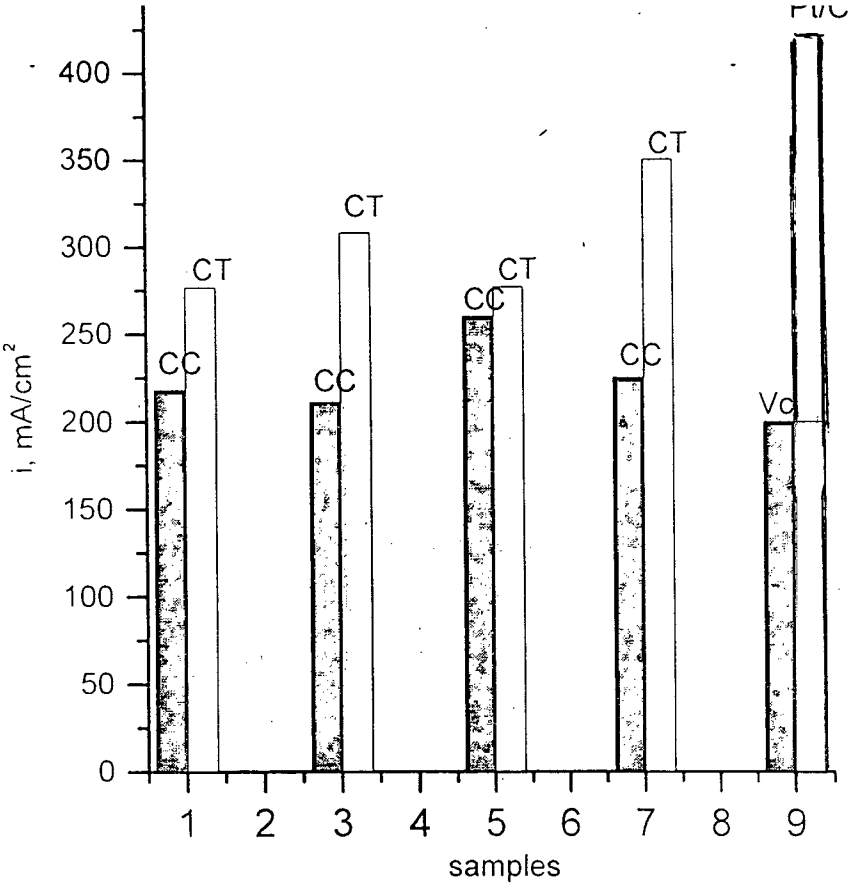

Fig. 4.30 Shows comparison of activity between CC-(P) and CT-(P) samples both by precursor methods

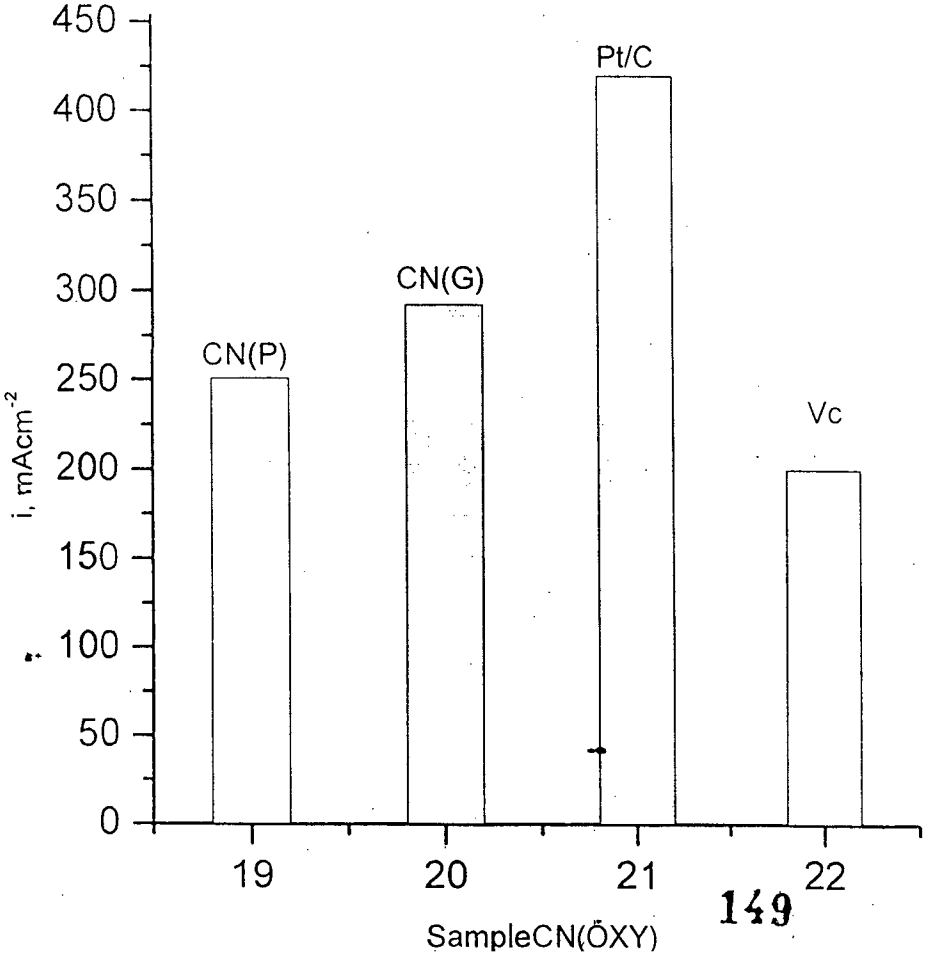

CC group. the precursor samples have higher activity in the CT group as compared to the corresponding CT samples obtained by physical mixing/ grinding.

3(ii) Fig 4.30 shows the comparison of activity of CC- (P) and CT- (P) samples both precursor methods. It is thus seen that the CT precursor method gives more active samples. than the CC precursor method. i.e. nitrilotriacetate complex produces better quality spinel oxide catalysts than the carbonate/hydrazido complex. Which could be due to bulky ligand present in the former precursor.

4 (i) Further comparison of activity between CT (P) samples. once again showed that sunlight mediated decomposition of precursor gave better activity for samples. irrespective of the nature of precursors.

(5) When comparison is made between the CN (P) and CN (G) samples. i. e. those prepared by nitrate method as shown in Fig. 4.31 like CC method here too the samples obtained by grinding shows higher activity than those obtained by precursor method. It may be the in situ preparation of the sample might have led to the sintering of the catalyst particles. with consequent reduction in the surface area. and hence electrocatalytic activity. That the surface areas are indeed reduced is evident from the values of the surface area obtained by BET method. and the surface morphology of these electrodes is shown in scanning micrographs in Fig. 4.32 (a). (b) .(c) and (d).

Pt/C = 92.99 m^2/g

CN-(P) = 90.96 m^2/g

CN-(G) = 190.91m^2/g

CN = 9.8 m^2/g

Vc = 250 m^2/g

Mag :x10000
Acc.V :20kV
Signal :SEI
WD :17mm
Spot size :23
———— :2.00um
File Name :
C:***\Co3o4.bmp

(a)

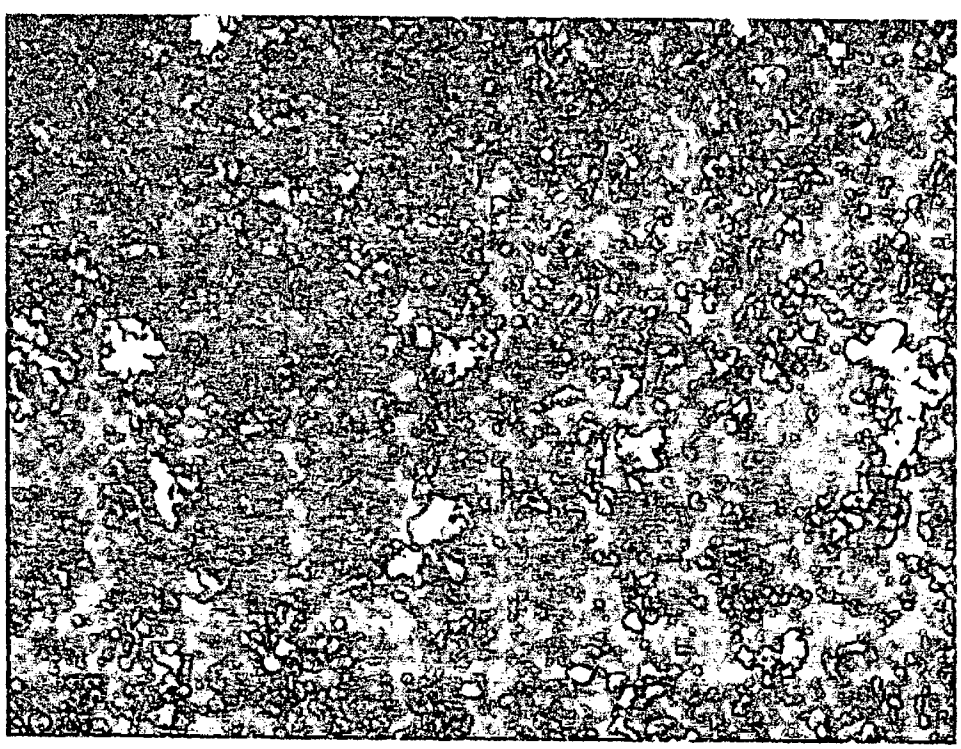

Mag :x10000
Acc.V :20kV
Signal :SEI
WD :16mm
Spot size :23
———— :2.00um
File Name :
C:***\Ptc20.bmp

(b)

Fig. 4.32 Scanning Electron Micrograph of (a) Co_3O_4 (CN)
(b) Pt/C

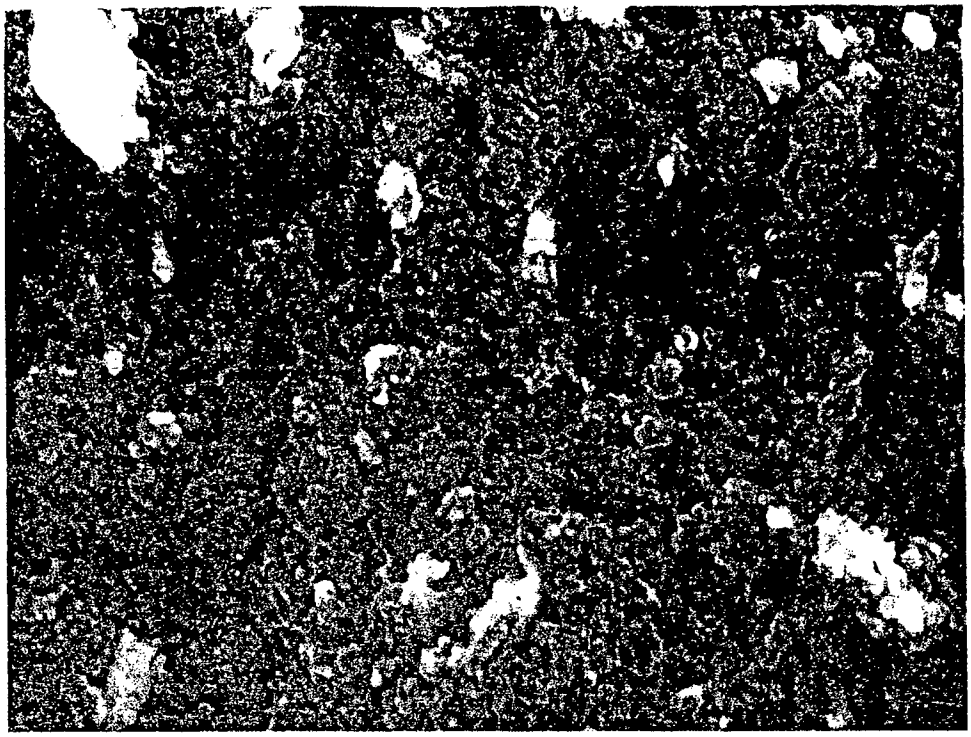

(c)

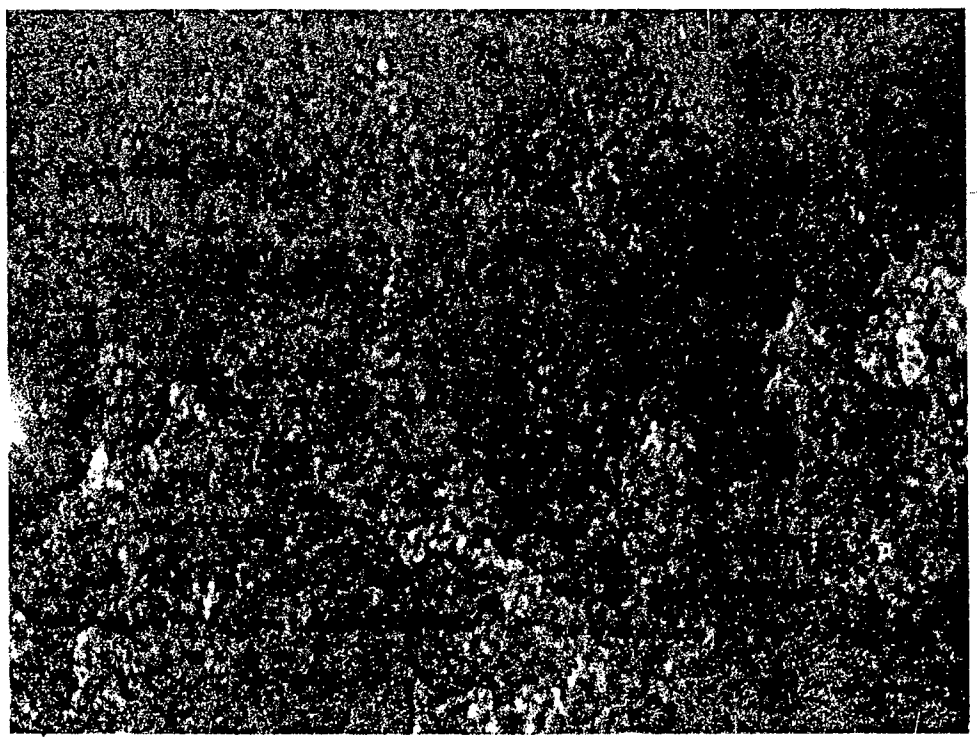

(d)

Fig. 4.32 Scanning Electron Micrograph of (c) (CN) (G)
(d) CN (P)

(6) Thus, by far the best sample is CT-IV (P), showing the highest electrocatalytic activity. It also shows the higher exchange current density $\sim 10^{-5} mA/cm^2$, much higher than the average value of $\sim 10^{-7} mA/cm^2$ shown by other samples; thus implying kinetically facile oxygen reduction on the CT-IV (P) electrode surface.

(7) In all the cases, the i_{400} activity values were lower for O_2 reduction from air, than when pure O_2 is taken for the experiment. It is probably due to the mass transport for diffusion of $O_{2\,(g)}$ up to the three-phase zone at the interface of the porous gas diffusion electrode. The plot for transport hindrance for Co_3O_4/C is shown in Fig. 4.26.

(8) Most of the samples showed Tafel slopes around 60 $mVdec^{-1}$, suggesting that the reduction mechanism generally follow $2e^-$ or the indirect pathway involving intermediate peroxide formation.

(h) The current potential data obtained by varying the concentration from 2%, 10% and 20% of Co_3O_4 for Co_3O_4/C gas diffusion electrode shows that there is increase in elelctrocatalytic activity from 2% to 10% but from 10% to 20% not much increase is detected.

4.3 CYCLIC VOLTAMMETRY

In cyclic voltammetry, the potential of a small stationary working electrode is changed linearly with time starting from a potential where no electrode reaction occur and moving to potential where reduction or oxidation of the electroactive species occurs.

The fundamental equations for cyclic voltammetry have been developed by Delahay and Shain. The basic feature observed in the voltammogram i.e a plot of

current vs. potential during cyclic voltammetry is the appearance of a current peak at a potential characteristic of the electrode reaction taking place. The position and the given shape of the voltammogram depend on the sweep rate, electrode material, solution composition and concentrations of the reactants.

The cyclic voltammetry can be used to identify the steps involved in the overall reaction, and the new species that are formed in the solution during electrolysis.

For a simple cathodic charge transfer process under reversible conditions, where both reactant and product are soluble, i_p in A cm^{-2} at 25°C is given by

$$|i_p| = 2.72 \times 10^5 \, n^{3/2} D^{1/2} C^o V^{1/2} \qquad 16$$

where 'D' is in $cm^2 sec^{-1}$, C^o in mole cm^{-3} and V in volts sec^{-1}.

Under totally irreversible conditions, i.e when the rate of the reverse reaction is negligible throughout the potential region studied, the following eqn. applies:

$$|i_p| = 3.01 \times 10^5 \, n(2.3RT/bF)^{1/2} D^{1/2} C^o V^{1/2} \qquad 17$$

In aqueous solution the potential window is limited on negative by the reduction of H_2O to H_2 and or the positive by the oxidation of H_2O to O_2. It is influenced by the choice of the working electrode, solvent and supporting electrolyte. The electrolysis of the species of interest must occur with this range. Fig 4.33 (a) gives the cyclic voltammogram (CV) of 0.1M KNO_3 with or without oxygen. The two cathodic peaks observed are due to the reduction of oxygen to peroxide and peroxide to OH^- [21]. If the oxide electrode contains a metal ion that can exist in different oxidation states the resulting curve will exhibit characteristic peak at the given redox potential. Fig 4.33(b) gives the CV spectrum of Co_3O_4 [22]. However as the potential of the redox couple Co^{2+}/Co^{3+} ($E^o = +1.92V$) would lay outside the potential window it is expected that the

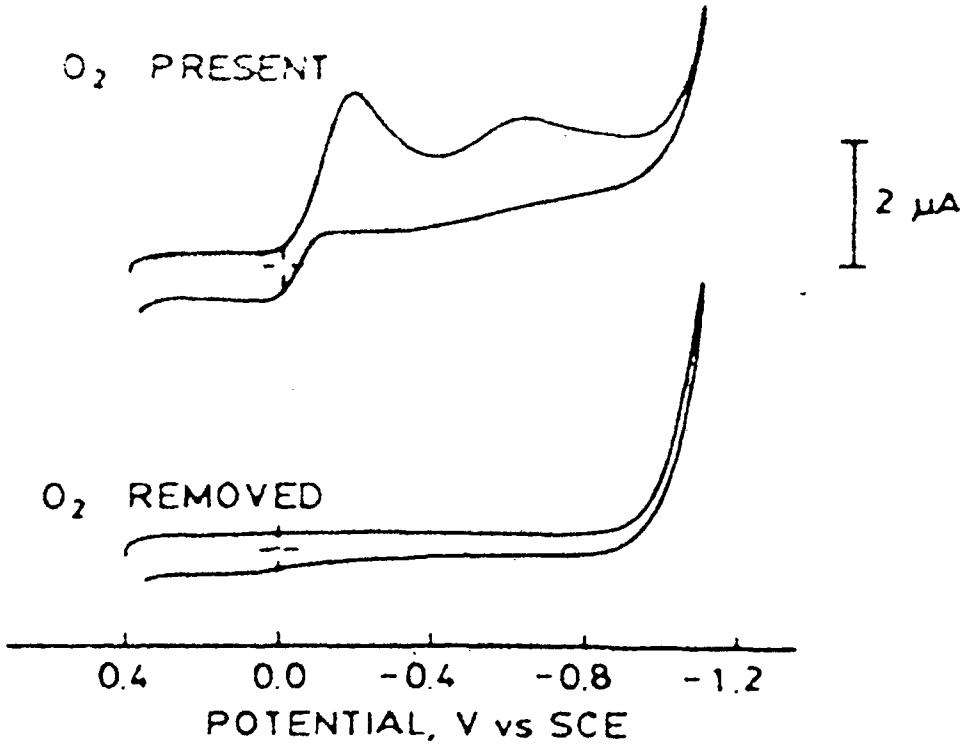

Fig. 4.33 (a) Cyclic voltammograms of 1.0 M KNO_3 showing affect of O_2. Oxygen removed by deoxygenating with N_2 for 10 minutes. Au electrode scan rate = to 50mV/s

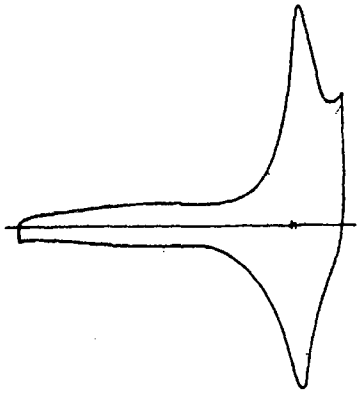

Fig. 4.33 (b) A Voltammetric "spectra" for CO_3O_4 in 1 mol/dm^3 KOH potential range : 0 to 0.5 V (SCE). Current range : arbitary units.

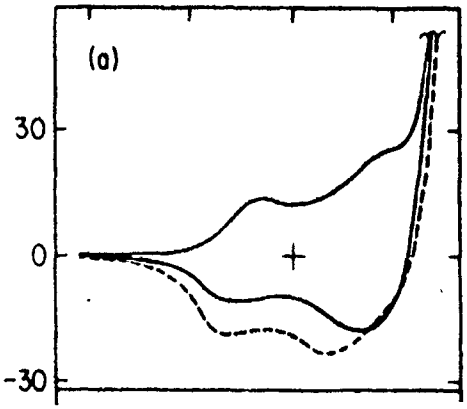

Fig. 4.33 (c) potentiodynamic profiles of cobalt oxide electrodes run at 0.1 V/sec in 2 M NaOH.

CV spectrum of Co_3O_4 would not interefere with the O_2 reduction peaks. Fig.4.34 (c) gives the CV spectrum of Co_3O_4 of spinel electrode in 2M NaOH showing oxygen reduction/oxygen evolution peaks [23].

4.3.1 CYCLIC VOLTAMMETRY AND GENERAL ACTIVITY CORELATION

Typical C-V profiles of some of the samples are presented through Figs 4.35 to Fig. 4.43. The CC-(G) samples I and IV, (Fig. 4.35 (b) to Fig. 4.38 (b) show three oxygen reduction peaks, which are well resolved only at high scan rates –350 or >350mV/s.

1. As mentioned earlier, the indirect oxygen reduction pathway involves two-stage reduction of $2e^-$ steps each.

   i) $O_2 + H_2O + 2e^- \xrightarrow{K_2} HO_2^- + OH^-$

   ii) $HO_2^- + H_2O + 2e^- \longrightarrow 3OH^-$

2. However Yeager [25] had first reported that peroxide formation precedes formation of adsorbed superoxide ion O_2^-. Following this suggestion, it seems pertinent to suggest here that the indirect reduction pathway involves the following three electrochemical steps:

   (a) $O_2 + e^- \longrightarrow O_2^-$ (adsorbed superoxide species)

   (b) $O_2^- + H_2O + e^- \longrightarrow HO_2^- + OH^-$

   (C) $HO_2^- + H_2O + 2e^- \longrightarrow 3OH^-$

so that the overall mechanism is the $4e^-$ transfer process;

$$O_2^- + H_2O + e^- \longrightarrow 4OH^-$$

The above mechanism thus explains the three oxygen reduction peaks observed in the C-V profiles obtained in this work.

3. As would be seen in the various figures, not all the samples show three step reduction. The numerical analysis of the CVs is presented in Tables 4.4 (a) and 4.4(b) for the CC and CT group samples, in relation to their corresponding electrochemical activity expressed as before in terms of the current density parameter i_{400}. Also included in the tables is the activation energy for the H_2O_2 decomposition reaction.

4. It is seen in the previous section of polarization studies that the CC-(G) samples had higher electrocatalytic activity than the CC-(P) samples. If now the O_2 reduction CV data is compared, it is found that the CC-(P) samples undergo reduction at less +ve values (by about log millivolts) for both peaks I and II indicating delayed reduction or less facile electrode kinetics, as compared to the CC-(G) samples. E. g. the value for CC-(P) samples ~+ 0.45 Volt and for CC-(G) samples it is ~ + 0.55Volt for the first reduction peak. This is evident in the Table 4.4 when these reduction peak potentials are read in relation to the i_{400} current density values. Thus CC- (P) has first peak potential 0.45 Volt and i value 218 mA/cm^2. While CC-I (G) has first peak potential 0.52 Volt and hence undergoes reduction more easily at more positive potential: therefore has higher activity i = 234mA/cm^2.

5. The comparative CV profiles of these samples are still more revealing refer Fig. 4.34 (a) and 4.37 (a). The CC (P) profiles on the reduction side (reverse scan) show the rapid decrease from the peak I current. Only two peaks are observed corresponding to the formation of superoxide ion O_2^- and a small current for the peroxide ion formation.

On the other hand the corresponding CC (G) shows a rising profile with all the three reduction peaks. It is therefore obvious that the reduction mechanism in the two cases is different. One may therefore conclude that the carbonate precursor derived Co_3O_4 spinel catalyze only partial reduction of oxygen up to the peroxide stage, and thus account for the observed lower activity.

6. Although these samples show very high initial current due to O_2^- formation, suppression of the subsequent reduction steps would simply increase in charge transfer ressistance owing to ohmic drop at the three-phase zone. This is confirmed by the fact that the uncompensated resistance Ru is seen to be significantly higher for the CC (P) samples than the CC (G) samples. Table 4.3 (a) and (b).

7. Eventhough the O_2^- formation is quite facile, as evident from the very high values of peak I currents, particularly for CC (P) samples, yet these samples show overall lower electrocatalytic activity. Therefore the superoxide ion formation may not be the rate-determining step (RDS) of the reduction mechanism. It is therefore conceivable that the peroxide ion formation or decomposition could be the RDS. Hence the activity of the samples for decomposition of the peroxide is studied separately. It is seen from Table 4.4 (a) and (b) or Fig 4.43 that the samples which show high electrochemical activity value for i_{400}, also show low i.e. favorable activation energy for peroxide decomposition reaction. Therefore it is concluded that in those cases where electrochemical reduction occurs through indirect pathway, the peroxide decomposition to OH^- is the RDS. Fig. 4.43 shows relation between electrocatalytic activity of samples and activation energy for peroxide decomposition.

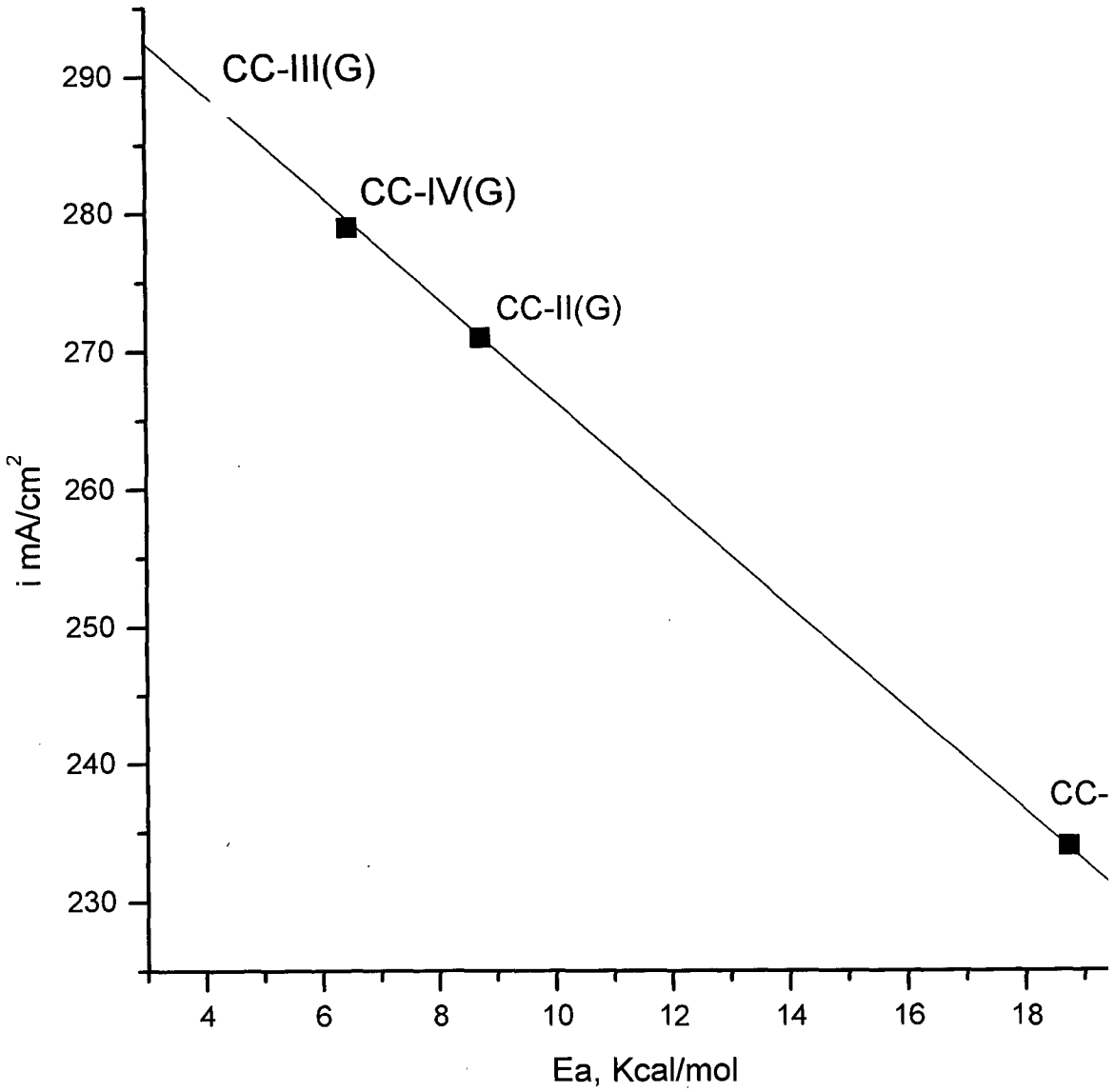

Fig. 4.43 Plot of showing the relation between electrocatalytic activity of the samples and activation energy for peroxide decomposition

8. Among the CT samples. it is shown in the previous section from the polarization studies. that unlike the CC samples the CT (P) samples are more active than the CT (G) samples. But further until the CC group which show different peak potentials for (P) and (G) samples the CV peak potentials in CT group were almost the same for the both (P) and (G) samples. Yet they showed significantly different activities. The samples CVs showing unique characteristics.

i) The low value of CT-I (G) could be due to rapid decay of peak I and II currents in contrast to CT- (P) (refer to Fig. 4.38).

ii) A very interesting result is obvious where the CV reduction profiles of CT-III (G) and CT-IV (G) are compared with CT-III (P) and CT-IV (P) refer Figs 4.40 and Fig 4.41. While the CT (G) profiles showed the expected three reduction peaks. the CT (P) profiles did not show peak I and peak II at 0.44and 0.28Volt respectively as observed for other CT samples (P) or (G). The CT (P) III and IV showed only one final reduction peak at ~ +0.5 Volt that correspond to the OH^- formation. Therefore the O_2 reduction on CT-III and IV (P) samples follow the direct one step $4e^-$ reduction pathway. This is the ultimate aim of the O_2 reduction catalyst search. for an alternate material to platinum. Interestingly the CT-IV(P) catalyst showed highest electrocatalytic activity.

Table 4.3 (a) Showing the different kinetic parameters obtained from steady state current potential data

Sample code	Method of prep.	i mA/cm^2		i_o	Tafel slopes mV/dec	R_u
		a (oxy)	b(air)			
Pt/c	Pt/C	420	376	$1.6E^{3}$	75	0.807
Vc	C	200	56	$2.0E^{-9}$	78	0.535
CC-I(P)	$Co_3O_4/C(P)/Si_b$	218	206	$7.2E^{-7}$	47	0.616
CC-I(G)	$Co_3O_4/C(G)$	234	204	$5.4E^{-9}$	30	0.581
CC-II(P)	$Co_3O_4/C(P)/Pt_b$	211	189	$3.7E^{-8}$	61	1.55
CC-II(G)	$Co_3O_4/C(G)$	271	209	$1.6E^{-8}$	60	0.189
CC-III(P)	$Co_3O_4/C(P)/Pt_b$	279	203	$2.8\ E^{-7}$	61	2.29
CC-III(G)	$Co_3O_4/C(G)$	288	249	$3.1E^{-6}$	58	0.267
CC-IV(P)	$Co_3O_4/C(P)/Si_b$	225	195	$4.8E^{-8}$	56	2.28
CC-IV(G)	$Co_3O_4/C(G)$	279	221	$3.8E^{-7}$	61	3.0

Table 4.3(b) Showing the different kinetic parameters obtained from steady state current potential data

Sample code	Method of prep.	i mA/cm^2		i_o	Tafel slopes mV/dec	R_u
		a (oxy)	b(air)			
Pt/c	Pt/C	420	376	$1.6E^3$	75	0.807
Vc	C	200	56	$2.2E^{-9}$	78	0.535
CT-I(P)	Co_3O_4/C(P)/Si_b	277	236	$1.6E^{-7}$	53	1.64
CT-I(G)	Co_3O_4/C(G)	210	181	$4.9E^{-7}$	52	1.18
CT-II(P)	Co_3O_4/C(P)/Pt_b	308	280	$1.8\ E^{-7}$	53	0.10
CT-II(G)	Co_3O_4/C(G)	240	205	$3.0E^{-6}$	61	3.0
CT-III(P)	Co_3O_4/C(P)/Pt_b	250	212	$2.8E^{-6}$	67	0.59
CT-III(G)	Co_3O_4/C(G)	266	223	$2.9E^{-6}$	50	1.3
CT-IV(P)	Co_3O_4/C(P)/Si_b	350	195	$1.6\ E^{-5}$	65.5	0.077
CT-IV(G)	Co_3O_4/C(G)	303	260	$6.74E^{-8}$	52.35	0.60
CN(P)	Co_3O_4/C(P)	248	238	$1.2E^{-7}$	64.41	0.237
CN(G)	Co_3O_4/C(G)	293	284	$3.5E^{-7}$	64	0.107

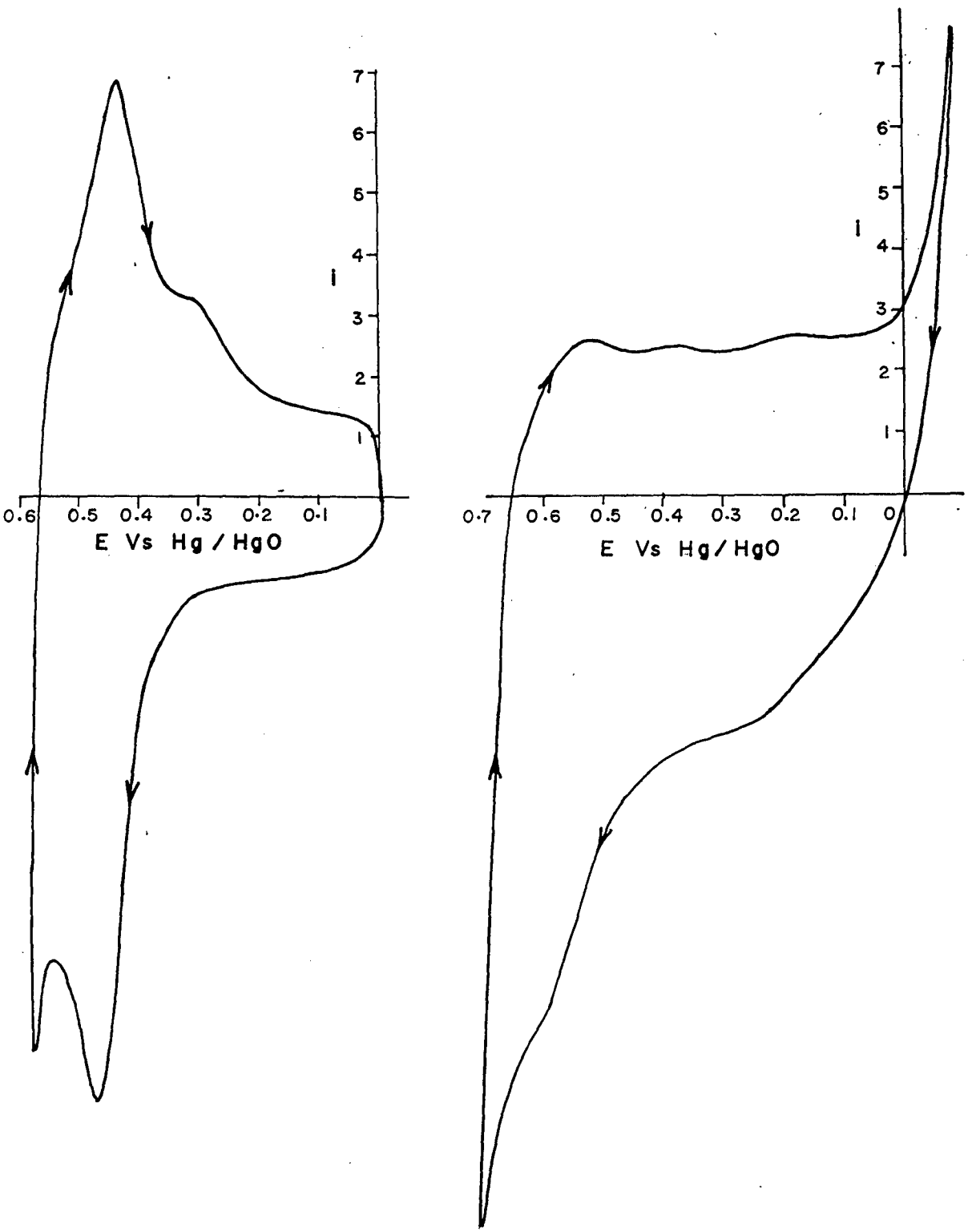

Fig. 4.34 The typical cyclic voltammogram for oxygen reduction reaction in 6 M KOH for a) CC-I (P) ; b) CC-I (G) at scan rate 200 mV/sec (a), 400 mV/sec (b).

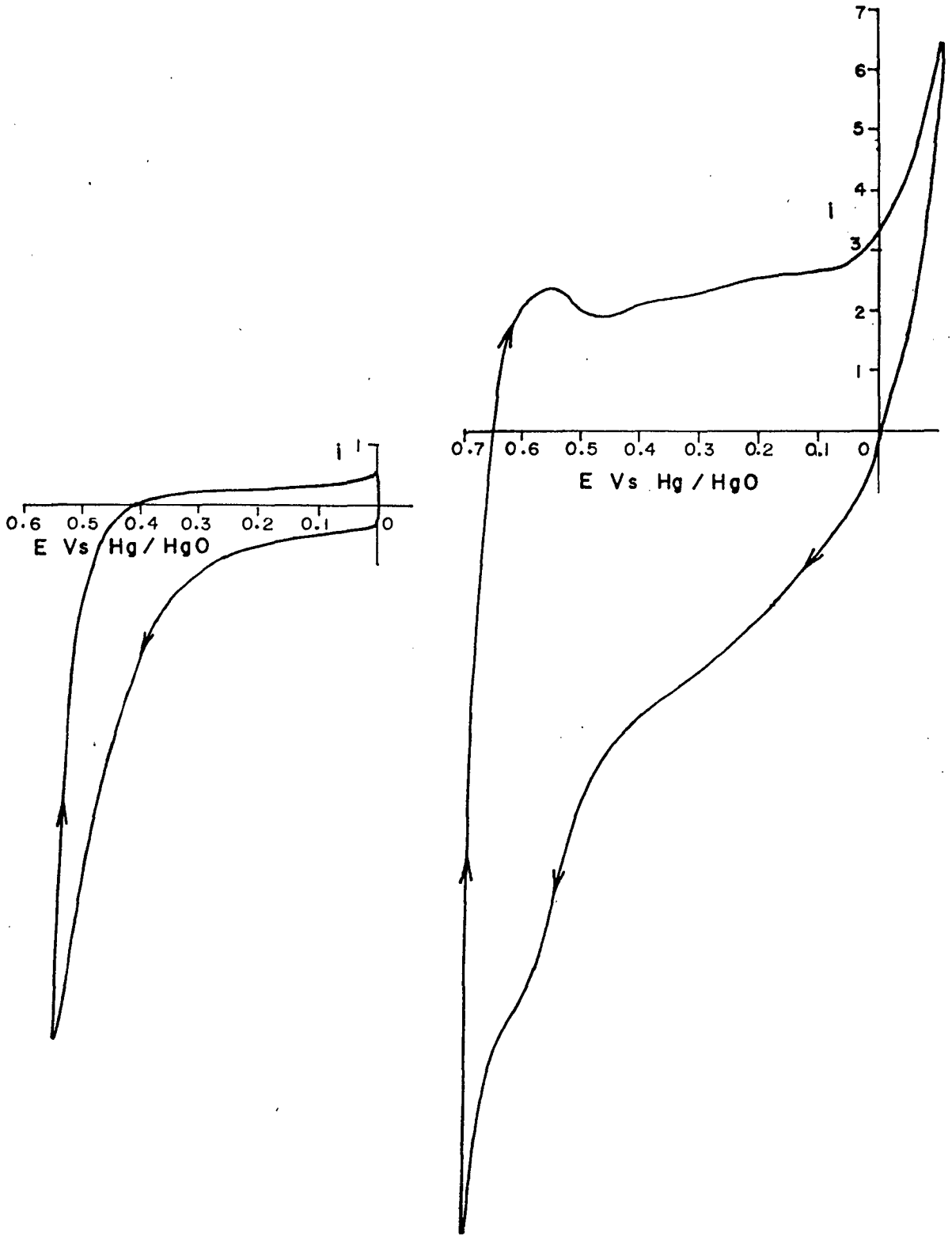

Fig. 4.35 The typical cyclic voltammogram for oxygen reduction reaction in 6 M KOH for a) CC-II (P) ; b) CC-II (G) at scan rate 400 mV/sec (b)

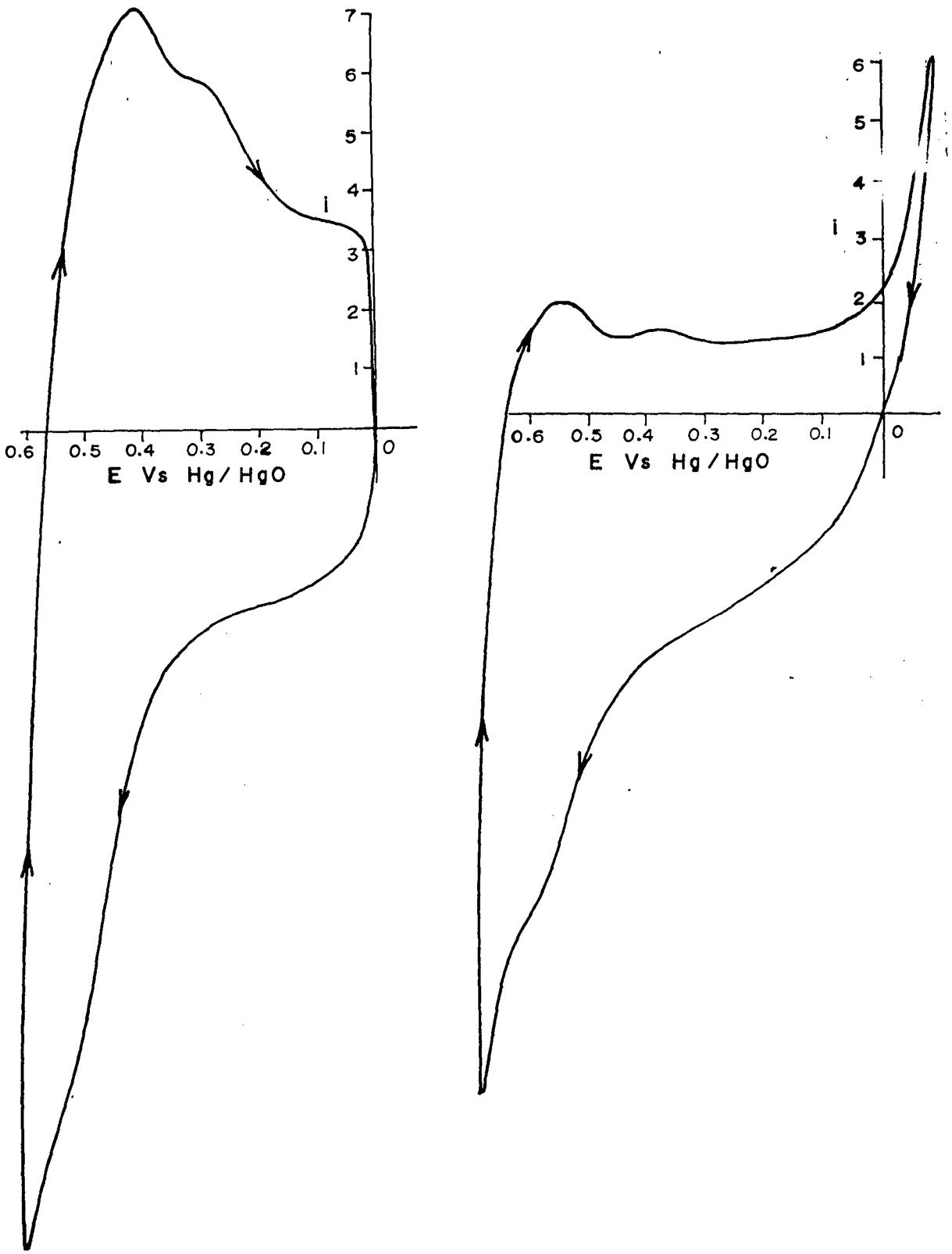

Fig. 4.36 The typical cyclic voltammogram for oxygen reduction reaction in 6 M KOH for a) CC-III (P) ; b) CC-III (G) at scan rate 200 mV/sec.(a) ; 400 mV/sec.(b)

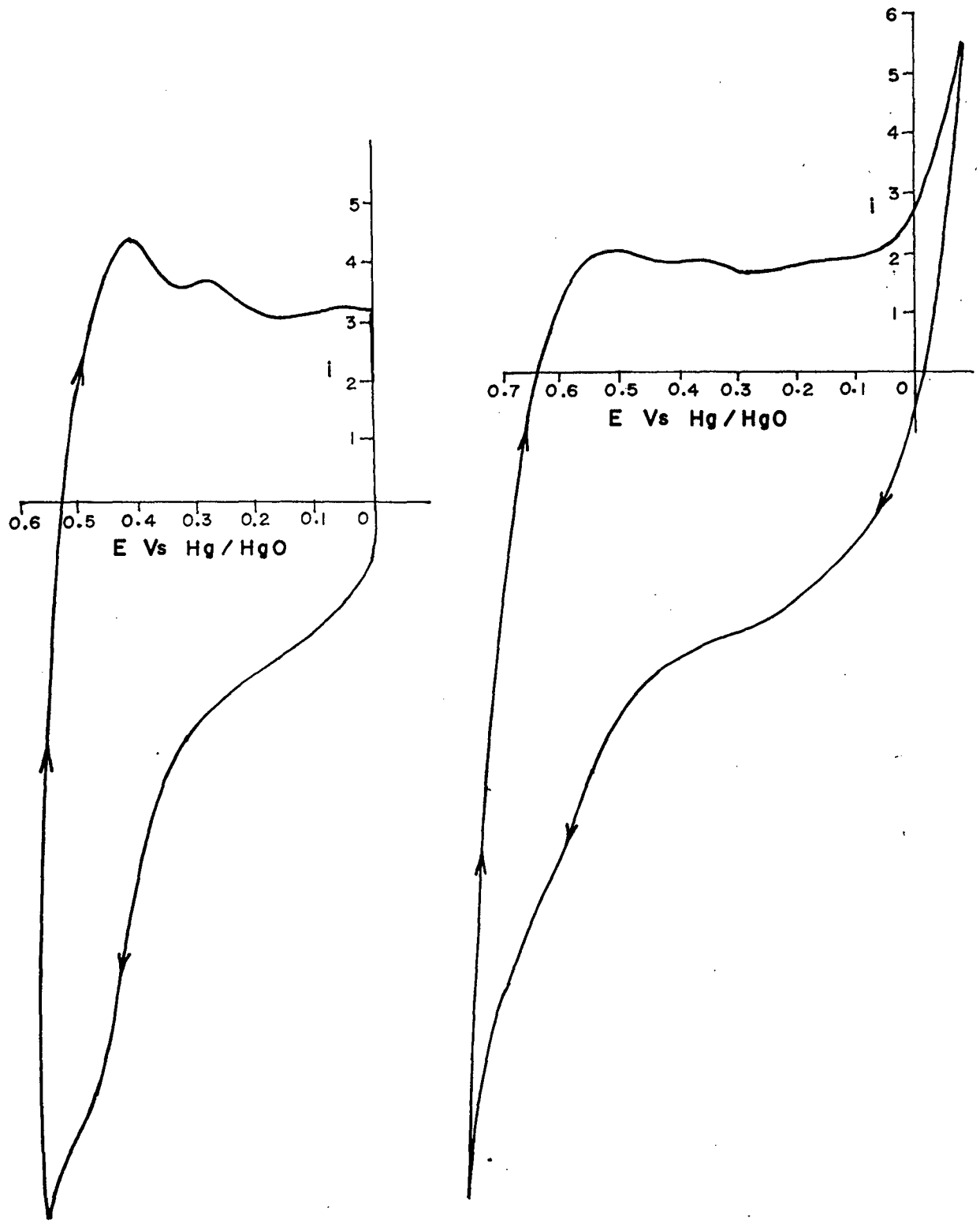

Fig. 4.37 The typical cyclic voltammogram for oxygen reductio reaction in 6 M KOH for a) CC-IV (P); b) CC-IV (G) at scan rate 350 mV/sec.(a), 400 mV/sec.(b)

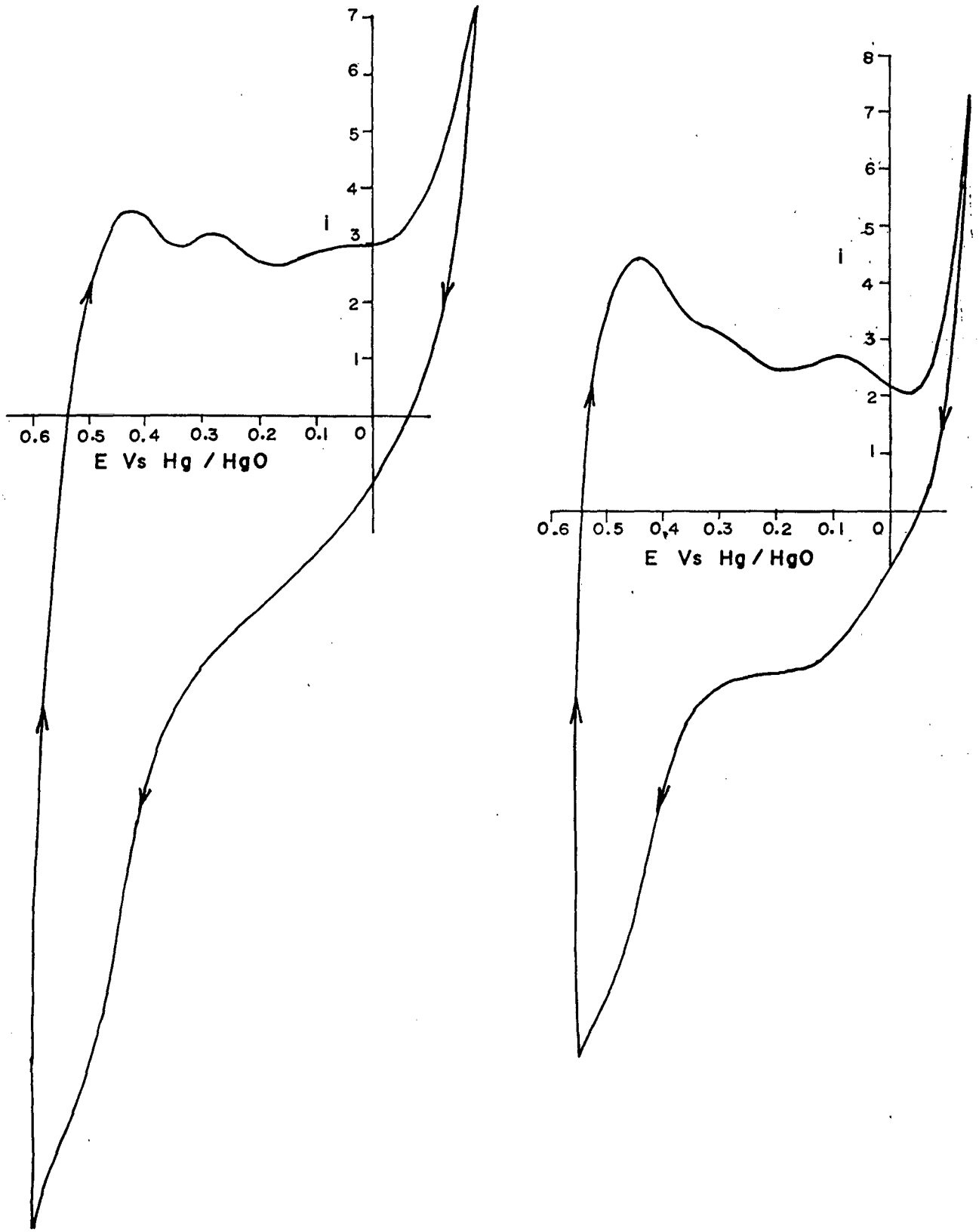

Fig. 4.38 The typical cyclic voltammogram for oxygen reduction reaction in 6 M KOH for a) CT-1 (P); b) CT-1 (G) at scan rate 350 mV/sec.

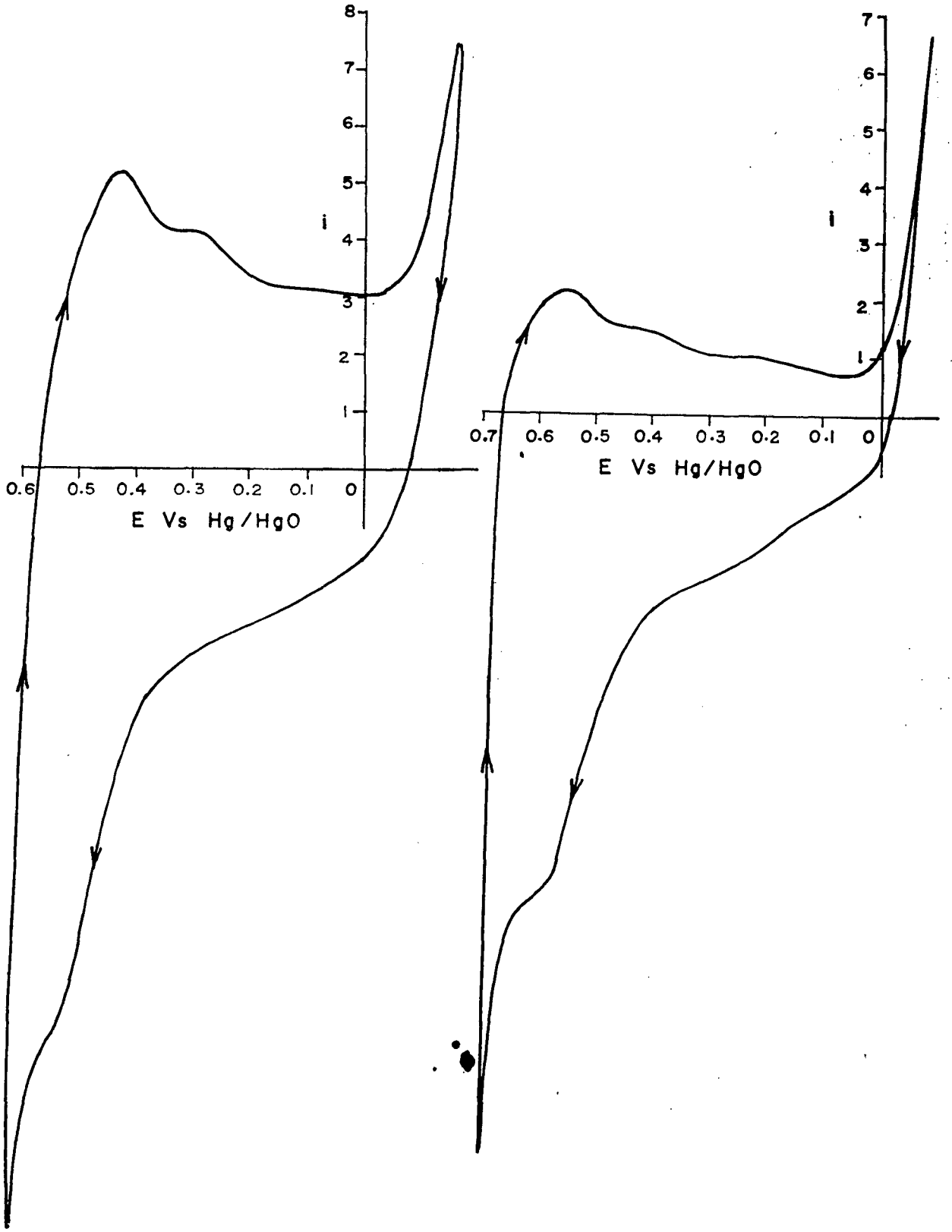

Fig. 4.39 The typical cyclic voltammogram for oxygen reduction reaction in 6 M KOH for a) CT-II (P) ; b) CT-II (G) at scan rate 400 mV/sec.(a), 300 mV/sec.(b)

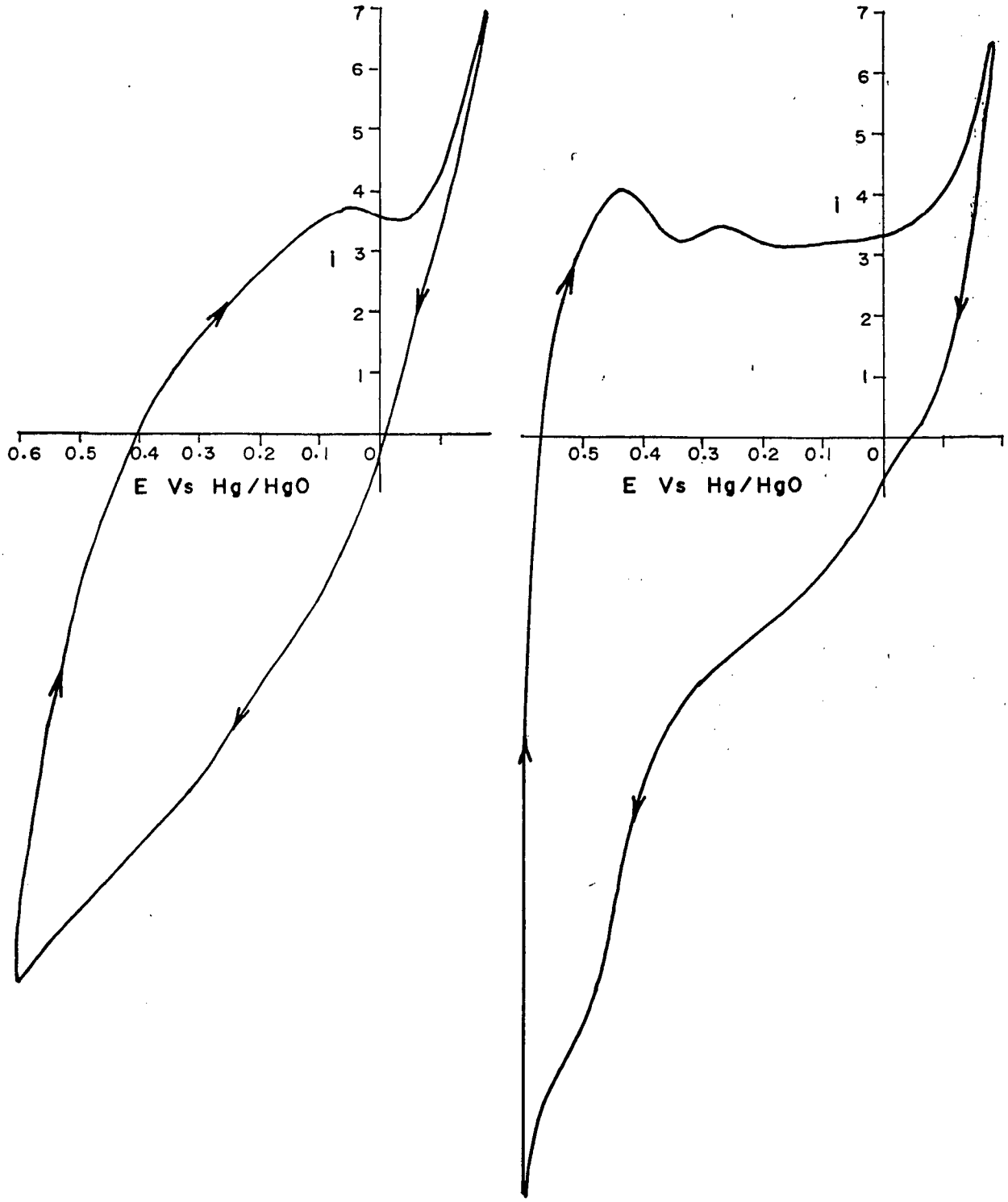

Fig. 4.40 The typical cyclic voltammogram for oxygen reducti reaction in 6 M KOH for a) CT-III (P) ; b) CT-III (G) at scan rate 200 mV/sec. (a), 400 mV/sec. (b)

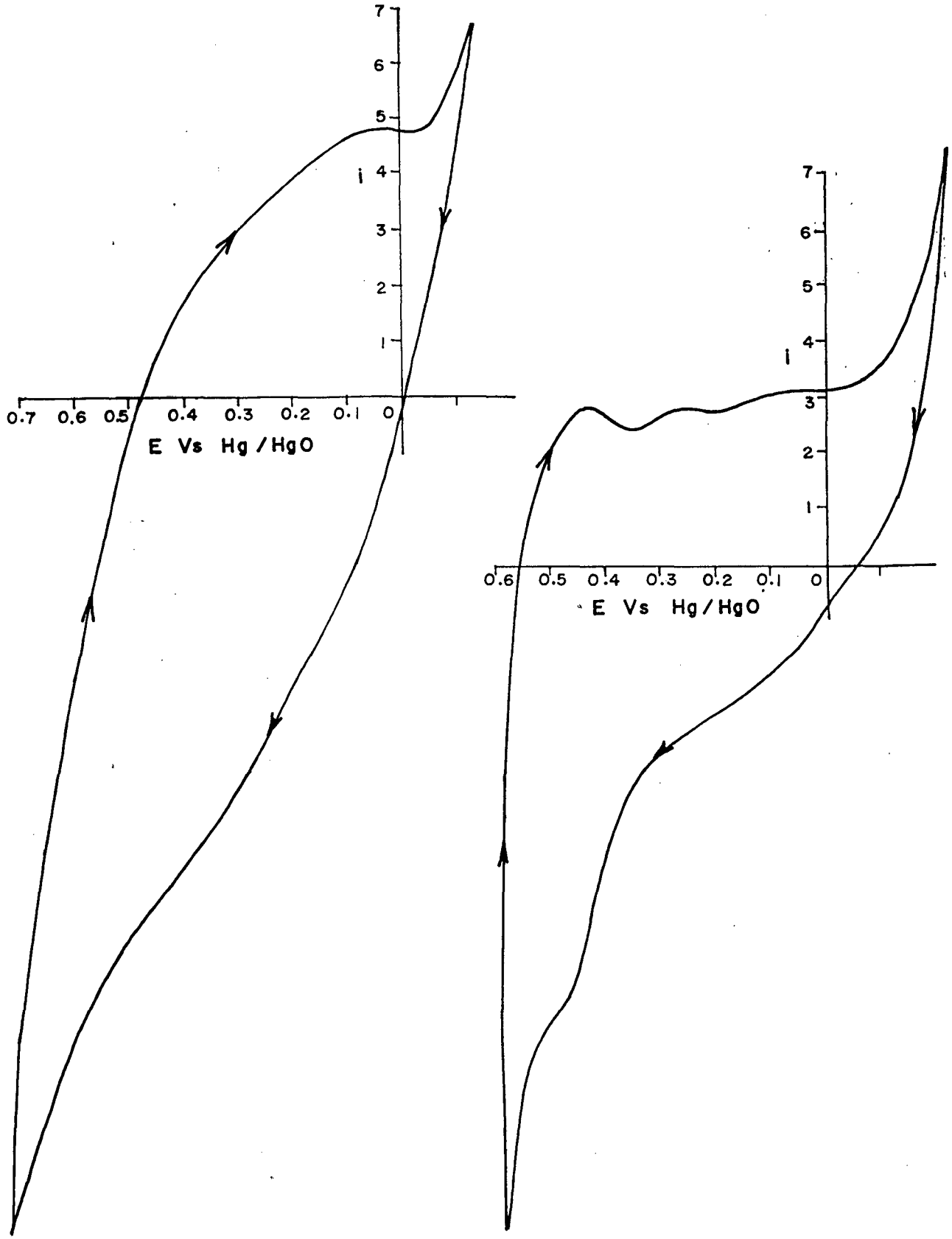

Fig. 4.41 The typical cyclic voltammogram for oxygen reduction reaction in 6 M KOH for a) CT-IV (P) ; b) CT-IV (G) at scan rate 300 mV / sec (a), 350 mV / sec. (b)

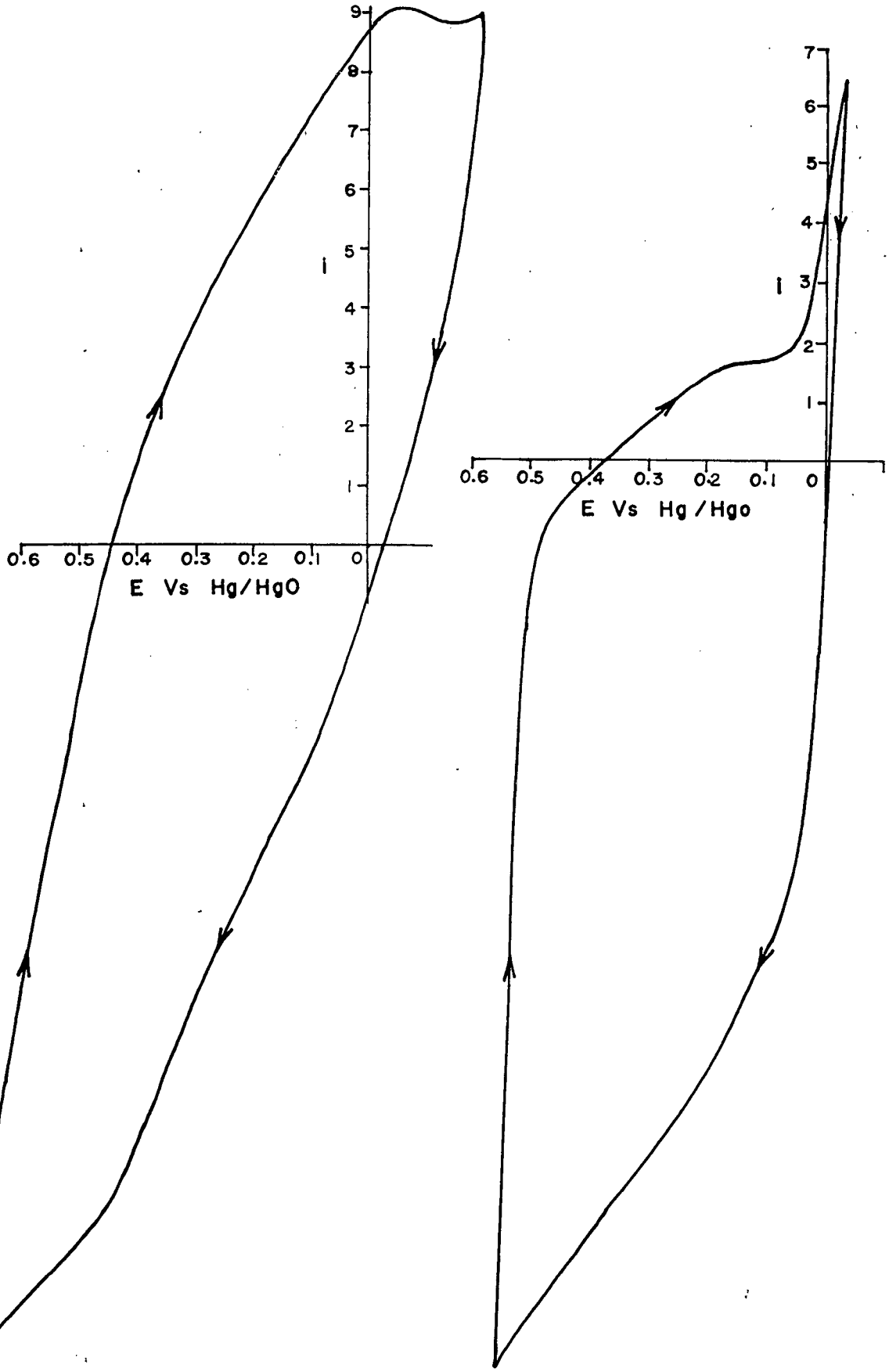

Fig. 4.42 The typical cyclic voltammogram for oxygen reduction reaction in 6 M KOH for a) CN-(P); b) CN-(G) at scan rate 200 mV/sec (a); 300 mV/sec (b).

Table 4.4 (a) Cyclic Voltammogram of samples in O_2 bubbled KOH solution

Samples	Peak I		Peak II		Peak III		i Oxy	Ea
	(Volts)	mA	mA	(Volts)	mA	(Volts)	mA/cm^2	Kcal/mol
CC-I(P)	0.45	5.6	0.30	3.2	-	-	218	25.62
CC-I(G)	0.52	2.6	0.38	2.5	0.18	1.7	234	7.18
CC-II(P)	0.43	5.7	0.28	3.0	-	-	211	3.46
CC-II(G)	0.54	2.5	0.38	2.2	0.2	2.4	271	6.95
CC-III(P)	0.41	7.0	0.28	5.8	-	-	279	3.57
CC-III(G)	0.55	2.4	0.37	2.1	0.14	1.3	288	2.97
CC-IV(P)	0.43	4.3	0.28	3.7	0.06	3.2	225	2.5
CC-IV(G)	0.53	2.0	0.36	1.9	0.17	1.8	279	6.9

Table 4.4 (b) Cyclic Voltammogram of samples in O_2 bubbled KOH solution.

Samples	Peak I		Peak II		Peak III		i Oxy	Ea
	(Volts)	mA	(Volts)	mA	(Volts)	mA	mA/cm^2	Kcal/mol
CT-I(P)	0.44	3.7	0.28	3.2	0.5	3.0	277	9.6
CT-I(G)	0.44	7.3	-	-	0.9	4.5	210	11.38
CT-II(P)	0.44	5.1	0.28	4.0	-	-	308	6.89
CT-II(G)	-	-	-	-	-	-	240	6.1
CT-III(P)	-	-	-	-	0.5	3.6	250	4.57
CT-III(G)	0.43	4.0	0.27	3.5	0.5	3.2	266	6.29
CT-IV(P)	-	-	-	-	0.5	0.8	350	2.5
CT-IV(G)	0.43	2.8	0.27	2.7	0.5	3.1	303	2.88
CN(P)	-	-	-	-	0.5	9.0	248	3.35
CN(G)	-	-	-	-	0.16	1.6	293	2.95

CONCLUSIONS

(1) Carbon supported Co_3O_4 spinel electrocatalysts are synthesized by several Precursor methods.

(2) Their electrocatalytic activity depended upon

(i) The nature of precursor (whether Carbonate, Nitrate, NTA complex, hydrazido ---etc)

(ii) Mode of decomposition:

Whether by use of direct thermal energy of a burner or by use of sunlight,

(iii) Whether catalyze by platinum or uncatalysed decomposition method of introducing carbon support whether by precursor method or mechanical grinding.

(3) Highly active samples were obtained when Cobalt (II) NTA complex is decomposed, in presence of silica and sunlight. The electrocatalytic activity of such a sample (20% Co_3O_4 /C) compared well with that of Platinum.

(4) It appears that Co_3O_4 alone prepared as above, could be a substitute electrocatalyst.

(a) However appropriate mixtures of (C/Co_3O_4 + Pt) could give high activities, with synergistic effects at the same time reducing the amount of noble metal catalyst that can be used. This could be a possible direction for future research - a consequence of the present investigation.

(b) These catalysts could also be tested in acidic electrolytes and for use in such fuel cells.

(c) It would be interesting to investigate doped Co_3O_4 with Cu^{2+}, Ni^{2+}, Pb^{2+} prepared by the method of CT-IV(P) as literature survey indicate improved performance with the above cations.

REFERENCES

1. J. R. Goldstein and A. C. C. Tseung, *J. Phys. Chem.,* 76 (1972) 3646.
2. H. M. Cota, J. Kalan, M. Chin and F. J. Schoenweis, *Nature,* (London) 203, (1964) 1281.
3. S. Jiang, and A.C. C. Tseung, *J. Electrochem.Soc.*,137 (1990) 76.
4 N. Sugumaran, and A. K. Shukla, *J. Power Sources,* 39 (1992) 249-254.
5 J. R. Goldstein, and A. C. C. Tseung, *J. Cata.,* 32 (1974) 452-465.
6. A. C. C. Tseung, and B. S. Hobbs, *Electrochim. Acta*, 17 (1972) 1557.
7. H. L. Bevan, and A. C. C. Tseung, *Electrochim. Acta*, 19 (1974) 201.
8. W. J. King, and A.C. C. Tseung, *Electrochim. Acta*,19 (1974) 485-491.
9. W. J. King, and A.C. C. Tseung, *Electrochim. Acta*, 19 (1974) 493.
10. G. Parravanno, *Proceeding of the IVth International Congress on Catalysis*, 1968 Moscow, P.149-165.
11. A. J. Appleby, J. Fleisch, and M. Savy, *J. Cata.,* 44 (1976) 281.
12. A. J. Appleby, and M. Savy, *Electrochim. Acta*, 21 (1976) 567.
13. S. Trassatti, *Electrodes of Conductive Mettalic Oxides.* (Elsevier Scientific Publishing comp.) Amsterdam (part A 1980, Part B 1981).
14. M. Hamdani, J. F. Koenig, and P. Chartier, *J. Appl. Electrochem.*, 28 (1998) 114-119.
15. G. K. Boreskov, *Kinet. Katal.* 14, (1973) 7.
16. S. Bagotsky, N. A. Shumulilova, and E. I. Kruscheva, *Electrochim, Acta*, 21 (1976).
17. S. Jiang, and A.C. C. Tseung, *J. Electrochem. Soc.*137, (1990) 764-769.
18. U. Morales, A. Campero, and O. Solorza-Feria, *J. New Materials for Electrochem.,*

Systems, 2 (1999) 89.

19. K. Kiros and S. Schwartz, *J. Power Sources,* 36 (1991) 547-555.

20. K. Kordesch, S. Jehangir, and M. Schautz, *Electrochim, Acta*,29 (1984) 1589-1596.

21. J. Van Benschoten, J. Y. Lewis, W.R. Heineman, A. Roston and P. T. Kissinger, *J. Chem. Educ.* 60 (1983) 772.

22. S. Trassatti, *Interfacial Electrochemistry of Conductive of Oxides for Electrocatalysis*, p. 769-792.

23. M. R. Gennero de Chialvo and A. C. Chialvo, *Electrochim. Acta*, 35 (1990) 437-443

24. L. Swette. N. Kackley and S.A. Mc Catty, *J. Power Sources*, 36 (1991)

25. E. Yeager, P. Krouse, and K.V. Rao, *Electrochim. Acta*, 9 (1964) 1057

ACNOWLEDGEMENTS

I was lucky to have been associated with Dr. Jayant. S. Budkuley. Professor and Head. Department of Chemistry. Goa University. for my Ph. D. studies. Without his keen interest. encouragement and valuable guidance. this thesis would not have been possible. It is with deep sense of gratitude that I thank my Guiding Teacher.

I will be failing in my moral duty. not to stress my overwhelming gratitude to Prof. A. K. Shukla. SSCU. Indian Institute of Science. Bangalore. for his ever active assistance. I am indebted to Prof. A. K. Shukla. without whose help this venture would not have been completed. I am grateful to him for extending all the available facilities to me for my research work.

I take this opportunity to thank Dr. Julio Fernandes. Goa University. for useful discussions. especially in electrochemical aspect in the thesis. I am grateful to Dr. Srinivasan. for helping me to interpret XRD data of my samples.

I am grateful to the chairman of the Ponda Education Society Shri Ravi S. Naik for granting me extraordinary leave and for his ever willing assistance. I extend my gratitude to the management of P.E.S. College for the help rendered.

My acknowledgement will be incomplete if I fail to thank our respected Principal of PES College. Dr. A.K. Heblekar. for being a constant source of encouragement and inspiration to me. I am also indebted to Dr. A. S. Dinge. Head. Dept. of Chemistry. PES College for his understanding. encouragement and support. I am grateful to all my colleagues in college. especially to Mr. Vikas Pissurlekar. Mr. Virendra Dangui. Mrs. Anuradha Kanolkar. and Mrs. Brenda Baretto for their valuable help. I extend my gratitude to my friend Mr. Sameer Patil. Bandekar College.

I am also grateful to Prof. Subrahamaniam. from Materials Division. IISC. Bangalore. for conducting the surface area of my electrodes. I am thankful to Mr. A. M. Kannan. SSCU. IISc. Bangalore. for undertaking SEM studies of my samples. and to Mr. Sariff from SSCU Workshop. Many thanks to Mr. Vijay Khedekar from NIO for having helped me in SEM studies. and Mr. U. Shirsat. for printing the SEM photographs. Thanks to Mr. Chitari. for undertaking the tracing work of my data.

I express my gratitude to Dr. H. S. Soni. Catalysis Division. NCL. Pune. for his assistance in carrying out studies in surface area. porosity measurements of my samples. I am also grateful to Dr. Pradhan. SIL. NCL. Pune for helping me carry out DTA-TGA-DTG of my samples. I acknowledge the help rendered to me by Dr. B. S. Rao. Deputy Director of NCL. My thanks to Dr. Vijaymohanan. Physical chemistry division. NCL. for the fruitful discussions.

I am thankful to Prof. Perisamy. for granting me permission to work in TIFR and Dr. Mrs. Nanda Haram. for helping me to conduct CV studies of the samples.

I am grateful to my friend from Fuel Cell Lab. Manoj Neergat. for helping me carry out half-cell polarization studies. to my friends from IISc. P. Sivakumar. B. Hariprakash. S. K. Martha. Raghuram. Suresh. Sriprakash. Kothandaraman. G. Nalini. Mandakini. Kamla. Digamber. Tapas. T. Shivakumar. K. Ramesha and to all my friends from IISc Who have helped me in some way or the other in my stay there a pleasant and a fruitful one.

I extend my gratitude to my friends. Karuna. Ranjeet. C.V. Dash. from NCL and Neel from TIFR. I am thankful to all teaching as well as non-teaching staff of the Chemistry Department. Goa University for being very nice to me throughout this venture.

Thanks to all my research student friends. I am thankful to Jayprakash and Lopes. from instrumentation for helping me in need.

I acknowledge the fellowship granted by the Department of Science and Technology. Government of India. New Delhi under funded project for some period during the study.

I am grateful to my brothers Girish and Shirish. my parents for helping me and understanding me at each and every step and to my uncle Shri Dharmanand Vaigankar. for being a constant source of inspiration and help. Thanks to Mr. Ramdas. I am also thankful to Mr. Mahendra Desai for checking my thesis.

Last but not the least. I remain grateful to anyone who may have either directly or indirectly helped me in the successful completion of my research thesis.

6/8/2001